Microsystems Engineering Assisted Cell and Tissue Culture Models: Detection and Therapeutic Applications of Botulinum Neurotoxin Type A

By

Won S. Hong

A dissertation submitted in partial fulfillment of

the requirement for the degree of

Doctor of Philosophy

(Biomedical Engineering)

at the

UNIVERSITY OF WISCONSIN-MADISON

2015

Date of final oral examination: 29 Apr 2015

The dissertation is approved by the following members of the Final Oral Committee:

David J. Beebe, Professor, Biomedical Engineering
Su-Chun Zhang, Professor, Neuroscience and Neurology
John S. Kuo, Associate Professor, Neurological Surgery and Human Oncology
Masatoshi Suzuki, Assistant Professor, Comparative Biosciences
Randolph Ashton, Assistant Professor, Biomedical Engineering

Abstract

Botulinum neurotoxins are the most lethal naturally produced neurotoxins. Due to the extreme toxicity, botulinum neurotoxins are implicated in bioterrorism; while, the specific mechanism of action and the long-lasting effect were found to be medically applicable in treating various neurological disorders.

Developing assays that can accurately determine toxicity of botulinum neurotoxins is therefore highly desirable to protect the public from bioterror threats and also to ensure the safety of patients on therapies derived from botulinum neurotoxins. In the first part of the thesis, I discuss different approaches that I've taken to develop physiologically relevant cell-based assays including (i) coculture of Schwann cells and neuronal cells, (ii) optimization of neural cell culture media, and (iii) development of an organotypic neuromuscular junction-like model to mimic muscle paralysis *in vitro*.

Additionally, I explored an alternative therapeutic application of botulinum neurotoxins. Synaptic vesicle 2 proteins are receptors of botulinum neurotoxin type A, which are highly expressed in neuroendocrine tumors and have been recognized as new biomarkers. I hypothesized that the nontoxic receptor-binding domain of botulinum neurotoxin type A can be used as a ligand to target synaptic vesicle 2 proteins expressed in neuroendocrine tumors without imposing neurotoxicity.

In the latter part of the thesis, I show that the nontoxic fragment of the heavy-chain receptor binding domain of botulinum neurotoxin type A preferentially recognizes and internalizes into neuroendocrine cancer cells originating from thyroid, lung, and pancreas. More intriguingly, this heavy-chain receptor binding domain does not only target neuroendocrine cancer cells but also suppresses expression of chromogranin A and achaete-scute complex 1,

neuroendocrine tumor markers, indicating potential application in palliative therapy and reversion of neuroendocrine differentiation.

To my amazing parents

and loving wife

Acknowledgements

I would like to thank my advisor, David Beebe, for being a great mentor throughout the graduate program, especially supporting my projects despite the diverging scope from the core research programs of the Microtechnology, Medicine, and Biology Laboratory (MMB lab). I also thank the former and current members of MMB lab, especially Edmond Young, who patiently worked with me through writing my first paper, and Kyung Sung and her husband Young Choi, who wholeheartedly supported my projects and occasionally helped me to relieve stresses from the lab. I wish to extend my appreciation to all members of MMB labs including Andrea Schuster and Jiwon Lim, undergraduate students in biomedical and chemical engineering programs respectively for assisting my research. I also had privilege to work with Dr. Herbert Chen and his research team members, Renata Jaskula-Sztul and April Harrison, whom I worked very closely on the neuroendocrine cancer research.

My greatest acknowledgement and gratitude go to my family for their support especially even after making the radical decision to quit my job to pursue graduate degree in biomedical engineering. My wife, Hyeduk, survived through the blazing subzero winter in Madison; my parents and parents-in-law for their prayers and encouragements; my sister and brother-in-law for taking out a poor graduate student couple out for many dinners.

Lastly but not least, I greatly appreciate and thank my former supervisor Jin Yin, colleagues David Scuderi and Eric Hayduk, and lifetime career advisors and mentors Gan Wei and Yasushi Saotome at the Shire Human Genetic Therapies who encouraged and pushed me to pursue graduate studies.

Thank you.

Table of Contents

List of Figures

List of Tables

Chapter 1 - Introduction

1.1 Background

Botulinum neurotoxins (BoNTs) are produced in *Clostridium botulinum* and they are the most potent and lethal toxins known to men. There are seven known and sequenced serotypes denoted A to G [1], and a recently discovered undisclosed strain which sequence was held from the public for safety reasons [2]. Of the seven sequenced and disclosed serotypes, type A is the most potent and its toxicity lasts for 3 to 6 months *in vivo*. Despite the implication in the bioterrorism due to the extreme potency, ease of production and transportation [3], the specific mechanism of actions and long-lasting effect were found medically applicable in treating neuromuscular dystonia and alleviating pain [4]. Currently, there are more than 150 ongoing clinical trials in the United States that use BoNTs as the active pharmaceutical ingredient [the U.S. National Institute of Health, Clinical Trials, http://clinicaltrials.gov, accessed: April, 2015]. With the growing number of medical applications of BoNTs expanding from already established muscle dystonia and spasms to the recent developments in treating gastric and breast cancer [5, 6], and controlling urinary tract [7], manufacturing and distribution of BoNTs is inevitable. Therefore, an assay that can not only detect the presence of the toxin but also can assess *in vivo* activity is highly desirable to protect the public from the misuse of the toxins and to ensure the safety of the patients in clinic.

Assays for detecting and determining the toxicity of BoNTs can be categorized into two in large depending on their intended applications: (1) infield testing in food supply chain to rapidly screen the fresh produces and (2) laboratory testing of active pharmaceutical ingredient for medical use. Previously, our laboratory developed microfluidic assisted BoNTs detection assays amenable for the infield testing that leveraged signal amplification in microchannels to

quantify catalytic activity of BoNTs [8] and measuring genome content of *Clostridium botulinum* [9]. Despite the advances and high sensitivity, these methods do not recapitulate physiological mechanism of action, which involves (i) the recognition of synaptic vesicle 2 (SV2) proteins and ganglioside GT1b receptors of the heavy-chain receptor binding domain (HCR) of BoNT/A, (ii) conformation change of the heavy-chain translocation domain (H_N) that repositions catalytic light-chain upon endocytosis, (iii) endosomal escape of the catalytic light-chain (LC) with acidification of endosome, and (iv) reduction of disulfide bond releasing LC into the cytoplasm [1]. The liberated LC then cleaves at least one of the components that form soluble *N*-ethylmaleimide-sensitive factor (NSF) attachment protein receptor (SNARE) complex, which mediates neurotransmitter containing vesicle exocytosis thus blocking acetylcholine release.

1.2 Need for Physiologically Relevant and Highly Sensitive Botulinum Neurotoxin Detection Assays.

In the past, mouse bioassay held its place as the gold standard for determining activity of BoNTs. The assay involves injecting mice with varying concentrations of BoNTs. Then highly skilled technicians closely monitor muscle paralysis of the mice and determine the minimum concentration required to kill the mice. The half concentration of the minimum lethal dose is defined as 1 LD_{50} U. Although the mouse bioassay is the most physiological form of the assay in determining the toxicity, it has disadvantages including (i) animal sacrifice, (ii) requirement of highly-skilled technicians, (iii) low throughput, (iv) high cost, and (v) low resolution and high assay variability [10]. Therefore, an *in vitro* assay that can replace the mouse bioassay without compromising detection sensitivity and physiological relevance is needed.

To develop the detection system with physiological relevance, selecting cholinergic neuronal cells with motor neuron-like characteristics as a model system is important. The most relevant model that does not require animal sacrifice available to date is the human motor neurons derived from human embryonic (hESC) or induced pluripotent stem cells (hiPSC). As an example of applying hESC for BoNT/A detection, hESC derived gamma aminoisobutyric acid (GABA)ergic neurons were tested as the sensors for detecting BoNT/A and showed the sensitivity surpassing that of the mouse bioassay [11]. Despite the advancement in using hESC derived neurons, the study was conducted using GABAergic neurons whereas the BoNT/A is known to act on cholinergic peripheral motor neurons [12]. Therefore, selected *in vitro* model for testing was not ideal. Additionally, differentiating hESC or hiPSC into cholinergic motor neurons include extensive time investment, which reportedly takes up to 60 days to deliver fully matured and functional motor neurons [13], and the differences in the qualities of the motor neurons vary from operator-to-operator [14]. On the other hand, identifying and selecting continuous neuronal cell lines with motor neuron-like characteristics offers advantages by providing (i) an unlimited source of the cells, (ii) minimized quality differences of the sensing cells, (iii) shortened cell culture duration, (iv) lower cost by using inexpensive reagents in cell culture, and (v) not necessitating highly-skilled technician to culture and differentiate hESC or hiPSC.

In 1970s, a group of researchers showed neuroblastoma hybrids cells display neuronal characteristics including the release of acetylcholine, neurite formation, and generation of action potentials upon electrical stimulations [15, 16]. One of the neuroblastoma and glioma fused cell line, NG108-15, was shown to be cholinergic [17], respond to pharmacological stimulation [18], and form synapsis with striated muscle cells [19, 20] suggesting motor neuron-like

characteristics. Additionally, NG108-15 cells can extend its neurites when cocultured with Schwann cells derived from human adipose stem cells [21]. Taken together, NG108-15 cell line is a good model that can be applied as the biosensor for detecting BoNT/A. However, the cell line suffers from far inferior detection sensitivity when compared to primary spinal cord and stem cell derived motor neurons (refer to Chapter 2).

The convenience of continuous neuronal cell line and motor neuron-like characteristics do not overweigh the detection sensitivity because 1.3-13 ng/kg body weight is enough to be lethal to men. To truly become useful as a biosensor, the detection limit must come down to picomolar range that can detect BoNT/A activity close or surpasses 1 LD_{50} U [3]. Therefore, the sensitivity to NG108-15 cell line must be improved. In my thesis, I proposed and conducted series of experiments to achieve detection limit of at least 1 LD_{50} U by (i) leveraging microscale engineering to accentuate soluble factor effects for increasing BoNT/A detection sensitivity, (ii) coculturing NG108-15 cells with Schwann cells providing more physiological relevant microenvironment, and (iii) optimizing NG108-15 culture media. The approaches and experimental outcomes are discussed in Chapter 2 and Chapter 3. Finally, the BoNT/A detection limit of NG108-15 cell line improved to 0.3 LD_{50} U.

After achieving a high BoNT/A detection sensitivity, I faced another challenge in utilizing cells as the sensor. The throughput of the sensor is limited by using Western blot as the end-point measurement. Although Western blot can distinguish cleaved and uncleaved portions of SNAP25 protein, the substrate of BoNT/A, upon intoxication of the cells, it requires laborious preparation, relies on the quality of antibody used, and takes several days to get the final readout. To address these limiting steps associated with Western blot, I leveraged microsystems engineering and applied tissue engineering technique to develop an organotypic neuromuscular

junction-like model. The model consists of neuronal NG108-15 cells and skeletal myoblast C2C12 cell line, and upon successful delivery of the organotypic model, muscle paralysis can be recapitulated upon BoNT/A intoxication *in vitro*. The proof-of-concept model is discussed in Chapter 4.

The interface where motor neurons innervate skeletal muscle fibers is called neuromuscular junction (NMJ). BoNT/A enters synaptic terminal of cholinergic motor neurons where the synaptic ends form synapsis with striated muscle fibers [12]. By developing an organotypic NMJ-like model, a higher degree of physiological relevance can be achieved and *in situ* measurement of muscle paralysis will enable high-throughput analysis and expedited readout.

1.3 Vertebrate Neuromuscular Junction

Vertebrate neuromuscular junction (NMJ) is a highly organized and complex system generated by axon terminals of motor neurons (MNs) innervating and forming synapses with skeletal muscle fibers. The synapses are capped by terminal non-myelinating Schwann cells providing, in part, structural stability of the synapse, while myelinating Schwann cells ensheath axons insulating from the loss of current as the signal travels down towards the synaptic ends. The network of these cells control voluntary motion in concert, thus disturbing the balance of this complex results in the loss of function and control in the muscle movements and can lead to neuromuscular disorders.

The molecular mechanisms and the physiology of NMJ are well-characterized. Membrane potential, created by differences in the charged ion concentrations between the inside and outside of the cell membrane, depolarizes firing action potential upon reaching the threshold, which propagates downwards towards axon terminal. Once the action potential reaches

presynaptic end, docked synaptic vesicles filled with acetylcholine (ACh) fuse with the cell membrane thereby releasing ACh to the synaptic cleft, an interface between the innervating axon terminal and innervated muscle fiber. The fusion of synaptic vesicles is mediated by SNARE complex. The released ACh molecules rapidly bind to nicotinic acetylcholine receptor (AChR), a voltage-gated sodium and potassium channel, depolarizing the cell membrane leading to muscle contraction. Unbound ACh molecules are rapidly hydrolyzed by acetylcholinesterase breaking down to choline and acetate for recycle [22]. Botulinum neurotoxins act at this interface by cleaving at least one of the components that make up SNARE complex. Inhibition of neurotransmitter release then leads to flaccid and muscle paralysis [12].

Despite the advancement in neuroscience research and tissue engineering, reliable and functional *in vitro* model of NMJ is not yet available mainly due to the difficulties in long-term culture of skeletal muscle required for the maturation of MNs and formation of functional synapses. Conventionally, cells are cultured on two-dimensional surface where cells adhere to the cell culture dish. As skeletal myoblasts fuse and form myotubes, they undergo spontaneous twitching creating tension on the cell membrane, which then pulls the fibers causing the detachment from the surface. The detached muscle fibers are no longer viable for MNs to form proper synapses. Additionally, even when the functional synapse can form in rare occasions, using electrophysiology to stimulate neurons to look at muscle contraction is painstaking and no quantitative analysis on muscle contractile force is possible [23]. Moreover, optimized medium that supports MN survival and skeletal muscle fibers is required for the long-term culture.

Research led by James Hickman adopted microelectromechanical systems engineering to fabricate microcantilever. The microcantilevers were treated with highly hydrophilic silane for cell adhesion, which was then used to culture myotubes. The elastic property of the

microcantilever reduced the membrane tension as cells twitch, allowing for a longer culture of myotubes. The contractile force then was measured by the degree of cantilever bending, which is measured by deflection of laser reflected off from the microcantilevers [24]. They additionally developed MN and skeletal muscle coculture media [25]. Despite the achievements, the system has several limitations: (i) fabrication of the microcantilevers requires a cleanroom facility equipped with sophisticated high-resolution microelectromechanical fabrication instrument, (ii) each microcantilever measures the force of individual myotube which forms synapse with undetermined body of a MN that limits good for single-cell analysis but not ideal for delineating function at tissue or organ level, (iii) MNs cannot be stimulated directly requiring pharmacological stimulation or (iv) further complicating the system by embedding electrical stimulation system, which then may stimulate myotubes causing false positives, and (v) the myotubes can be detached from the microcantilever with extensive stimulation for functional analysis. I sought to address these limitations to create functional NMJ. By adopting simple fabrication technique that does not require cleanroom, transfecting MNs with channel rhodopsin 2 for stimulating MNs, and using three-dimensional cell and tissue culture method for increasing culture duration, I established NMJ-like model *in vitro*. The approach I discussed in Chapter 4 is simpler, quantitative, and can be performed in any bioscience research labs. The *in vitro* NMJ-like model is at the proof-of-concept stage; however, it will serve as a biomimetic model to recapitulate muscle paralysis *in vitro,* thus offering rapid physiologic readout in quantifying activity of BoNT/A, which the tissue can later be collected to analyze cleavage of SNARE components to determine specificity and origin of toxin, including BoNT/A. Additionally, the model will foster basic neuroscience and applied translational researches and developmental sciences with the emergence in the stem cell research.

1.4 Importance of Glia

The fundamental functional units of NMJ are MN and skeletal muscle fibers. Another important player, which was not discussed in the previous sections is glial cells present in both central (CNS) and peripheral nervous systems (PNS). I will focus on the glial cells of PNS since the thesis is limited to BoNT/A and NMJ.

Peripheral glia Schwann cells, another member forming NMJ, were regarded as a passive player where its roles were limited to (i) maintaining currents passing through the axons by forming myelin sheets around the axons and (ii) providing structural integrity of synapses formed between the axon terminal of MNs and skeletal muscle fibers [26]. Nonetheless, Ullian *et al.* observed significantly increased number of synapses and synaptic activities of purified rat spinal cord MNs when cocultured with purified rat Schwann cells *in vitro* [27]. Subsequently, paracrine signaling between Schwann cells and MNs was found responsible for modulating synaptic activities [28], of which one of them is transforming growth factor-beta1 (TGFβ1). TGFβ1 is thought to work either independently or cooperatively with yet unidentified small biomolecule [29]. Additionally, Schwann cells interact with MNs for survival [30] and also involved in regeneration of axons [31]. Taken together, increasing number of evidences support involvement of intricate intercellular interactions between MNs and Schwann cells at NMJ, signaling for survival, development, maturation, and maintenance. Therefore, introducing Schwann cells to NMJ model will offer more physiologic, mature, and structurally sound model.

Taking advantage of the Schwann cells interaction with MNs, I applied Schwan and cholinergic neuronal cell coculture to increase the detecting sensitivity of BoNT/A, which is described in Chapter 2.

1.5 Clinical and Therapeutic Applications of Botulinum Neurotoxin Type A

The following Chapter 2 to Chapter 4 of the thesis focused in developing *in vitro* models for detecting BoNT/A. Ultimately, I want to apply these models to study basic and translational neuroscience, developmental biology, and neurodegenerative diseases. Changing gears from the emphasis on the *in vitro* cell and tissue model development, I looked at utilities of BoNT/A and how these models can serve as tools towards drug discovery and development.

Currently, there are over 150 on-going clinical trials using BoNT/A or its genetic variants under the United States Food and Drug Administration [the U.S. National Institute of Health, Clinical Trials, http://clinicaltrials.gov, accessed: April, 2015]. Already approved uses for BoNT/A and ongoing clinical trials focus narrowly on pain relief and muscle dystonia and spasms. Additionally in research and development phases, modular design of BoNT/A consisting (i) heavy-chain receptor binding domain (HCR) that recognizes SV2 and ganglioside GT1b as co-receptors, (ii) heavy-chain translocation domain (H_N) that positions catalytic light-chain of BoNT/A for endosomal escape, and (iii) light-chain catalytic domain (LC) that cleaves SNAP25 [1] was shown to be repurposed through genetic engineering. These efforts include altering the function of LC to cleave different substrates or utilizing HCR and H_N for delivering drugs to peripheral neurons [4, 32]. Interestingly, continued translational research on BoNT/A found its use in treating overly active bladder, breast cancer, and even gastric cancer [5-7] expanding the utility of the most lethal toxin known to man.

With the earlier part of the thesis that emphasizes on the development of model and potentially yielding valuable NMJ disease model by using iPSC derived MNs, skeletal myoblasts, and Schwann cells in combination, using BoNT/A as means of delivering therapeutic reagent to MNs may reveal significant impact in human health in treating debilitating MN diseases such as

amyotrophic lateral sclerosis (ALS) and spinal muscular atrophy (SMA) where no treatment is available. Developing a physiologically relevant organotypic model of NMJ and adopting it for high-throughput drug screening platform, new compounds and potential targets for therapies may surface. In that, HCR holds promise as a ligand for targeted drug delivery to peripheral neurons while utilizing the H_N to unload biologics to cytoplasm as demonstrated in the past [33].

Though many applications of BoNT/A in clinic are explored to apply to PNS diseases and the first four chapters of my thesis put emphasis on such application enabling studies, I identified an unique opportunity to apply BoNT/A in neuroendocrine cancer. Neuroendocrine malignancies arise from hormone and neurotransmitter secreting heterogeneous neoplasm originating from lung, thyroid, and pancreas. The uncontrolled hypersecretion of bioactive hormones and neurotransmitters cause debilitating symptoms including excessive diarrhea, hemorrhage, and cardiac failure for example. Early in the 2000s, considered new biomarker for neuroendocrine tumors SV2 was identified [34-37], which later coincidently discovered as the receptor for BoNT/A [38]. In Chapter 5, I discuss how non-toxic HCR can be used as a therapy for treating neuroendocrine cancers and show a novel function of the HCR.

1.6 Overview of the Thesis

One of the long-term goals of my research is to provide therapies to patients suffering from neurodegenerative diseases, especially in the peripheral nervous system. Complex and intricate interactions among the constituents of neuromuscular junction convolutes proper diagnose and understanding these devastating motor neuron diseases and muscle dystrophies. In my thesis, I aimed to provide tools that allow deconvoluting intercellular interactions by adopting microsystems engineering to develop functional physiologically relevant organotypic

models. Although still at primitive stage, the data I collected in my research takes the first step towards providing insights and therapies associated with neuromuscular junction and an untouched area in neuroendocrine cancer.

Using botulinum neurotoxin type A as the main theme, I show the importance of glial cells in Chapter 2, media optimization that will aid neurons and skeletal muscle fiber coculture in Chapter 3, organotypic neuromuscular junction-like micro-tissue model that will enable rapid quantification of functional outputs in Chapter 4, and a novel function and potential clinical applications of botulinum neurotoxin that will open new opportunities for applying botulinum neurotoxins in Chapter 5.

Chapter 2 – A Microscale Neuron and Schwann Cell Coculture Model for Increasing Detection Sensitivity of Botulinum Neurotoxin Type A

2.1 Introduction

Botulinum neurotoxin (BoNT) is an N-terminal Zinc-metalloprotease consisting of seven serotypes (A-G) that are produced by the bacterium species *Clostridium botulinum* [1]. BoNT is well known for its clinical efficacy in both cosmetics and neuromuscular distonias [39], achieved via the blocking of acetylcholine release [12]. Additionally, BoNT is known for its extremely high specific toxicity, which together with its ease of production makes it a serious threat in bioterrorism [3]. Understanding the effects of BoNT on neural response and function, and the mechanisms underlying BoNT-associated cell signaling, is crucial to our ability to both harness its useful application in clinical settings and control its potential danger to public health and safety.

In vivo, BoNT activity occurs specifically at the pre-synaptic ends of neuromuscular junctions (NMJs), a complex cellular microenvironment primarily comprised of the axon terminal of a motor neuron forming a synapse with a skeletal muscle fiber, which is further capped by terminal Schwann cells and kranocytes [40]. While motor neurons and muscle fibers are the fundamental units of NMJs, terminal Schwann cells also play an essential role in the microenvironment by being involved in synaptogenesis, synaptic activity, regeneration of damaged synapses, and synaptic maturation of NMJs [40, 41]. Thus, the behavior and function of neurons at an NMJ, including their response to BoNT, is likely dependent on the complex microenvironmental cues at the NMJ, particularly signals provided by neighboring cell types.

BoNTs consist of covalently linked ~100 kDa heavy-chain (HC) and catalytic ~50 kDa light-chain (LC) domains. The HC binds two different types of surface receptors, polysialogangliosides and cell surface protein receptors, which are present at post-synaptic ends of cholinergic neurons, and are responsible for internalizing BoNT into the cell by endocytosis in active synapses. The LC is delivered into the cytosol through a channel in the endocytotic vesicle formed by the N-terminus of the HC. The LC then cleaves a specific peptide bond in a protein of the soluble N-ethylmaleimide-sensitive factor attachment protein receptor (SNARE) complex, blocking the release of neurotransmitters [1, 12]. BoNT serotypes A and E cleave synaptosomal-associated protein 25 (SNAP25), serotypes B, D, F, and G cleave synaptobrevin on synaptic vesicles, and serotype C cleaves both SNAP25 and syntaxin on the plasma membrane [1]. Because of the high degree of specificity in cleavage of SNARE proteins by BoNTs, many assays have been developed to measure SNARE cleavage to detect and quantify toxicity of BoNT [42].

Currently available BoNT assays can be divided into four basic categories: (1) *in vitro* cell-free, (2) *in vitro* cell-based, (3) *ex vivo*, and (4) *in vivo* assays [42]. *Ex vivo* and *in vivo* assays, including the standard *in vivo* mouse bioassay (also known as in vivo mouse LD_{50} assay), are highly sensitive and physiologically relevant models, but suffer from high cost, low throughput, high variability, and various practical and ethical issues related to animal testing [43]. In contrast, while *in vitro* cell-free assays such as enzyme-linked immunoabsorbent assay [44] and synthetic SNAP25 substrate peptide cleavage assay in microfluidic channel [8] are very sensitive and high throughput methods [45], these assays do not measure all relevant steps for intoxication disregarding important physiologic mechanisms [46]. Although *in vitro* cell-free

assays do not capture physiologic mechanisms, they are useful in positive and negative testing for BoNT, where cell culture and animal care facilities are not accessible.

Cell-based assays are attractive because they represent living functional units that exhibit physiologic mechanisms, but have lower cost and can be better standardized than *in vivo* methods [43]. Therefore, cell-based assays are great alternatives to *in vivo* mouse bioassay in determining specific toxicity of BoNT for pharmaceutical applications. Despite high sensitivity and physiologic relevance, cell-based assays relying on fastidious primary [10] and stem cell-derived neurons [47, 48] are difficult to isolate and require several weeks of cell culture before used for BoNT detection. In the past, studies had demonstrated utility of neuronal cell lines in detecting BoNTs but they suffered from low sensitivity [49, 50]. Recently, however, direct differentiation of neuronal cell lines using soluble factors achieved high sensitivity of the cell lines [51, 52]. Alternatively, an *in vitro* cell-based assay that labeled different SNARE substrates with fluorescence resonance energy transfer (FRET) sensors in cells has shown promise for higher throughput and multiplex potential [53], but challenges associated with widespread accessibility and technical difficulties in detecting the FRET signal still remain. Importantly, a limitation of current cell-based assays, which has been largely overlooked, is they do not account for many critical aspects of the NMJ microenvironment, such as the presence and putative role of Schwann cells [54], and the importance of controlling diffusion that affects cell signaling through soluble factors [55, 56] to more closely mimic physiologic conditions [57]. It is possible that improvements in the design and control of the *in vitro* microenvironment may increase sensitivity of BoNT detection by addressing the key issues related to current *in vitro* cell-based platforms, and thus offer an alternative to existing assays.

Recent advances in microfluidic cell-based technologies have provided a unique opportunity to test this hypothesis. Microscale cellular systems leverage microfabrication techniques to yield customized geometries that improve spatiotemporal control of the microenvironment, including the organization of different cell types and improved control of soluble factor diffusion. Here, we describe a microscale coculture model consisting of neurons and Schwann cells that recapitulate important aspects of the cellular interactions of the NMJ microenvironment, with specific application to the detection of BoNT. As a baseline for the microscale experiments, we first tested macroscale coculture of the neuronal NG108-15 with S16 Schwann cell lines and discovered that it significantly increased sensitivity compared to that of NG108-15 monoculture. We further found that culturing at the microscale versus macroscale in the absence of S16 cells has significant effects on sensitivity, and that, through the spatial arrangement of NG108-15 and S16 cells in microenvironments, soluble factors from the S16 cells are the likely contributors to the increased BoNT/A sensitivity observed.

2.2 Materials and Methods

Cell Lines and Cell Culture: A hybrid mouse neuroblastoma and rat glioma cell line, NG108-15, was purchased from ATCC (Manassas, VA), and maintained in growth medium composed of Dulbecco's Modified Eagle Medium (DMEM; Invitrogen, Carlsbad, CA) with 10% fetal bovine serum (FBS; Invitrogen), 1% penicillin-streptomycin (P/S; Invitrogen), and supplemented with 0.1 mM hypoxanthine, 400 nM aminopterin, and 16 μM thymidine (HAT; Sigma-Aldrich, St. Louis, MO). A rat Schwann cell line, S16, was purchased from ATCC, cultured in T-75 flasks coated with poly-L-lysine (PLL; Sigma-Aldrich), and maintained in growth medium composed of DMEM with 10% FBS, 1% P/S, and 110 mg/L sodium pyruvate

(Sigma-Aldrich). Both NG108-15 and S16 cells were incubated at 37°C with 5.0% CO_2, subcultured as suggested by the supplier, and discarded after 20 passages.

***S16 Conditioned Medium*:** 3 x 10^5 S16 cells were cultured in PLL-coated T-75 flasks in the S16 growth medium described above. Cells were washed with PBS after one day of culture and then fed with 20 ml of fresh supplemented S16 growth medium free of FBS. After three additional days of culture without media exchange, conditioned medium (CM), was collected and centrifuged for 10 min at 2000 rpm, and supernatant was stored at -20°C until ready for use. For CM experiment at the macroscale, 50 µl of CM was mixed with 150 µl of fresh serum-free NG108-15 growth medium. FBS was then added subsequently to make 1% FBS by volume. Thus the overall dilution of the soluble factors in CM was approximately 270 nl/cell (20 ml per 300,000 cells followed by 1:4 dilution).

Microfluidic Device Design: The microfluidic device consisted of a 3 x 4 array of independent micro-culture systems each consisting of three separate microchambers connected by diffusion ports (Figure 1A). The device design allowed independent experimental conditions in each micro-culture system, while the interconnected design of the micro-culture system allowed cell-cell communication via soluble factors without the influence of physical cues. Details of design and operation are described elsewhere [58]. For all microscale coculture experiments in this study, NG108-15 cells were seeded in the middle microchamber, and S16 cells were seeded in either the two side microchambers or in the middle mixed with NG108-15 cells (Figure 1B). Cells, medium, BoNT/A, and fixing and immunostaining reagents were all introduced into the microchambers by passive pumping using only a micropipettor [59].

Microfluidic Device Fabrication: The microfluidic device was fabricated using established soft lithography techniques [60, 61]. Briefly, master molds were made by spin-

coating different grades of SU-8 (Microchem, Bedford, MA) followed by pre-bake, ultraviolet (UV) light exposure, post-bake, and development steps. Polydimethylsiloxane (PDMS; Dow Corning, Midland, MI) was mixed in a 10:1 ratio of pre-polymer base and crosslinking agent, vacuumed, poured on the master molds, and cured at 80°C for 4 h on a hot plate. Cured PDMS layers were then removed from the master molds, and soxhlet-extracted with 100% ethanol for at least 4 h to remove uncrosslinked PDMS oligomers known to leach from the bulk into culture media [62]. PDMS layers and a glass slide were sequentially plasma treated and irreversibly bonded, as described previously [58]. The assembled device was heated at 70°C for 10 min on a hot plate prior to use.

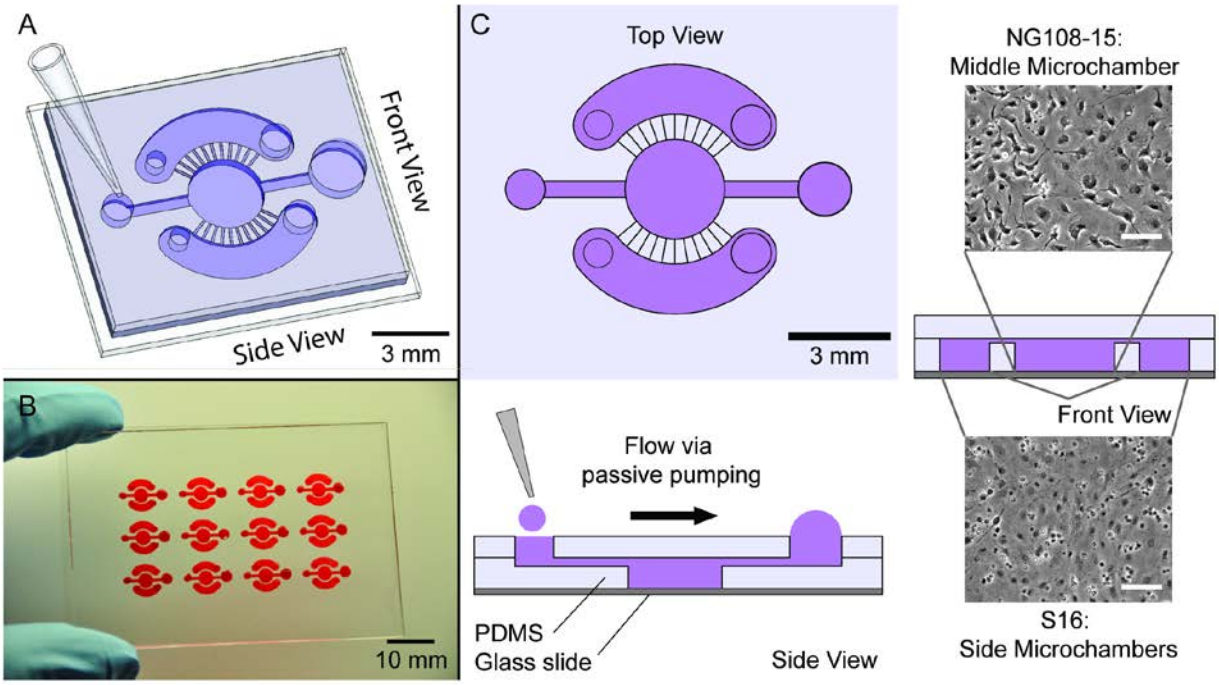

Figure 1: Design of the microfluidic device
(A) 3-D view of the micro-culture system. (B) Image of the device with 3 x 4 array of micro-culture systems. (C) Top view of a micro-culture system consisting of three microchambers, one in the middle and two on each side; side view of the micro-culture system with arrow indicating the direction of flow by passive pumping; front view of the device where NG108-15 cells were seeded in the middle and S16 cells in the side microchambers. Diffusion ports were placed approximately 250 μm above the glass surface where cells adhered. Scale bars on cell images represent 100 μm.

Immunofluorescence Microscopy: Antibodies used include the following: for primary antibodies, mouse monoclonal IgG anti-SNAP25 (Synaptic Systems, Gottingen, Germany) and rabbit polyclonal IgG anti-S100 (Thermo Scientific, Rockford, IL); and for secondary antibodies, AlexaFluor488 goat anti-mouse and AlexaFluor647 goat anti-rabbit (Invitrogen). DAPI nuclear staining dye was acquired from Invitrogen. Cells were fixed with 4% paraformaldehyde (PFA) prior to staining. Both S100 and SNAP25 primary antibodies were diluted 1:200 in 1% bovine serum albumin (BSA; Sigma-Aldrich), incubated overnight at 4°C. The secondary antibodies were diluted 1:500 in 1% BSA and incubated for 30 min at ambient. For all staining and washing, passive pumping was used. Fluorescence microscopy was performed on a Nikon Eclipse Ti inverted fluorescence microscope with a PlanFluor 4x or 20x objective (Nikon Instruments, Melville, NY), and images were captured with a with a Nikon DS-Qil Mc CCD camera and acquired with NIS-Element Version D 3.10 software.

Microscale Cell Viability Assay: Cells were cultured in the microchambers as described above. Cells were washed with PBS (with Ca^{2+}/Mg^{2+}) two days after seeding, and incubated at ambient temperature for 20 min with a Live/Dead cytotoxicity assay (Invitrogen) consisting of Calcein AM (green) for live cells and ethidium homodimer-1 for dead cells. DAPI was added to the samples after washing the cells. Nikon Eclipse Ti inverted fluorescent microscope with PlanFluor 4x objective and additional 1.5x intermediate magnification was used for image acquisition. Cell viability assay was performed in triplicates.

***Macroscale SNAP25 Cleavage Toxicity Assay*:** Each well of a 96-well plate (Becton Dickinson and Company, Franklin Lakes, NJ) was coated with 50 µl of 0.083 mg/ml Matrigel (BD Bioscience, San Jose, CA) prior to cell seeding. Each well was seeded with ~15,000 NG108-15 cells either alone or with ~3,750 or ~15,000 S16 cells. Cells were cultured for two

days in 200 µl of DMEM with 1% FBS, 1% P/S, and HAT. BoNT/A at 8 U/pg specific toxicity was serially diluted in culture medium to the desired concentration, and 50 µl of the diluted BoNT/A was added to each well after aspirating spent medium. Cells were collected for Western blot two days after treatment. All materials that contacted BoNT/A were disinfected with 10% household bleach before disposal.

Microscale SNAP25 Cleavage Toxicity Assay: Micro-culture systems were filled with 70% ethanol, coated with PLL, washed three times with sterile deionized (DI) water, and coated with 30 µl of 0.083 mg/ml Matrigel. For monoculture and mixed coculture, ~15,000 NG108-15 cells were seeded either alone or mixed with ~15,000 S16 cells in the middle microchamber using passive pumping. For compartmentalized coculture, ~15,000 NG108-15 cells were seeded in the middle microchamber and ~1, 875 or ~7,500 S16 cells were seeded in both side microchambers totaling ~3,750 or ~15,000 S16 cells per micro-culture system. Spent medium was aspirated and 30 µl of fresh medium was added daily for two days. BoNT/A was diluted to desired concentration in the medium and 30 µl of the BoNT/A (10 µl in each microchamber) was added to each micro-culture system after aspirating spent medium. Two days after BoNT/A treatment, 10 µl of 2x lithium dodecyl sulfate buffer (LDS; Invitrogen) was directly added to the middle microchambers via passive pumping and then collected. This lysis and collection step was repeated once. All materials that contacted BoNT/A were disinfected with 10% household bleach before disposal.

Western Blot: LDS was added directly to the BoNT/A-treated cells and heated for 10 min at 70-80°C. Samples were loaded onto a 12% Bis-Tris gel (Invitrogen), and electrophoretically separated in SDS MOPS buffer (Invitrogen) by applying 200 V for 75 min. The gel was transferred onto a Mini Nitrocellulose Transfer Pack by Trans-Blot Turbo Transfer

System (Bio-Rad, Hercules, CA). The blot was stained with mouse monoclonal IgG anti-SNAP25 (Synaptic Systems) and rabbit polyclonal IgG anti-β-actin (Thermo Scientific) primary antibodies. Anti-mouse IRDye800 and anti-rabbit IRDye700 (LiCor, Lincoln, NE) IgG secondary antibodies were used for detection with a LICOR Odyssey two-channel infrared imager (LiCor). An optical densitometry tool from ImageJ (NIH) was used to quantify relative ratio of cleaved to uncleaved SNAP25. The half maximal effective concentration (EC_{50}) for each sigmoidal curve was calculated using GraphPad Prism 5 software (GraphPad, La Jolla, CA).

Statistical Analysis: For all of the EC_{50} comparisons, log transformed one-way analysis of variance (ANOVA) followed by Tukey method were performed using R software version 2.12.1 (* $p < 0.05$; ** $p < 0.01$; *** $p < 0.001$). All error bars represent standard error.

2.3 Results

Macroscale SNAP25 cleavage toxicity assay in 96-well plate: To verify that the NG108-15 cell line used was functional for BoNT/A internalization and SNAP25 cleavage, we first demonstrated that NG108-15 cells expressed both SNAP25 and SV2A by Western blotting (Supplement 1A-B). In contrast, S16 cells were shown not to express either SNAP25 or SV2A, as expected. To determine BoNT/A sensitivity of NG108-15 cells at the macroscale, we cultured NG108-15 cells in 96-well plates, either in monoculture or in coculture with S16 cells, and measured SNAP25 cleavage by Western blotting. BoNT/A was found to cleave SNAP25 in a dose-dependent manner, with an EC_{50} of 12.5 ng/µl (Figure 2A-C). To test our hypothesis that culturing neurons with Schwann cells would increase assay sensitivity by creating a more physiologic NMJ microenvironment, we cocultured ~15,000 NG108-15 cells with either ~3,750 or ~15,000 S16 cells (i.e., 4:1 and 1:1 NG108-15-to-S16 cell ratio). In cocultures, EC_{50}

decreased to 5.1 ng/µl for 4:1 cell ratio, and further decreased to 0.8 ng/µl for 1:1 cell ratio (Figure 2A-C). This represented a 16-fold increase in sensitivity compared to monoculture of NG108-15 cells. Because these cocultures were performed in wells without compartmentalization of cell types, it is possible that soluble factors, physical factors, or a combination of both were responsible for the measured increase in sensitivity. To decouple the effects of chemical and physical signals from S16 cells, serum-free S16 conditioned medium (CM) was mixed with fresh medium (FM) in 1:3 CM-to-FM volume ratio, and used to culture NG108-15 cells alone. In CM experiments, we found that EC_{50} decreased slightly to 8.8 ng/µl (Figure 2A-C), but without statistical significance ($p = 0.622$).

Cell Viability and Characterization in Micro-culture Systems: Similar EC_{50} between monoculture and CM condition suggested that both contact and soluble factors regulate sensitivity of NG108-15 cells. However, it is also possible that the reduced effects of S16-derived CM compared to direct coculture of S16 cells with NG108-15 cells at the macroscale may have been due to (1) high dilution of the soluble factors from S16-derived CM prepared in large T-75 flasks, or (2) potential loss or degradation of soluble factors from freezing and thawing samples and additional liquid handling. To reduce these issues related to CM-based experiments, we used a micro-culture system that compartmentalized the two cell types to eliminate physical contact and allow communication via soluble factors only (Figure 1).

An independent micro-culture system consisted of three separate cell culture microchambers connected by diffusion ports. To prevent cells from migrating across microchambers and contaminating compartmentalized cultures, diffusion ports were positioned ~250 µm above the glass surface where cells adhered (Figure 1C). Proper compartmentalization of NG108-15 and S16 cells was verified by immunofluorescence microscopy.

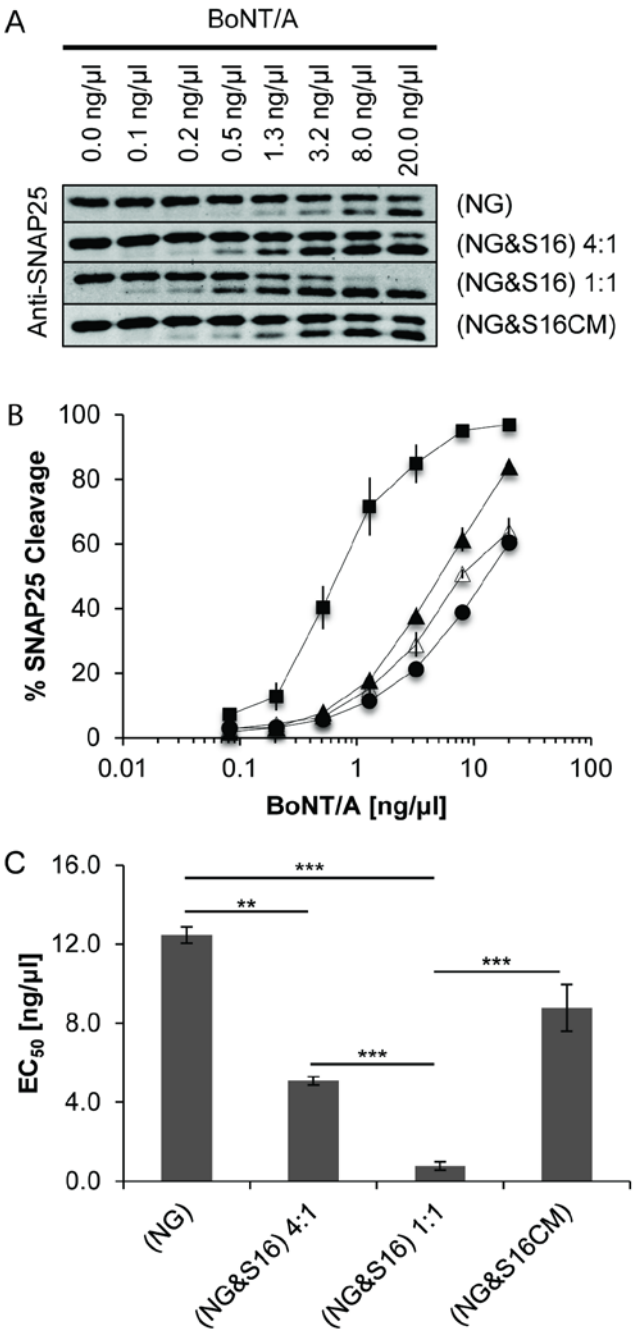

Figure 2: NG108-15 and S16 cell coculture in macroscale 96-well plate.
(A) Western blot of SNAP25 cleavage at different concentrations of BoNT/A. The upper and lower bands indicate uncleaved and cleaved SNAP25 respectively. (B) Dose-response curve of the percentage of cleavage of SNAP25 at different concentrations of BoNT/A. (C) The concentration of BoNT/A required to cleave 50% of SNAP25, denoted as EC_{50}. NG108-15 monoculture ((NG)), closed circle; NG108-15 and S16 coculture at 4:1 cell ratio in the same well ((NG&S16) 4:1), closed triangle; NG108-15 and S16 cocultured at 1:1 cell ratio in the same well ((NG&S16) 1:1), closed square; NG108-15 cultured in S16 conditioned medium ((NG&S16CM)), open triangle. *P*-values (* $p < 0.05$; ** $p < 0.01$; *** $p < 0.001$) of the three independently repeated experiments ($n = 3$).

S16 cells showed S100, which is highly expressed in glial cells (Figure 3E), but did not express SNAP25 (Figure 3F, Supplementary Figure 1A). In contrast, NG108-15 cells expressed both S100 and SNAP25 because of their hybrid neuroblastoma/glioma phenotype (Figure 3B-C). Images also showed that cells remained in their respective microchambers after two days of culture (Figure 3A-I). In addition, both NG108-15 and S16 cells demonstrated high viability in the micro-culture systems (Figure 4A-F).

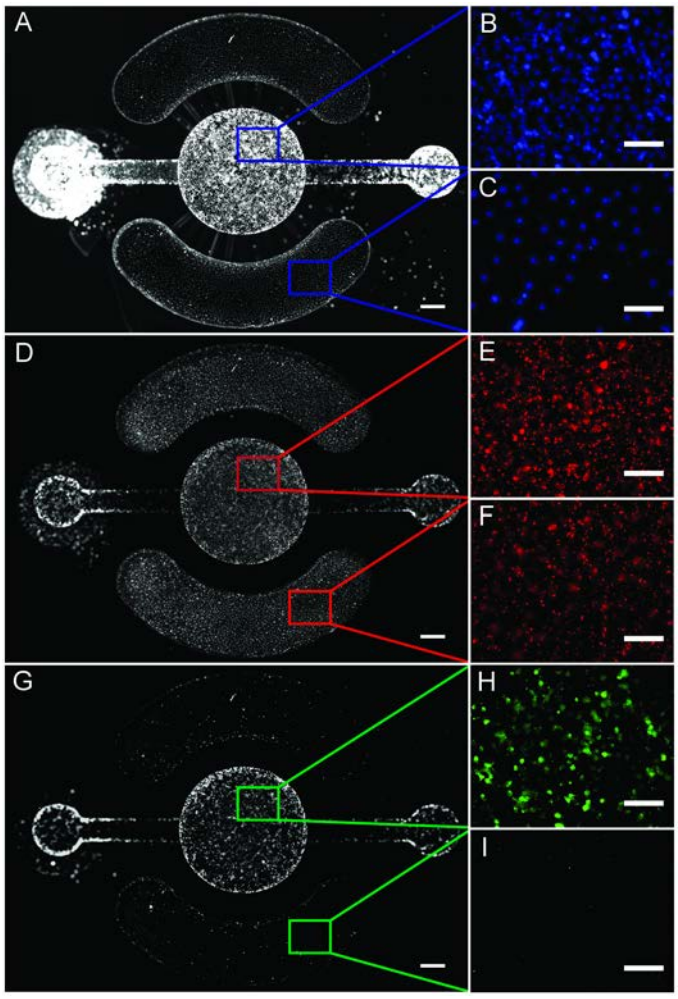

Figure 3: Separation of NG108-15 and S16 cells in the microchambers. Immunofluorescence images of the micro-culture system stained with (A) DAPI, (D) S100, and (G) SNAP25; scale bar represents 500 μm. Higher resolution fluorescent microscope images of the middle and side microchambers seeded with NG1080-15 and S16 cells, respectively. All of the microchambers were stained with (B-C) DAPI, (E-F) S100, and (H-I) SNAP25; scale bar represents 200 μm. The experiments were done in triplicates.

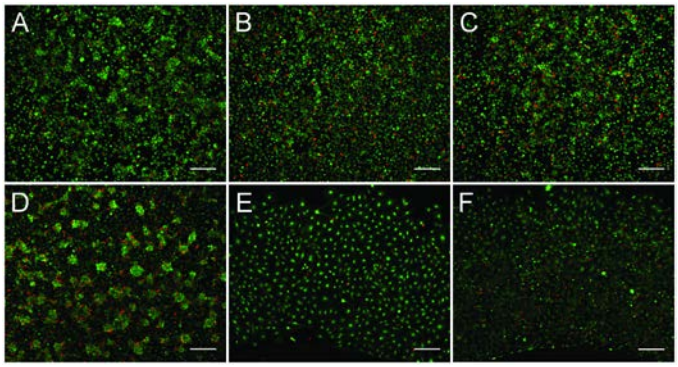

Figure 4: Cytotoxicity assay of the cells in the microchambers.
NG108-15 and S16 cells were stained with Calcein AM (green) and ethidium homodimer-1 (red) showing live and dead cells respectively. (A-C) NG108-15 cells in μ(NG), μ(NG)(S16) 4:1, and μ(NG)(S16) 1:1, respectively. (D) Both NG108-15 and S16 in μ(NG&S16) 1:1. (E-F) S16 cells in μ(NG)(S16) 4:1 and μ(NG)(S16) 1:1. Representative images of three replicates; scale bars represent 200 μm.

Microscale SNAP25 cleavage toxicity assay in microfluidic device: To test the hypothesis that soluble factor signaling in microscale environments can improve assay sensitivity, we compared monoculture of NG108-15 cells alone at the macroscale with monoculture of NG108-15 cells alone in microchambers, and found that EC_{50} at the microscale decreased significantly to 2.6 ng/μl compared to macroscale culture in 96-well plates (Figure 6A). Compartmentalized microscale coculture at 4:1 cell ratio showed no significant difference in EC_{50} compared to monoculture (2.2 ng/μl, p = 0.977; Figure 5A-C). However, microscale coculture at 1:1 cell ratio, in both separate microchambers (μ(NG)(S16)) and in the same middle microchamber (μ(NG&S16)), further decreased EC_{50} to 1.2 ng/μl and 1.1 ng/μl, respectively (Figure 5C). Surprisingly, EC_{50} of microscale versus macroscale coculture conditions did not show statistical difference (p = 0.692; Figure 6B), whereas EC_{50} of microscale versus macroscale monoculture conditions did show statistical difference (Figure 6A). The results for EC_{50} under various conditions are summarized in Table 1.

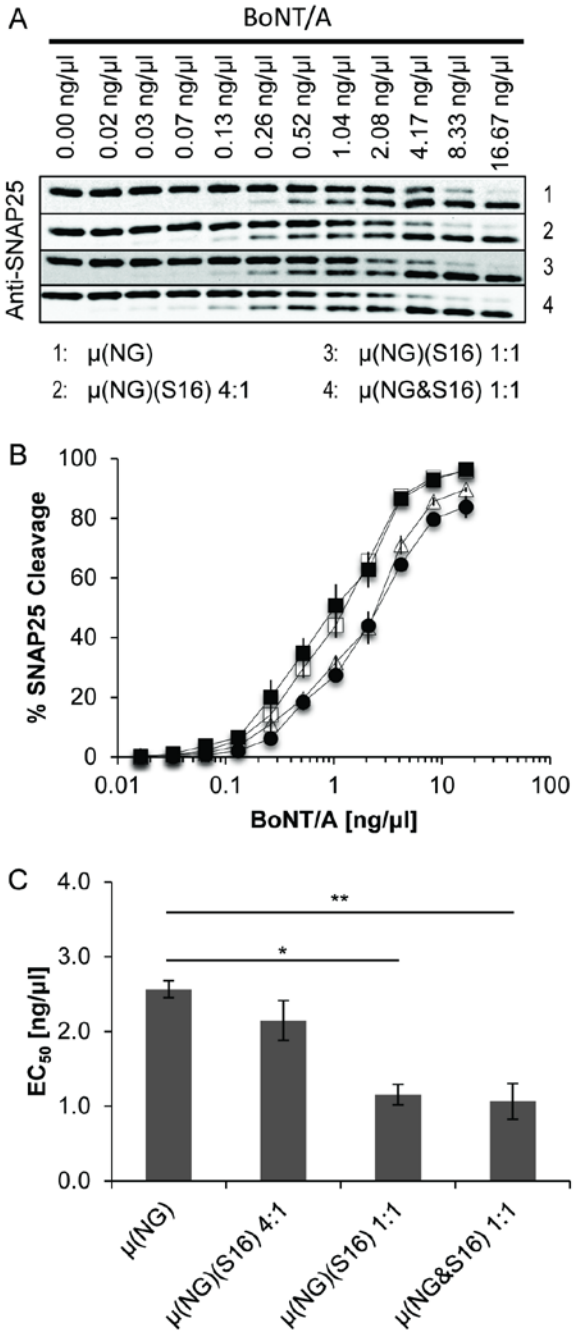

Figure 5: NG108-15 and S15 cell coculture in the microchambers.
(A) Western blot of SNAP25 cleavage at different concentrations of BoNT/A. The upper and lower bands indicate uncleaved and cleaved SNAP25 respectively. (B) Dose-response curve of the percentage of cleavage of SNAP25 at different concentrations of BoNT/A. (C) The concentration of BoNT/A required to cleave 50% of SNAP25, denoted as EC_{50}. NG108-15 monoculture (µ(NG)), closed circle; NG108-15 and S16 coculture at 4:1 cell ratio in the separated wells (µ(NG)(S16) 4:1), open triangle; NG108-15 and S16 cocultured at 1:1 cell ratio in the separated well (µ(NG)(S16) 1:1), open square; NG108-15 cultured in S16 cultured in the same well ((NG&S16) 1:1), closed triangle. *P*-values (* $p < 0.05$; ** $p < 0.01$) of the three independently repeated experiments (n = 3).

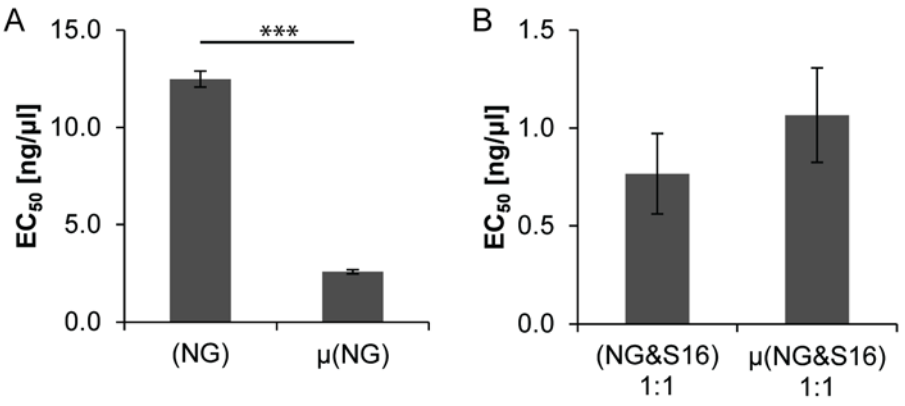

Figure 6: Differences in the sensitivity at different scales.
(A) EC_{50} of NG108-15 monoculture in 96-well plate and in micro-culture system (*** $p < 0.001$). (B) EC_{50} of NG108-15 and S16 coculture in 96-well plate and in micro-culture system where the two cell types were cultured in physical contacts.

2.4 Discussion

There is an important need to develop assays that can detect and quantify BoNT in a sensitive and robust manner. Existing assays either suffer from high variability and poor reproducibility such as *in vivo* mouse bioassays, or have poor physiological relevance such as *in vitro* cell-free assays [63]. On the other hand, cell lines are physiologically relevant and their inherently low sensitivity can be increased by promoting differentiation [51, 52]. In this report, we described a microscale cell culture system that was developed to improve both sensitivity and physiologic relevance simultaneously. This was achieved by making two important, distinct advances to traditional cell-based assays: (1) using coculture of neurons with Schwann cells instead of monoculture of neurons alone, and (2) using microscale instead of macroscale culture environments to reduce soluble factor diffusion and control spatial organization. Results from these two advances, alone and in concert, are summarized in Table 1.

We chose to develop an assay that relied on cell lines, including the NG108-15 neuronal cell line and the S16 Schwann cell line, as opposed to fastidious primary or stem cells. Unlike primary and stem cells that require extracting tissue from animals or necessitate prolonged cell culture and differentiation steps, cell lines are readily available, easily cultured and maintained, and more robust in terms of run-to-run variability. NG108-15 cell line was previously shown to form cholinergic synapses with myotubes [17, 18], and differentiate with elevated levels of endogenous cyclic adenosine monophosphate (cAMP) and other soluble factors such as retinoic acid and purmorphamine [52, 64, 65]. S16 is a well characterized and commercially available Schwann cell line with phenotype most similar to primary cells [66]. The main drawback of employing cell lines was the lack of sensitivity prior to differentiation and non-functional synapses. Thus, our primary objective was to choose a cell line that forms active synapses and provide culture conditions that would improve sensitivity.

Table 1: Relative EC_{50} and fold increase in sensitivity.
Measured EC_{50} values are normalized to NG108-15 monoculture in 96-well plate, and the inverse of the normalized EC_{50} was taken to calculate relative fold increase in sensitivity (in parenthesis). Microscale culture conditions where NG108-15 and S16 were cultured in separate microchambers were used for the calculation.

Culture Condition \ Scale	Macroscale	Microscale
NG108-15 alone	1.0 (-)	0.21 (4.9 x)***
NG108-15 & S16 (4:1)	0.41 (2.5 x)**	0.17 (5.8 x)***
NG108-15 & S16 (1:1)	0.06 (16 x)***	0.09 (11 x)***

(* $p < 0.05$; ** $p < 0.01$; *** $p < 0.001$)

First, we compared conventional monoculture of neurons and the coculture of neurons and Schwann cells in macroscale 96-well plates, and found that cocultured cells were

significantly more sensitive to BoNT/A treatment than monocultured cells. This effect was enhanced with increasing density of cocultured Schwann cells, up to 16-fold more sensitive than original monoculture. The sensitivity increase was likely aided by Schwann cells' synaptogenic potential and modulation of synaptic activities, as previous reports demonstrated that Schwann cell-derived CM was enough to increase number of synapses of rat spinal motor neurons [27] and increase synaptic activities at the developing NMJs [28]. Interestingly, when conditioned medium was collected from S16 cells and applied to monocultured NG108-15 cells, the sensitivity was not significantly different than monoculture. This suggested that the soluble factor signals in the conditioned medium were either (1) acting in concert with physical signals when both cell types were cultured in the same compartment, or (2) inactivated or mitigated in its effectiveness because of handling or an overly high dilution factor. Concentration of S16-derived soluble factors in coculture at 4:1 cell ratio was roughly 90-fold higher than CM culture (i.e., ~3 nl/cell in coculture compared to ~ 270 nl/cell in CM culture, see Methods). Based on previous evidence that soluble factors from Schwann cells were enough to induce synaptogenesis and synaptic activity, highly diluted CM likely caused the reduced effect of S16 soluble factors.

To accentuate the effect of soluble factors by reducing diffusion distances, we designed a microscale coculture system that allows improved soluble factor sensitivity by compartmentalization and by eliminating the need for conditioned medium experiments. Using the microscale NG108-15 monoculture, we observed a significant 5-fold increase in sensitivity compared to macroscale NG108-15 monoculture. This increased sensitivity is due to reduced culture volume in microscale culture for a single cell type, suggesting that accentuated autocrine effects may be responsible. Interestingly, the effect of coculture on assay sensitivity at the microscale (from EC_{50} of 2.6 to 1.2 ng/μL) was much less significant compared to the effect of

coculture on sensitivity at the macroscale (from EC_{50} of 12.5 to 0.8 ng/μL). We had hypothesized that the combination of coculture and the microscale may synergistically increase the sensitivity compared to that of either macroscale coculture or microscale monoculture alone. However, this synergistic effect did not materialize as the largest fold increase in sensitivity was achieved by macroscale coculture. Decreasing the culture scale form macro to micro showed more improvement in sensitivity than coculturing at microscale. This rather surprising result may be due to: (1) the existence of a coculture "detection limit", or (2) absorption of S16-derived soluble factors into the surrounding PDMS material.

While it is possible that the effects of coculture may reach a limit due to saturation of surface receptors that associate with S16-secreted soluble factors, this is unlikely because glial cells outnumber neurons in vertebrate nervous system, and furthermore, the sensitivity gain at 4:1 cell ratio at the microscale was insignificant (Figure 5C). A more likely cause for the diminished effect would be the absorption of S16-secreted soluble factors that mediate cell-cell communication and impact assay sensitivity. The microfluidic device was fabricated from PDMS, which is known to absorb hydrophobic molecules and abrogate associated cellular responses [62]. The influence of small hydrophobic molecule absorption is further aggravated at microscale due to the increased surface-to-volume ratio. It is known that transforming growth factor-β1 (TGFβ-1) associates with TGF-β binding proteins through hydrophobic interactions [67], and TGFβ-1 is one of the secreted factors from Schwann cells that modulates synaptic activity at the developing NMJ [29]. Therefore, it is plausible that some of S16-secreted soluble factors were absorbed in PDMS along with TGFβ-1, thereby diminishing the coculture effect at the microscale. Fabricating devices from a more bio-inert material such as polystyrene or other

polymers [68] so that we can confirm our hypothesis may be included in future studies to validate our platform for application of BoNT cell-based assay.

In summary, we demonstrated proof-of-concept that a neuronal cell line can be sensitized by coculturing with Schwann cells and by culturing at the microscale. Further improvements could allow the assay to match or surpass the sensitivity of *in vivo* and primary or stem cell derived neuron cell-based methods. For example, one potentially viable option may be to use coculture in combination with supplementing cell culture medium with gangliosides, factors that increase endogenous cAMP and differentiating the cell lines [50, 52, 64]. Furthermore, alternative end-point readouts may be considered for cell-based assays to eliminate the use of Western blots that are time consuming to perform. Continuous improvement in FRET sensor technology [69] may alleviate a major bottleneck in adopting cell-based assays. Together with our microscale coculture platform and emerging sensor technologies, robust and sensitive cell-based BoNT detection assays have potential to replace *in vivo* assays in the future.

2.5 Supplementary Data

Two cell lines used for the experiments were evaluated for expression of the proteins required for BoNT detection using Western blot. NG108-15 cells expressed both SNAP25 (Synaptic Systems) and β tubulin III (Sigma) confirming neuronal lineage whereas S16 cells were negative of both SNAP25 and β tubulin III (Supplementary Figure 1). In addition, NG108-15 expressed SV2A (Synaptic Systems), one of the known BoNT co-receptors; however, S16 did not (Supplementary Figure 2).

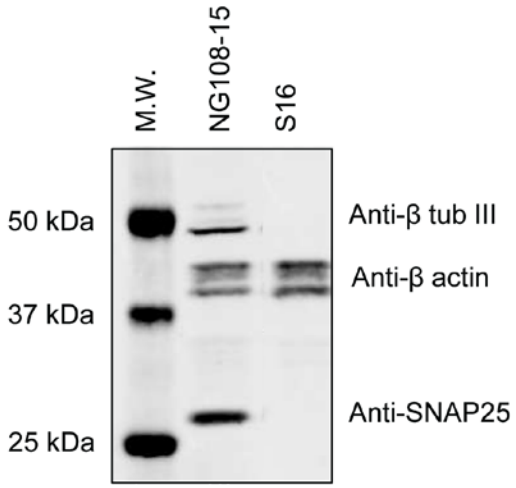

Supplementary Figure 1: Western blot of β actin, β tubulin III, and SNAP25 of the two cell lines.
NG108-15 cells expressed β tubulin III and SNAP25 whereas S16 cells did not.

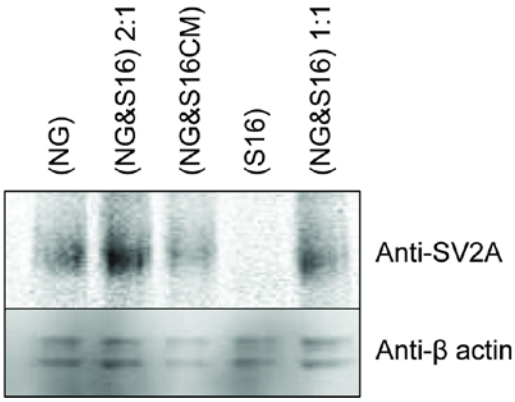

Supplementary Figure 2: BoNT/A surface receptor expression.
NG108-15 cells expressed SV2A protein, a surface receptor for BoNT/A. However, S16 did not express SV2A.

2.6 Acknowledgements

We would like to thank Xiyu Wang, an undergraduate student for making the microfluidic devices and Thomas Havighurst for assisting statistical analysis. We would like to also acknowledge Sabine Pellett and Regina Whitemarsh in Eric Johnson's Lab for productive and helpful discussions. This work was supported by the National Center for Food Protection and Defense [2010-ST-061-FD0001]. DHS Science and Technology Assistance Agreement No. 2007-ST-061-000003 awarded by the U.S. Department of Homeland Security. It has not been formally reviewed by DHS. The views and conclusions contained in this document are those of the authors and should not be interpreted as necessarily representing the official policies, either expressed or implied, of the U.S. Department of Homeland Security. The Department of Homeland Security does not endorse any products or commercial services mentioned in this publication.

Chapter 3 – Development of a Highly Sensitive Cell-Based Assay for Detecting Botulinum Neurotoxin Type A through Neural Culture Media Optimization.

3.1 Introduction

Botulinum neurotoxin (BoNT) is the most potent naturally produced toxin with lethal doses ranging 1.3-13 ng/kg body weight depending on the exposure method. Produced by *Clostridium botulinum*, there are seven disclosed BoNT serotypes (A – G) [3] and undisclosed serotype H of which the sequence is held due to security reasons [2]. Despite the bioterrorism potential of BoNTs, the potency and specific biological mechanisms have found a role in medicine. Among the seven disclosed serotypes, BoNT/A was found to be applicable in treating neuromuscular dystonia. Due to the extreme potency of BoNT/A, accurate quantification of the toxin is required to avoid serious side-effects including muscle numbness, difficulty breathing, and even death [4]. Therefore, highly sensitive BoNTs detection assays capable of infield testing at various food supply chain and distribution sites to product against bioterrorism, and physiologic assays that can reliably quantify BoNT/A toxicity for medical use are highly desired.

Previously, we have developed *in vitro* assays which leverage a microfluidic device to enable a highly sensitive *in vitro* assay measures DNA content of *Clostridium botulinum* [9] and the catalytic activity of the toxin (i.e. proteolysis activity of LC) in food matrices such as milk and orange juice [8], while other laboratories reported an ELISA-based detection system [44]. Although these *in vitro* biochemical assays are suitable for infield testing against biological threats and were also shown to be highly sensitive, they do not recapitulate physiological mechanisms.

The physiologic mechanism of action of BoNTs is well studied and their structure plays important role in imposing neurotoxicity. BoNT/A, as well as the other serotypes, weighs approximately 150 kDa, including a 50 kDa heavy-chain receptor binding domain (HCR), a 50 kDa heavy-chain translocational domain (H_N), and a 50 kDa light-chain catalytic domain (LC). Although the HCR and H_N are covalently linked, non-covalent disulfide bonds link the LC to the heavy-chain domains. To impose toxicity, HCR of BoNT/A associates synaptic vesicle 2 (SV2) and ganglioside GT1b to enter cholinergic neurons upon synaptic activities [70]. The endocytosed toxins are then exposed to low endosomal pH leading to a conformational change that liberates the LC in the cytosol. The LC then cleaves SNAP25, a component of soluble *N*-ethylmaleimide sensitive fusion attachment protein receptor complex (SNARE), blocking neurotransmitter release and leading to the flaccid paralysis associated with botulism [1, 12]. To develop a physiologically relevant assay, these each of these intoxication steps must be taken into consideration. As the functionality and therefore lethality of BoNT cannot be determined by simple ligand-receptor binding (functionality of the LC), ensuring the proper function of the other domains (HCR, H_N) is required for accurate and reliable detection of BoNT.

Mouse lethality assay (MLA) is the most physiologic relevant form of the BoNT/A assay and has been considered the gold standard for detecting and determining specific toxicity of BoNTs. In MLA, varying concentrations of BoNTs are injected into mice and the minimum concentration required to kill the half of the mice is denoted as 1 LD_{50} U [63]. Currently, the MLA has set the benchmark for detection sensitivity achieving a sensitivity of 7 – 15 pg/mL (equivalent to 0.05 – 0.1 pM or 1 – 2 LD_{50} U) [63]. Although this method has proven to be effective, it requires special animal facilities, highly skilled technicians, and animal sacrifice in

addition to large errors ranging from 30 to 60% [10] thus developing *in vitro* assays is highly desirable (reviewed Singh *et al.* [71]).

The most cell-based assays involve several steps including the culture of neuronal cells, treating the cells with BoNT/A, and directly lysing the cells to measure the amount of SNAP25 cleaved using Western blot. In order for BoNT/A to enter the cells and cleave their substrates, the heavy-chain domains and LC must be intact, H_N must present LC towards cytoplasm with a conformational change occurring at endosomal pH, and finally the LC must escape out of the endosome reducing the disulfide bonds linked to the heavy-chains [1]. Therefore, the cell-based assay systems are still able to accurately recapitulate the physiologic intoxication mechanisms of BoNT ensuring the full functionality and toxicity of BoNT is detected, minimizing false readouts.

Initially, *ex vivo* primary spinal cord neurons demonstrated great potential, showing comparable sensitive to the MLA [10]. Stem cell derived neuron-based assays were also shown to be just as sensitive [47, 48, 72]. However, the laborious process of obtaining primary neurons still requires animal sacrifice while differentiating stem cells takes several weeks with varying quality of the differentiated cells [14]. Despite the readily available continuous neuronal cell lines that are able to mitigate these major drawbacks of primary and stem cell derived neurons, they have exhibited far inferior sensitivity to BoNTs.

In the developing of a BoNT detection assay with continuous neuronal cell lines, recent studies developed methods to improve detection sensitivities of the neuronal cell lines. The human neuroblastoma cell line, SiMA, exhibited EC_{50} (amount of BoNT/A required to cleave 50% of SNAP25) of ~6.5 pM [51]. Although SiMA showed high sensitivity, the cell line is not well characterized and does not have motor neuron-like characteristics. As BoNTs enter neurons at the neuromuscular junction, which is formed by synaptic terminal of motor neurons and skeletal

muscle fibers. Thus scouting and using cell lines with motor neuron-like characteristics will offer the most representative physiologic response. NG108-15 is a cholinergic neuronal cell line, which was shown to form functional synapsis with skeletal muscle fibers [17, 18] and extend neurites when cultured with Schwann cells differentiated from adipose-derived stem cells [21] indicating motor neuron-like characteristics. However, NG108-15 cells suffer from low BoNT/A detection sensitivity in their native state. Previously, we observed enhanced BoNT/A detection sensitivity when cocultured with Schwann cells, which demonstrated potential for sensitizing and further strengthening motor-neuron characteristics of the NG108-15 cell line [73]. Additionally, Whitemarsh *et al.* showed culturing NG108-15 cell line in a neural differentiation medium increased the BoNT/A detection sensitivity to EC_{50} of ~11.5 U (equivalent to ~12.3 pM) upon addition of GT1b a day prior to treating cells with BoNT/A but effects of the different components were not thoroughly investigated [52]. Despite these advances, further interrogation of NG108-15 cells and their culture conditions could provide the advanced sensitivity to allow their use in an *in vitro* cell based BoNTs detection assay.

In this study, we focused our efforts on optimizing neural culture media to further assess the effects of different media components by improving neural cell culture conditions with the continual neuron cell line NG108-15. We screened and looked at the combinatorial effect of three commercially available neural supplements. Additionally, varying concentrations of retinoic acid (RA), purmorphamine (Pur), TGFβ1 and GT1b were tested for their impact. Through our optimization study, we developed a highly sensitive cell-based assay that can detect BoNT/A without introducing media additives throughout the culture, and achieved higher sensitivity than the previous report that used NG108-15.

3.2 Materials and Methods

Cell Culture: NG108-15 cells were purchased from ATCC (Manassas, VA) and were maintained as suggested by the supplier. Briefly, DMEM (Invitrogen, Carlsbad, CA) basal medium that was supplemented with hypoxanthine, aminopterin, and thymidine (HAT supplement; Sigma, St. Louis, MO), 10% fetal bovine serum (FBS), and 1% penicillin-streptomycin (P/S; Gibco) was used to expand and maintain the cell line. To initiate BoNT/A detection assay, NG108-15 cells were plated at ~15,000 cells/well in 96-well plate coated with 1:100 diluted growth factor reduced Matrigel (BD Biosciences, San Jose, CA). The cells were seeded in full growth medium and incubated at 37 ˚C with 5% CO_2 overnight. On the following day, the complete growth medium was replaced with neural differentiation media. The neural differentiation media contained varying combinations of neural supplements B27, N2 (Invitrogen), and GS21 (GlobalStem, Rockville, MD) in Neurobasal medium containing GlutaMAX (Invitrogen) and P/S. The neural differentiation media was then further supplemented with varying concentrations of retinoic acid (Sigma), purmorphamine (Cayman Chemical, Ann Arbor, MI), GT1b (Matreya, Pleasant Gap, PA), and transforming growth factor β1 (TGFβ1; PeproTech, Rocky Hill, NJ). The neural differentiation media was replaced every other day for 6 days. On day 7, varying concentration of BoNT/A (8 pg/U specific toxicity, Johnson Laboratory, University of Wisconsin in Madison, WI) was diluted in 50 µl of the respective differentiation media, and incubated for an additional two days. Cells were then directly lysed using LDS buffer (Invitrogen) mixed with a protease inhibitor cocktail (Thermo Scientific, Rockford, IL) before being collected for Western blot analysis.

Western Blot: Gel electrophoresis was performed using Novex NuPAGE 12% Bis-Tris gel in SDS MOPS running buffer (Invitrogen) at 200 V for 1 hr. The gel was then transferred

onto a nitrocellulose membrane using Trans-Blot Turbo Transfer System (Bio-Rad, Hercules, CA), blocked and stained with primary and subsequently with secondary antibodies. Mouse anti-SNAP25 at 1:4,000 dilution (Synaptic Systems, Gottingen, Germany), and mouse anti-β-actin at 1:10,000 dilution (Sigma) were used for the primary antibodies. Anti-mouse IR800 (Li-Cor) at 1:10,000 dilution was used as the secondary antibody. Odyssey Infrared Imager (Li-Cor) was used to scan blots and the relative amount of SNAP25 cleavage was quantified using ImageJ (National Institute of Health, Bethesda, MD).

Statistical Analysis: Prism GraphPad 6.0 (La Jolla, CA) was used to fit dose-response curves, computing EC_{50} of SNAP25 cleavage, and for all statistical analysis. Error bars on all dose-response curves and EC_{50} bar graphs indicate standard errors. All experiments were repeated at least three times.

Safety Considerations: BoNT/A is highly toxic and must be handled carefully in a biosafety hood. All materials and supplies that were in contact with BoNT/A were disinfected using 10% bleach for a minimum of 10 minutes before being discarded in biohazard waste containers.

3.3 Results and Discussion

Neural Culture Media Supplements: We began our media optimization studies by confirming the previously reported EC_{50} ~60 U (measured by amount of BoNT/A required to cleave 50% of SNAP25) upon differentiating NG108-15 in neural differentiation medium supplemented with B27 [52]. After differentiating NG108-15 cells for 6 days followed by 2 days of BoNT/A treatment, we obtained similar EC_{50} at 67.2 U in B27 supplemented Neurobasal media (Figure 7A-B). Additionally, we tested two more neural supplements, N2 and GS21, to

generate baselines on the effects of the three neural supplements on BoNT/A detection sensitivity in NG108-15. Interestingly, culturing NG108-15 in GS21 neural supplement significantly reduced the EC_{50} to 27.4 U, whereas the cells in N2 neural supplemented media increased the EC_{50} to 99.5 U, although it failed to show statistical significance against B27 (Figure 7A-B). This experiment showed that the neural supplement alone significantly affects BoNT/A detection sensitivity as GS21 appeared superior to the other tested supplements in facilitating BoNT/A detection.

B27 is the most widely used neural culture supplement. However, its formulation is kept proprietary and the lot-to-lot variability has been a concern [74]. In the efforts to reduce the lot-to-lot variability and fully-define the elements required to culture neural cells, Chen *et al*. developed a new neural supplement (NS21) that contains 21 components (GS21 is commercially available analogue of NS21) and disclosed its full formulation. NS21 was shown to be a superior alternative to B27 in hippocampal neuron culture that reduced degeneration of soma and axons that were seen in B27 supplemented media [75]. Also evident in our results, GS21 provided a different environment for neuronal cell culture, and culturing NG108-15 in GS21 supplemented medium significantly improved the condition for BoNT/A detection. The increased sensitivity with GS21 neural supplement was encouraging, and we moved forward to media optimization.

Concentrated Neural Supplements in Combination with RA and Pur: N2 neural supplement contains five components that can be used minimally for culturing neuronal cells compared to the B27 and GS21 we tested. Although these neural supplements are pre-formulated to the recommended final overall concentration at 1x, using them at higher concentrations and in combination were not thoroughly investigated. We hypothesized that the

quantity of specific components in each neural supplement may be limiting; thus increasing the concentrations or using them in combination may enhance the neural cell culture condition and increase BoNT/A detection sensitivity.

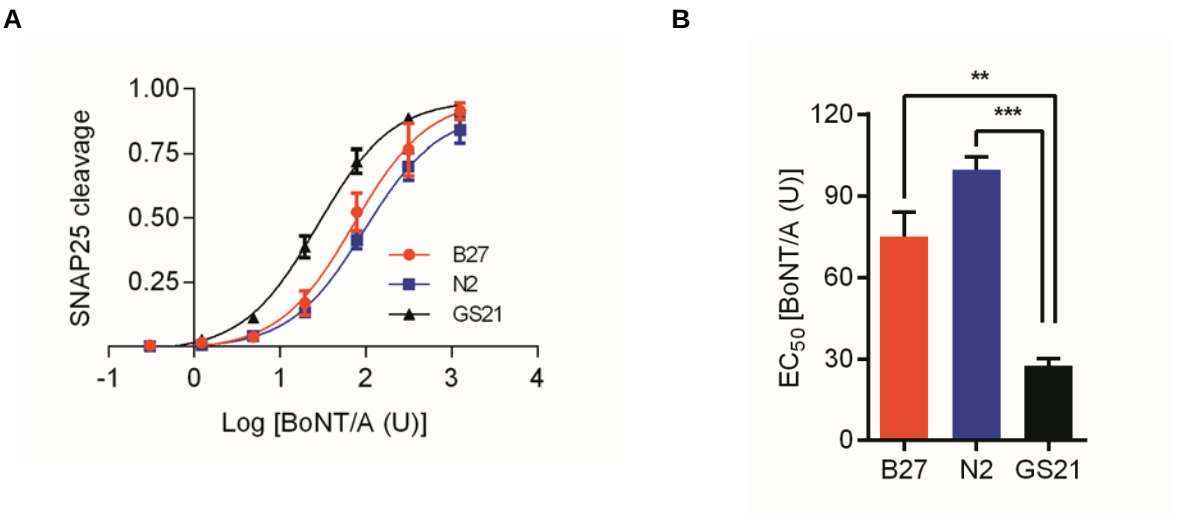

Figure 7: SNAP25 cleavage in different neural supplements.
(A) Dose-response curve of SNAP25 cleavage in NG108-15 cells cultured in Neurobasal medium supplemented with B27, N2, or GS21. (B) The dose-response curves were analyzed to calculate amount of BoNT/A required to cleave 50% of SNAP25, denoted EC_{50} and plotted. One-way ANOVA followed by Tukey's multiple comparison test was used for statistical analysis (** $p < 0.005$ and *** $p < 0.001$).

To begin with, we designed a 5-factor 4-level Taguchi design-of-experiment (Supplementary Table S1) that takes account for varying concentrations of neural supplements in combination with RA and Pur. RA and Pur were tested because they were shown to increase BoNT/A detection sensitivity [52] and required in differentiating human pluripotent stem cell derived neural progenitor cells towards motor neuron lineage [13]. The measured EC_{50} was the lowest at 2x B27, 3x N2, and 4x GS21 in combination with 2.5 μM Pur, followed by 2x B27, 4x N2, and 3x GS21 (Supplementary Figure 3A). Next, we analyzed the main-effect of means and

signal-to-noise ratios to identify suggested optimal concentrations of the five factors that were tested. The analysis indicated that adding 2x B27, 4x N2, and 3x GS21 with 2.5 to 10 μM of RA and 2.5 or 10 μM of Pur is the most probable optimized culture condition (Supplementary Figure 3B-C).

Table 2: Tested experimental conditions at elevated concentrations of neural supplements.

Study Condition Number	Study Condition Code	B27	N2	GS21	Retinoic acid (μM)	Purmorphamine (μM)	EC_{50} (U)
1	(1,0,0,0,0)	1	0	0	0	0	90.9
2	(0,1,0,0,0)	0	1	0	0	0	99.5
3	(0,0,1,0,0)	0	0	1	0	0	27.1
4	(2,3,4,0,0)	2	3	4	0	0	24.1
5	(2,3,4,0,1)	2	3	4	0	2.5	21.4
6	(2,3,4,0,2)	2	3	4	0	5.0	18.5
7	(2,3,4,0,3)	2	3	4	0	7.5	17.9
8	(2,3,4,0,4)	2	3	4	0	10.0	15.2
9	(2,3,4,1,3)	2	3	4	2.5	7.5	14.0
10	(2,3,4,2,3)	2	3	4	5.0	7.5	15.1
11	(2,3,4,3,3)	2	3	4	7.5	7.5	16.0
12	(2,3,4,4,3)	2	3	4	10.0	7.5	22.1
13	(2,4,3,0,0)	2	4	3	0	0	21.4
14	(2,4,3,0,1)	2	4	3	0	2.5	20.6
15	(2,4,3,0,2)	2	4	3	0	5.0	19.0
16	(2,4,3,0,3)	2	4	3	0	7.5	16.8
17	(2,4,3,0,4)	2	4	3	0	10.0	12.8
18	(2,4,3,1,3)	2	4	3	2.5	7.5	12.3
19	(2,4,3,2,3)	2	4	3	5.0	7.5	15.8
20	(2,4,3,3,3)	2	4	3	7.5	7.5	14.7
21	(2,4,3,4,3)	2	4	3	10.0	7.5	13.5

After analyzing Taguchi's design-of-experiment, we narrowed the study parameters for further investigation. The concentrations of the neural supplements were fixed based on the EC_{50} in Supplementary Figure 3A and main-effect and signal-to-noise plots in Supplementary

Figure 3B-C to either 2x, 3x, and 4x or 2x, 4x, and 3x concentration of B27, N2, and GS21 respectively. Tested concentrations of RA and Pur ranged from 2.5 to 10 μM. As baselines, 1x concentration of each neural supplement and all three combined at 1x each were also tested (Table 2). Surprisingly, only the presence and absence of GS21 in media showed statistical significance. The results also suggested that the differences in the EC_{50} that we obtained from Taguchi study were mainly due to the addition of RA and Pur, rather than the concentrations of neural supplements. It appeared that higher concentrations of neural supplements in the culture media did not significantly contribute to BoNT/A detection sensitivity (Figure 8). It is also interesting to note that the EC_{50} diverged with the increased amount of RA in different combinations of neural supplements (Study Conditions 9-12 vs. 18-21 in Table 2). When computed using Student's two-tailed t-test, the conditions containing different combinations of neural supplements but the same amount of RA and Pur (Study Conditions 12 and 21 in Table 2) showed significant difference in the EC_{50} (Figure 8), confirming that the all parameters that we so far tested have non-linear relationship.

Combination of Neural Supplements: The previous set of experiments showed that that the components in at least GS21 are not limiting. Additionally, it was surprising that GS21 was the only significant contributor to decreasing the EC_{50} in BoNT/A detection sensitivity (Figure 8). To further determine the optimized media condition for culturing neurons to increase BoNT/A detection sensitivity, we lowered the concentrations of neural supplements to 1x and tested the following conditions: (1) GS21 alone, (2) GS21 and N2, and (3) GS21, N2, and B27. In this study, we saw significant decrease in the EC_{50} only when GS21 was combined with N2, which also indicated that components in these two neural supplements acted synergistically in the detection sensitivity. Although adding B27 to GS21 and N2 combined media also lowered the

EC_{50}, it failed to show statistical significance thus suggested a possible negative effect (Figure 9A-B).

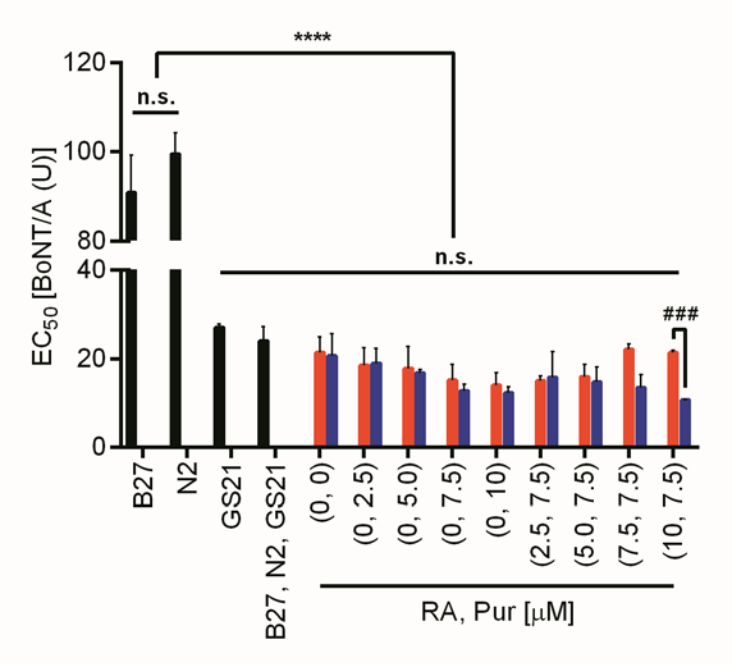

Figure 8: Effect of RA and Pur in concentrated neural supplement media.
EC_{50} of SNAP25 cleavage was plotted in NG108-15 cells cultured in Neurobasal media supplemented with 1x concentrations of B27, N2, GS21, or all three supplements were added at 1x concentrations each B27&N2&GS21 combined (black). Significant decrease in the EC_{50} was observed in media containing GS21 and all three supplements compared to media with B27 or N2 alone. Increased concentration of the neural supplements at 2x B27, 3x N2, and 4x GS21 (red) and 2x B27, 4x N2, and 3x GS21 (blue) were tested with varying concentrations of RA and Pur. No significance was observed compared to GS21 alone or combined B27, N2, and GS21 at 1x concentration each. One-way ANOVA followed by Tukey's multiple comparison test was used for statistical analysis (**** $p < 0.0001$). Student's t-test used to compare statistical difference between the conditions containing different neural supplements but with same amount of RA and Pur ($^{###}$ $p < 0.001$).

Combinatorial Effect of Neural Supplements, RA, and Pur: Finally, we deduced the desired amount and combination of neural supplements. Yet, the concentrations of RA and Pur required to achieve the optimal medium for the highest sensitivity were not evaluated. In this set

of experiments, we decided to fix the concentration of Pur at 7.5 μM instead of testing all combinations of RA and Pur. The concentration of Pur was determined by the observation where we saw diverging trend of the EC_{50} with addition of RA (Figure 8). Additionally, we tested 2.5 and 10 μM RA (the lowest and the highest concentration we tested throughout this report) to test whether RA work with or against the neural supplements and Pur. Although GS21 combined with N2 showed the lowest EC_{50}, we evaluated all three combinations of neural supplements that we tested in Figure 9 in case of non-linear combinatorial effects of RA and Pur.

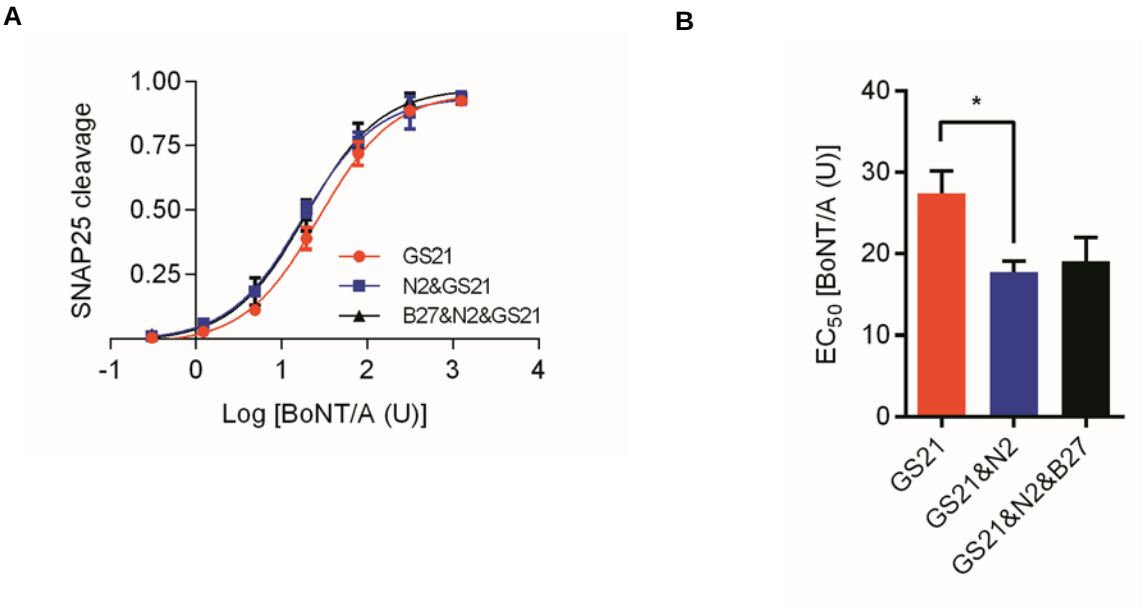

Figure 9: Effect of GS21 in combination with N2 and B27 neural supplements.
(A) Dose-response curve of SNAP25 cleavage in different combinations of neural supplement each at 1x concentration. (B) Analyzed EC_{50} of the three tested conditions showed significant decrease in the EC_{50} when GS21 was supplemented with N2. One-way ANOVA followed by Tukey's multiple comparison test was used for statistical analysis (* $p < 0.05$).

In conditions that only contained neural supplement GS21 (Group 1), the lowest EC_{50} was achieved when 2.5 μM RA and 7.5 μM Pur was added. Increasing the concentration of RA

from 2.5 to 10 μM did not show significant change in the EC_{50} (Figure 10A and D). In media supplemented with GS21 and N2 (Group 2), we did not see any statistical difference when RA and Pur were introduced. However in contrast to Group 1, increasing RA from 2.5 to 10 μM significantly increased EC_{50} (Figure 10B and D). Lastly, significant decrease in the EC_{50} was observed with the addition of 2.5 μM RA in the group that contained all three neural supplements (Group 3) and it was the most BoNT/A sensitive condition of all (Figure 10C and D).

From the results of Figure 9, we expected the most sensitive condition to only contain GS21 and N2 neural supplements in addition to RA and Pur. To our surprise, we saw the most gain in the sensitivity was in the media that contained all three neural supplements. When we performed group t-test of the means, Group 1 to 3 and Group 2 to 3 were statistically significant (Figure 10D). This set of experiment again indicated a non-linear combinatorial effect of the components contributing to increased BoNT/A detection sensitivity.

Effect of TGFβ1 and GT1B: After thorough investigation on the effect of the neural supplements, RA and Pur on BoNT/A detection sensitivity, we tested two more media additives that might further enhance our assay. In a previous study, we showed 16-fold increase in the BoNT/A detection sensitivity when NG108-15 cells were cocultured with Schwann cells [73]. Schwann cells were shown to promote synaptogenesis and synaptic activities of primary spinal cord motor neurons by secreting TGFβ1 [27, 29]. In addition, ganglioside GT1b was shown to significantly increase the BoNT assay detection sensitivity [51, 52]. Therefore, we investigated the effect of GT1b and TGFβ1 in our final media that contained all three neural supplements, 2.5 μM RA and 7.5 μM Pur.

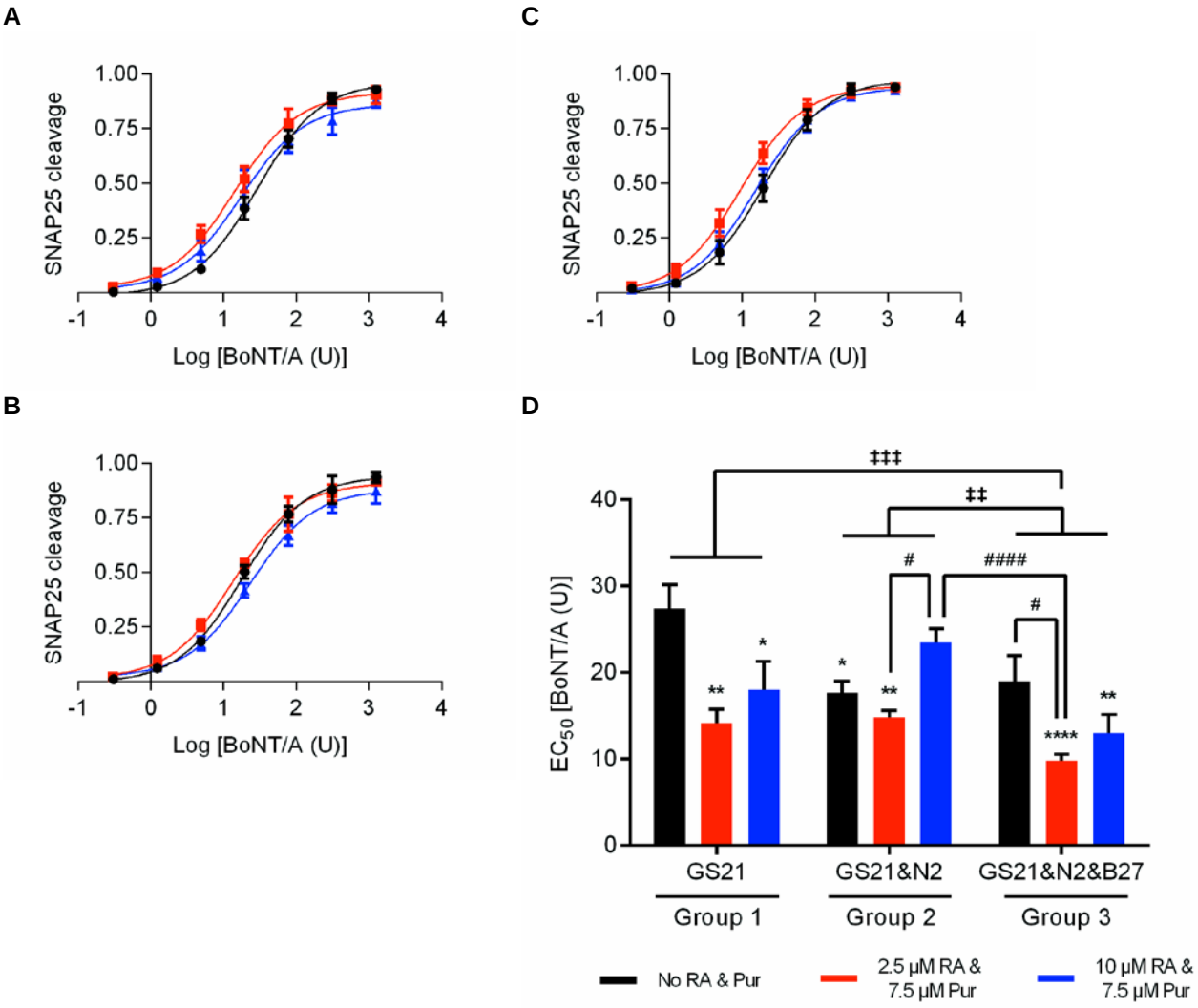

Figure 10: Combinatorial effects of RA and Pur in GS21, N2, and B27 supplemented media.

(A) Dose-response curve of SNAP25 cleavage when cultured in media supplemented with GS21 only, (B) GS21 and N2 combined, and (C) GS21, N2 and B27 combined. To all neural supplement media, varying concentrations of RA and Pur were added to test their combinatorial effects in the EC_{50}. Colors of both dose-response curves and EC_{50} plots indicate the amount of RA and Pur added to the media: no RA and no Pur (black); 2.5 µM RA and 7.5 µM Pur (red); 10 µM RA and 7.5 µM Pur (blue). (D) Analyzed EC_{50} of the dose-response curves were plotted. One-way ANOVA followed by Tukey's multiple comparison test was used for statistical analysis and the *p*-value against the condition that only contained GS21 (Group 1 black bar) is marked with asterisk (*) and the rest were indicated with pound sign ($^{\#}$). Multiple group t-t-test of the means (‡) showed statistical significance of Group 3 to both Group 1 and Group 2. For all statistical tests, * $p < 0.05$, ** $p < 0.01$, **** $p < 0.0001$, $^{\#}$ $p < 0.05$, $^{\#\#\#\#}$ $p < 0.0001$, and ‡ $p < 0.05$.

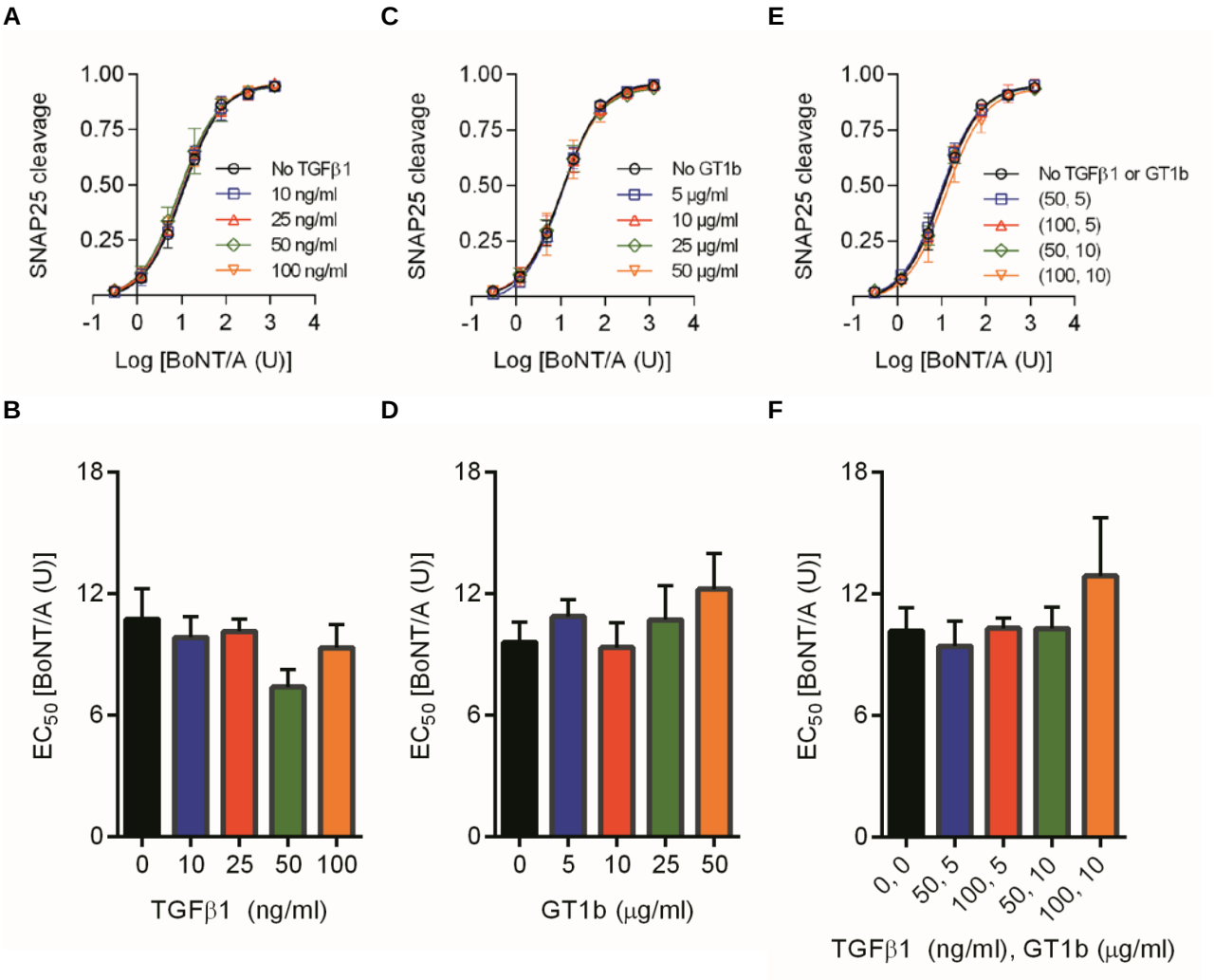

Figure 11: Effect of TGFβ1and GT1b.
EC_{50} of the optimized media containing all three neural supplements, 2.5 µM RA, and 7.5 µM Pur was tested with varying concentrations of (A) TGFβ1, (B) GTb1, and (C) TGFβ1 and GT1b. A small decrease in the EC_{50} was observed when 50 ng/ml TGFβ1 was added to the culture medium, but none of the tested conditions showed statistical significance.

At 50 ng/ml of TGFβ1, we observed a slight gain in the sensitivity further decreasing EC_{50} from 10.7 to 7.4 U although without statistical significance (Figure 11A-B). Despite the previous reports showed that GT1b increases the BoNT/A detection sensitivity, we did not see additional benefits of adding GT1b to our culture medium (Figure 11C-D). Furthermore, addition of both TGFβ1 and GT1b did not show any gain in the detection sensitivity (Figure

11E-F). The final medium that included TGFβ1 reached the limit of detection between 0.3 and 1.2 U (Figure 12).

3.4 Conclusions

We focused our efforts in increasing the sensitivity of the motor neuron-like NG108-15 cell line through combinatorial optimization of neural cell culture medium with the final formulation of 1x B27, 1x N2, 1x GS21, 2.5 μM RA, 7.5 μM Pur, and 50 ng/ml TGFβ1 to achieve a detection sensitivity of EC_{50} ~7.4 U (equivalent to ~7.9 pM), with detection limit between 0.3 and 1.2 U. The sensitivity does not surpass that of *in vivo* MLA (1 – 2 LD_{50} U), and *ex vivo* primary (EC_{50} 3.8 U) and *in vitro* stem cell derived neuron (EC_{50} 0.98 U) cell-based assays [10, 47], but the detection range is comparable.

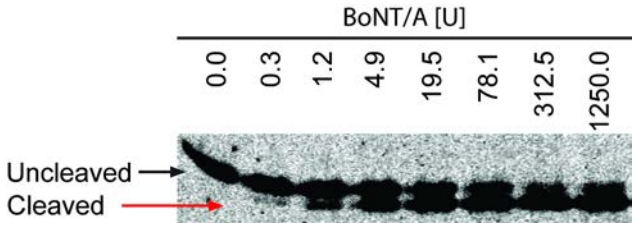

Figure 12: Western blot of SNAP25 cleavage in the final medium.
The Western blot image stained with SNAP25 antibody shows cleaved and uncleaved portion of SNAP25 protein in the final medium composed of 1x B27, 1x N2 and 1x GS21 neural supplements and 2.5 μM RA, 7.5 μM Pur, and 50 ng/ml TGFβ1 additives. The lower bands indicate cleaved SNAP25 and visible starting 0.3 U.

The cell-based assay we report here is suitable for testing pharmaceutical reagents to determine concentration and activity of the toxin and not intended to use as the primary assay for infield testing. The assay, however, can be accompanied with biochemical detection assays that

are amenable for infield testing to accurately determine the toxicity if BoNT is detected in food supplies. We quantified the relative amount of SNAP25 cleavage using Western blot as the end-point measurement to assess the specificity of BoNT/A and the sensitivity of the assay. Although Western blot is not amenable for high-throughput and difficult to validate, it can be replaced with ELISA as Fernandez *et al.* demonstrated with a proprietary antibody specific to cleaved SNAP25. The ELISA method for detection also attributed to a 2-fold gain in the sensitivity [51], which may be applicable to our culture to further improve our method.

Through step-by-step media optimization study, we developed a highly sensitive cell-based BoNT/A detection assay using a neuronal cell line that was characterized to behave like motor neurons. The assay sensitivity is comparable to the sensitivity reported with the MLA and eliminates the need for the animal sacrifice and laborious steps involved in obtaining primary or stem cell derived neurons. This approach provides a good example in the development and refinement of new *in vitro* cell-based approaches for BoNT detection.

3.5 Supplementary Data

Supplementary Table S1: Taguchi five-factor and four-level design of experiment.

Taguchi Study Matrix Code	B27	N2	GS21	Retinoic acid (µM)	Purmorphamine (µM)
(1,1,1,0,0)	1	1	1	0	0
(1,2,2,1,1)	1	2	2	2.5	2.5
(1,3,3,2,2)	1	3	3	5.0	5.0
(1,4,4,4,4)	1	4	4	10.0	10.0
(2,1,2,2,4)	2	1	2	5.0	10.0
(2,2,1,4,2)	2	2	1	10.0	5.0
(2,3,4,0,1)	2	3	4	0	2.5
(2,4,3,1,0)	2	4	3	2.5	0
(3,1,3,4,1)	3	1	3	10.0	2.5
(3,2,4,2,0)	3	2	4	5.0	0
(3,3,1,1,4)	3	3	1	2.5	10.0
(3,4,2,0,2)	3	4	2	0.0	5.0
(4,1,4,1,2)	4	1	4	2.5	5.0
(4,2,3,0,4)	4	2	3	0	10.0
(4,3,2,4,0)	4	3	2	10.0	0
(4,4,1,2,1)	4	4	1	5.0	2.5

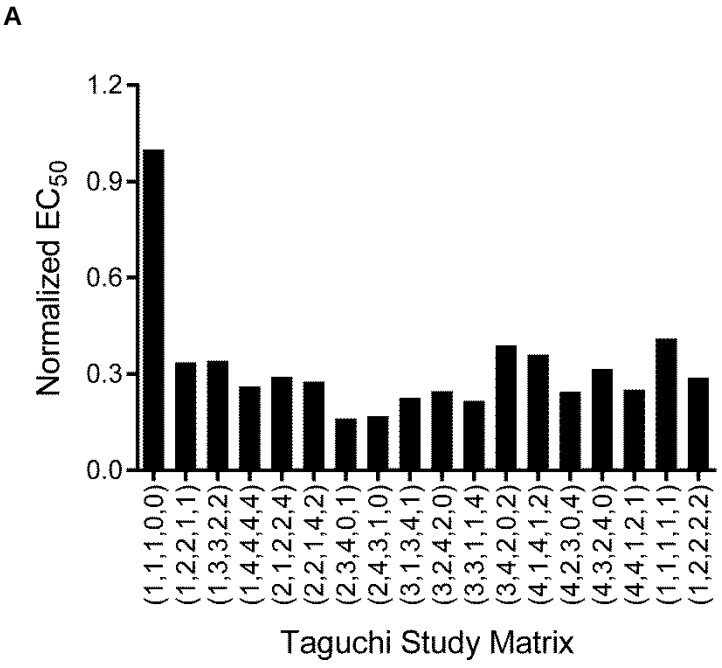

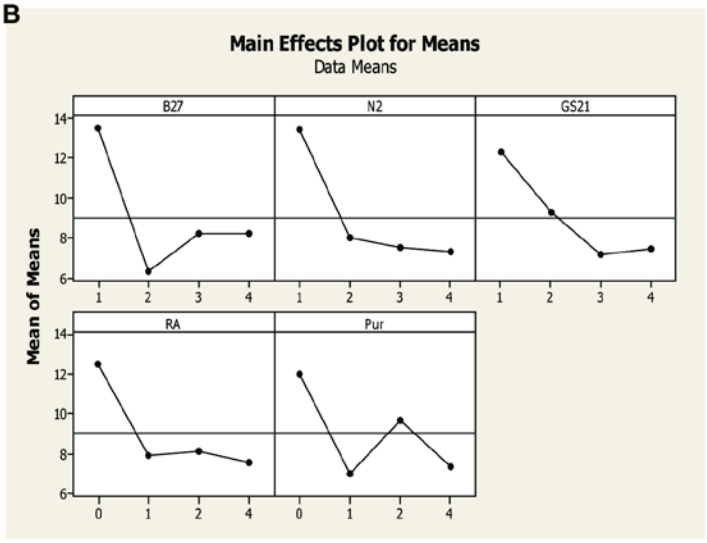

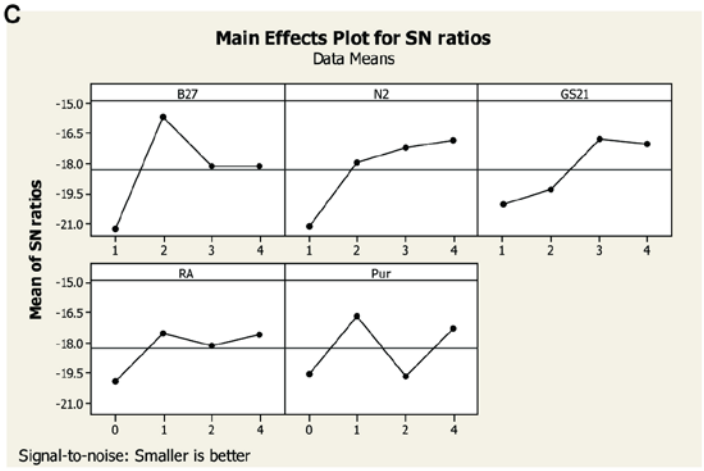

Supplementary Figure 3: Taguchi design of experiment.
(A) A five-factor four-level study was designed using Taguchi design of experiment. For each condition, dose-response curve was generated and the corresponding normalized EC_{50} was calculated and plotted. (B) Main-effect of means and (C) signal-to-noise ratio plots were generated. Plots indicated that 2x B27, 4x N2, and 3x GS21 was optimal concentrations of neural supplements, and 2.5 to 10 μM RA and either 2.5 or 10 μM Pur was shown as the optimal media condition. The Taguchi study design and analysis was performed using Minitab16 and the study was not repeated.

3.6 Acknowledgements

We thank Dr. Eric Johnson, Sabine Pellett, and William Tepp at the University of Wisconsin-Madison for supplying BoNT/A and their insight in this project.

Funding: This research was supported by the U.S. Department of Homeland Security Science and Technology Assistance Agreement No. 2007-ST-061-000003, National Center for Food Protection and Defense (2010-ST-061-FD0001), the National Research Service Award (NRSA) T32 EB011434, University of Wisconsin Carbone Cancer Center Support Grant P30 CA014520, and Bill and Melinda Gates Foundation OPP1028788-Microfluidic Immiscible Phase Barrier: Simplified Sample Preparation for POC Diagnostics in the Developing World.

Disclaimer: The views and conclusions contained in this document are those of the authors and should not be interpreted as necessarily representing the official policies, either expressed or implied, of the U.S. Department of Homeland Security. The Department of Homeland Security does not endorse any products or commercial services mentioned in this publication.

Chapter 4 – 3D Printer Aided Micro-pillars Fabrication Method for Long-Term Culture of Skeletal Muscle Tissue and Functional Analysis.

4.1 Abstract

Skeletal muscle tissue is responsible for the voluntary movement, and defects in the development and degeneration in skeletal muscle can be devastating. To provide tools to study muscle physiology, genetic defects, and degeneration, an *in vitro* model with proper organization of the muscle tissue and force quantification is necessary. Previously, microscale pillars with overhangs were fabricated to anchor muscle tissues and measured the pillar deflection to quantify muscle force. In this study, the skeletal muscle tissue was directly actuated by supplying electrical current using electrodes [76]. Although this approach allows quantification of muscle force, it is difficult to position electrodes to each tissue limiting throughput of the approach, and does not differentiate mature and immature development of the muscle tissue such as muscle-specific kinase (MuSK) aggregation and accumulation responsible for receiving signal from the innervating neurons. Alternatively, channel rhodopsin 2 (ChR2) was expressed in skeletal myoblast to enable light stimulation thus does not require electrodes [77]. However, ChR2 creates artificial flux of calcium, thus does not truly recapitulate the physiological process of muscle contraction. Additionally, the muscle contractions stimulated directly on muscle does not guarantee proper communication from the innervating nerves from motor neurons similar to direct electrical stimulation.

To foster basic and translational research in development, degeneration, and regeneration of muscle and motor neurons, I developed a simple fabrication technique that can be adopted in any research laboratories to make the micro-pillar devices for muscle force quantification. And

by coculturing skeletal muscle tissue and ChR2 expressing cholinergic motor neuron-like cells, I demonstrate that muscle contraction can be actuated by stimulating neuronal cells by light. The approach I've taken best mimics human physiology, gives an easy access to the engineering tool for tissue culture, and has a high potential towards generating functional neuromuscular junction to accelerate translational researches especially in treating skeletal muscular dystrophies and motor neuron diseases.

4.2 Device Fabrication

Master Mold Fabrication – Photolithography: The master mold of the device configured with micro-pillars in micro-wells (μPW) was first fabricated using silicon wafer deposited with layers of SU-8 photoresist. The fabrication and device was first developed to culture cardiomyocytes, which I reconfigured to a larger scale so that μPW can be loaded with micropipette instead of centrifugation [78, 79]. Seeding cells via centrifuge severely undermines the reproducibility of the tissue in each well because the volume and cell number of each well is not controlled. Moreover, one set of devices or array can only accommodate one condition, thus not amenable for high-throughput screening. The device I designed allows seeding cells and extracellular matrix in each well separately, thus gives more control and reproducibility. To fabricate the master mold for the μPW devices, high-resolution photomasks designed to create base, micro-pillars, and overhang for anchoring muscle tissues were printed (Figure 13). The micro-pillars were placed inside the 4.5 mm diameter micro-wells, which media reservoir was created on the peripheries of the micro-wells for feeding cells without disturbing the tissue (Figure 14).

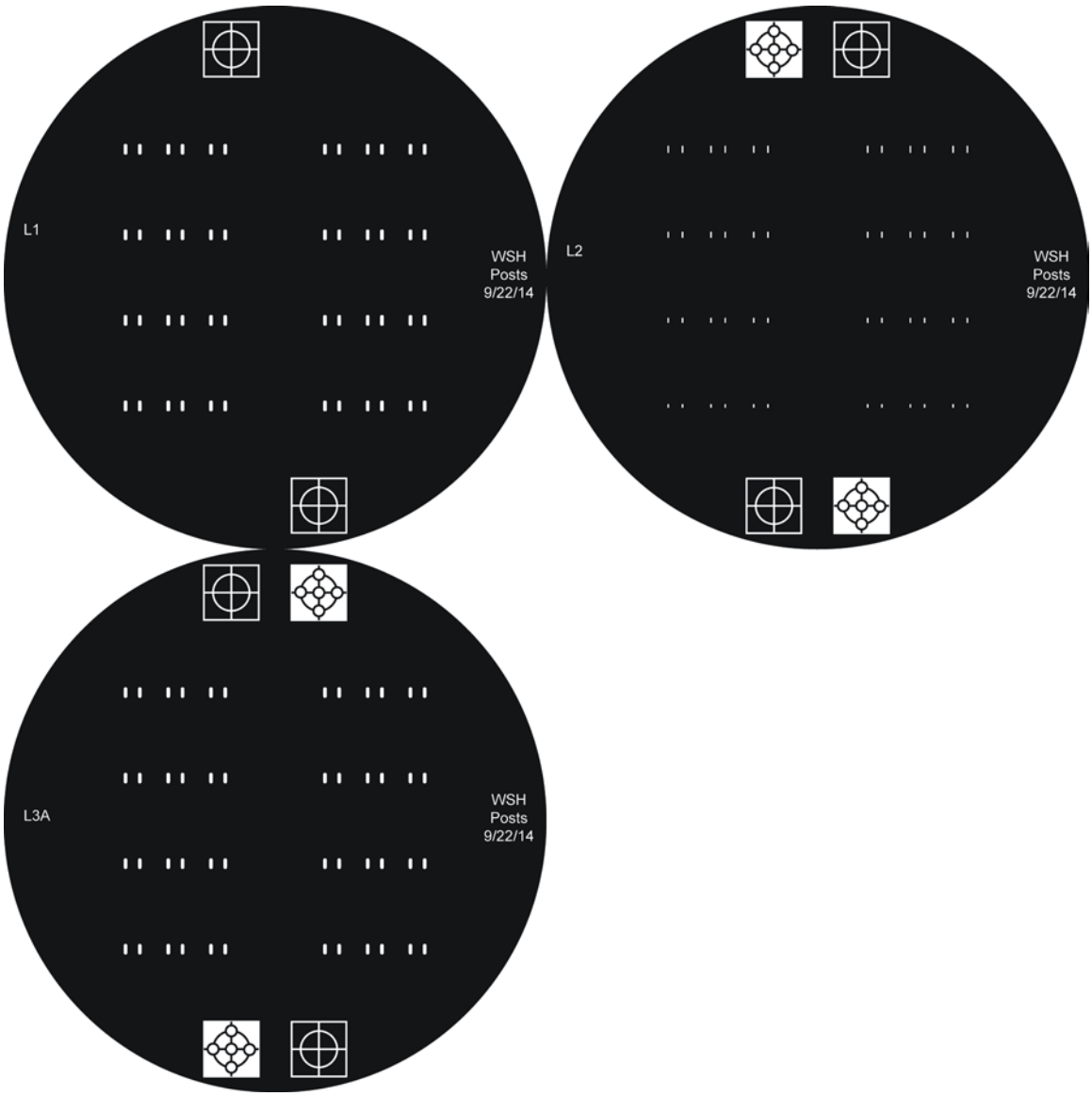

Figure 13: Micro-pillar photomasks with overhangs.
L1 layer (top left) creates the base where the micro-pillars sit, L2 layer (top right) creates the actual micro-pillars, and L3A (bottom left) layer creates overhang on top of the micro-pillars.

To fabricate the silicon wafer SU-8 master mold, (i) each layer of the photoresist was spun down using a spin coater, (ii) baked at 95 °C for several hours, depending on the thickness of each layer, to allow solvent to evaporate, and (iii) exposed to ultraviolet (UV) light to crosslink the negative photoresist SU-8.

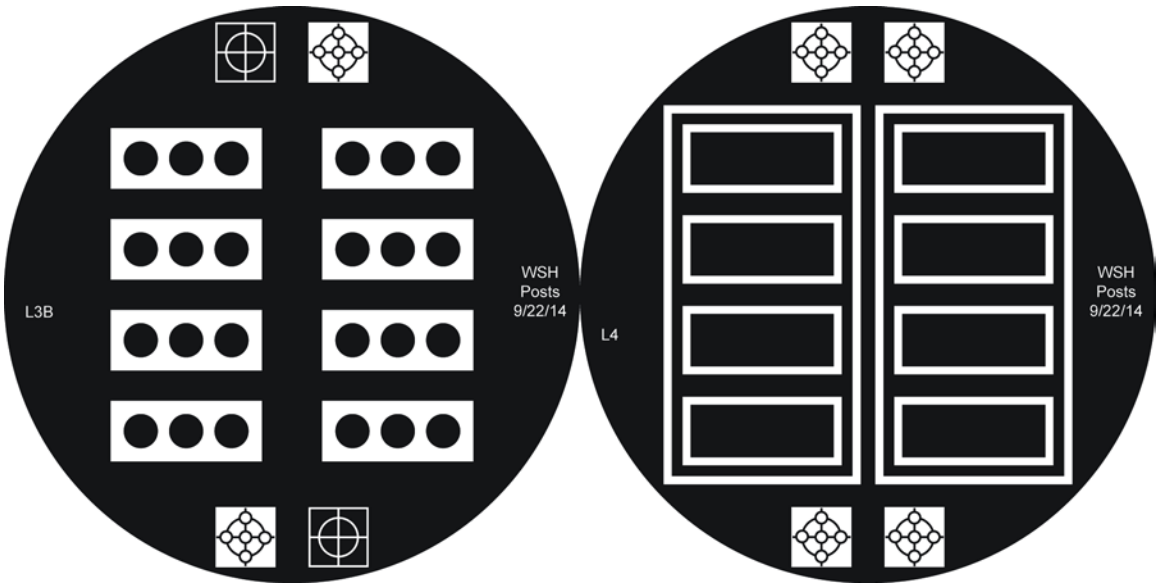

Figure 14: Micro-well photomasks with media reservoir.
L3B layer (left) creates micro-wells where the micro-pillars are placed and L4 layer (right) creates reservoir for medium feed.

Each layer followed the standard photolithography protocol except for the sacrificial layer required to generate overhangs on top of the micro-pillars. The sacrificial layer is the mixture of 85% SU-8 100 and 15% Shipley, a positive photoresist, which was spun down after the micro-pillar layer in order to block UV light to penetrate downward beyond the sacrificial layer; therefore, crosslinking of the SU-8 photoresist only occurs on the layers deposited on top of the sacrificial layer unless overexposed [80]. Covering the micro-pillar layer with the sacrificial layer is a critical step and the sacrificial layer thickness and the UV exposure was optimized to create the overhangs. Subsequently, the micro-wells and media reservoirs were created. The process of creating the silicon SU-8 master takes about 2 – 3 days (Figure 15).

The μPW device master mold fabricated with photolithography yielded overhangs for tissue anchorage (Figure 16). The minimum resolution of the micro-pillars was limited due to the equipment used for fabrication, and the height of the micro-pillars was also limited due to the

innate capacity of the process in generating high aspect ratio features. Overall, we were able to achieve the photolithography yielded micro-pillar dimensions at approximately at 200 µm x 1000 µm x 1000 µm (W x L x H). Creating smaller feature size is feasible in cleanroom facility with mask aligner but I did not challenge the scale of the device to create smaller features.

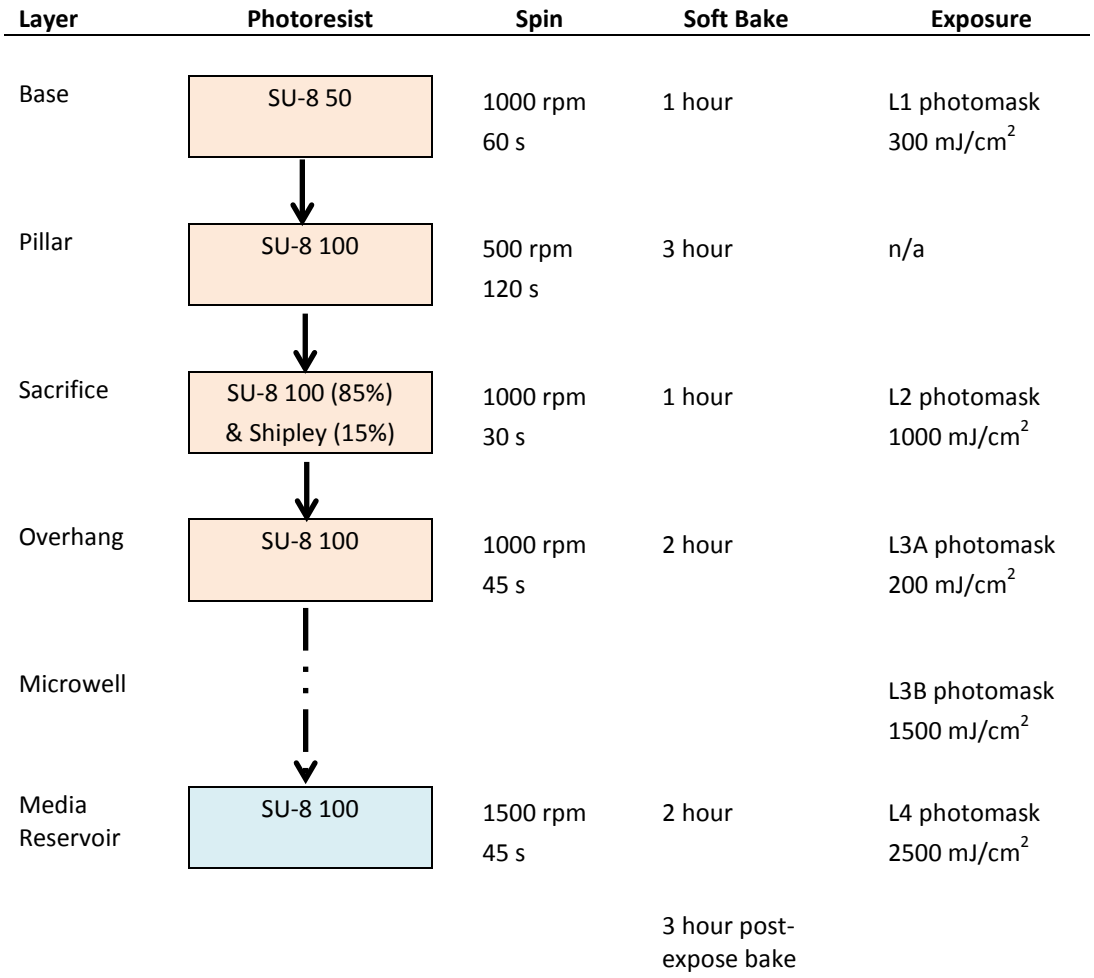

Figure 15: Silicon master mold fabrication steps using photo lithography technique for generating µPW device.
Master mold fabrication process scheme using photo lithography technique is described. The photomasks under exposure column are displayed in Figure 13 and Figure 14. Overall, the process takes 2 – 3 days from spinning down the first layer to developing the master mold. Mixture of SU-8 and Shipley is required to create sacrificial layer to create overhangs on pillars.

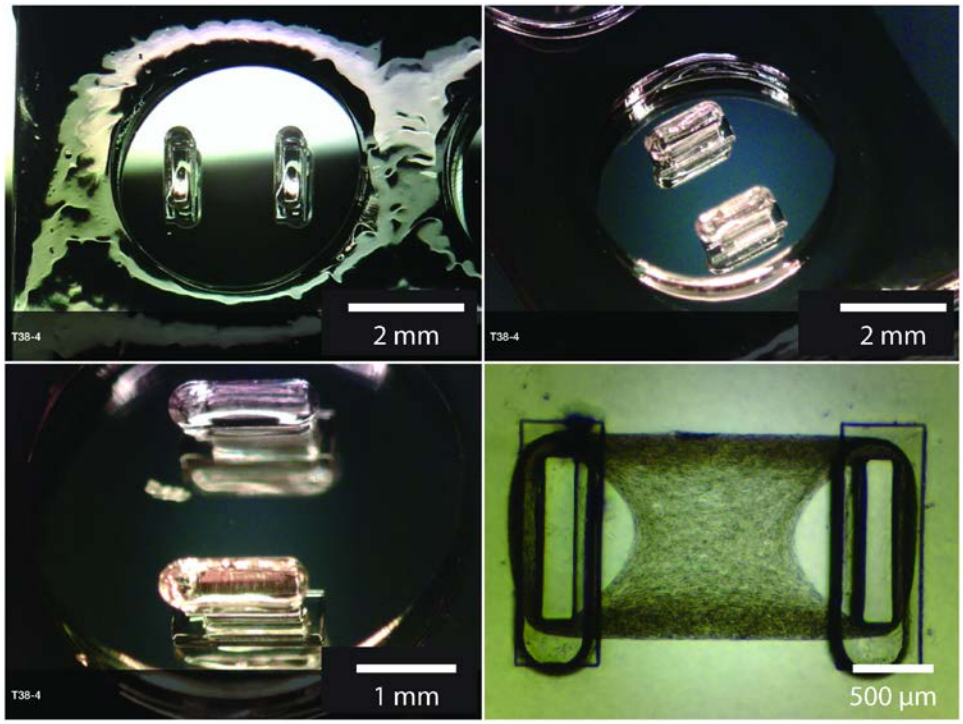

Figure 16: Silicon master mold fabricated using photo lithography technique.
The µPW device fabricated using SU-8 on silicon wafer is displayed above. The micro-pillars are placed inside of the micro-wells (top left) and the overhangs are placed on top of the pillars (top right and bottom left). The master mold was then used to fabricate PDMS mold, followed by PDMS µPW devices, and cultured C2C12 skeletal muscle tissue in 3 mg/mL fibrin gel (bottom right).

Master Mold Fabrication – 3D Printing: Despite the success in fabricating µPW device using photolithography, the process requires equipment not easily accessible to many research laboratories, and also the feature size is limited unless equipped with high resolution photomask aligner and UV light. Instead of challenging the resolution the features using photolithography technique, which requires cleanroom facility and access to expensive systems, I used Viper Si2 3D printer capable of printing at micron scale (Figure 17). The 3D printer adds a thin layer of liquid resin polymer, and exposes the resin with laser to crosslink the polymer. Acura60 resin was used, which the formula is based on durable polycarbonate.

Figure 17: Viper Si2 3D printer used to fabricate master mold.
Acura60 resin was used to fabricate master mold using 3D printer shown above. The 3D printing simplifies the master mold fabrication process, which shortens the process from 2 – 3 days to 3 – 4 hours. The resin is polycarbonate base, which is more durable than SU-8 fabricated features and can create high-aspect ratio features.

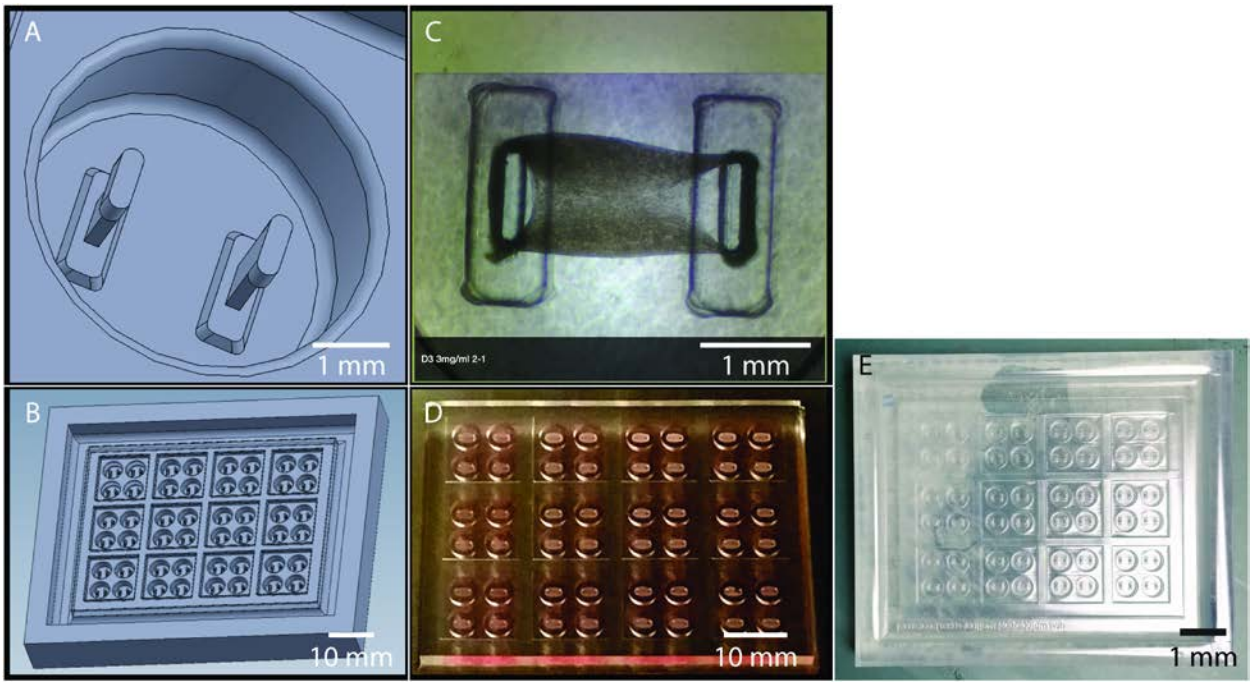

Figure 18: 3D printed master mold using Viper Si2 and Aura60 resin.
The master mold of the μPW device was printed using 3D printer. The master mold was used to create PDMS mold, which was then silane coated to fabricate μPW device. The micro-pillars are place inside a micro-well (top left) and placed in arrays (bottom left) to enable high-throughput screening. Skeletal muscle tissue was cultured in fibrin gel (top right) and the array of muscle tissues are shown on the bottom right.

To 3D print the master mold, the μPW tissue array device was designed using SolidWorks as shown in Figure 18A-B. The design consists of quads of micro-wells for replicates. Each quad has separate media reservoir allowing 12 different conditions comprising 48 tissues for each tissue array device. The 3D printer printed the micro-pillars down to 100 x 800 x 1500 μm in width x length x height with overhangs, which the feature resolution and the aspect ratio were superior to the photolithography technique used as shown in Figure 16. The master mold was then used to cast PDMS mold, which was then plasma treated and silane coated to fabricate and detach PDMS devices. The final μPW tissue array device is shown in Figure 18D-E.

4.3 Long-Term Culture of Skeletal Muscle Tissue

C2C12 Skeletal Muscle Tissue Culture in μPW Devices: The μPW devices were used to culture C2C12 cells in fibrin and Matrigel to support tissue formation. Fibrin gels were shown to be superior to collagen type I fibers in terms of longevity of the skeletal muscle tissue culture, and also allows cell migration [81, 82]. Additionally, Matrigel was shown to promote muscle maturation when combined with other matrix [83]. In the μPW devices, the cell and tissue matrix supported tissue culture for at least up to 3 weeks without deteriorating the tissue as previously reported, which limited skeletal muscle tissue culture duration. The skeletal tissue were anchored around the micro-pillars, and held down by the overhangs eliminating the issues of muscle fibers detaching from the surface and rolling up (Figure 19).

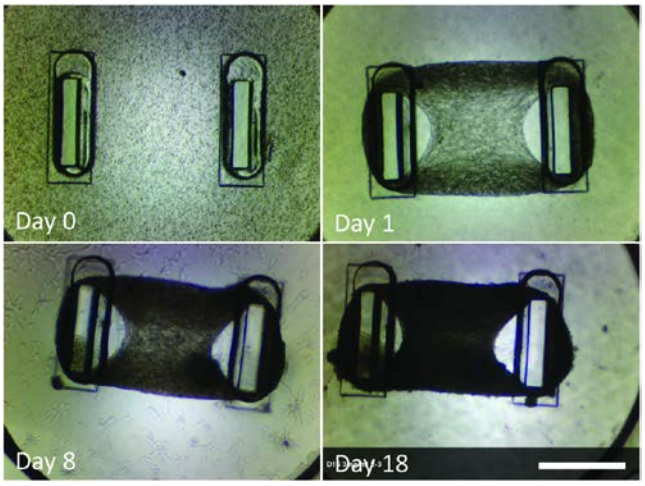

Figure 19: C2C12 culture in µPW device with fibrin gel.
C2C12 skeletal myoblasts were mixed with 3 mg/mL fibrin gel and 10% growth factor reduced Matrigel. The cell and matrix mixture was loaded into micro-well and cultured for up to 3 weeks. The gel matrix contracted and formed ring around the micro-pillars within 24 hours after seeding and maintained the tissue for over 3 weeks. Scale bar: 1 mm.

While culturing skeletal muscle tissues, deflection of the micro-pillars was observed not only to support tissue formation but also elastic enough to be displaced with muscle contraction. The dimension of the micro-pillars fabricated using photolithography technique and 3D printing were 200 x 1000 x 1000 µm and 100 x 800 x 1500 µm respectively in width x length x height. Starting 5 – 6 days in differentiation, C2C12 cells underwent spontaneous twitching. The photolithography mold fabricated micro-pillars were too stiff—due to the dimension, not the elastic property of the PDMS—to see meaningful displacement of the pillars for quantification (Supplementary Video 1); however, 3D print mold fabricated micro-pillars were elastic enough to see the displacement (Supplementary Video 2). The spontaneous twitching of C2C12 tissue continued for up to 2 weeks in differentiation, but significantly slowed down afterwards (Supplementary Video 3).

4.4 Cholinergic Neurons and Skeletal Muscle Coculture

Channel Rhodopsin 2 Transfection in Cholinergic NG108-15 Neuronal Cells: Neuroblastoma and glioma hybrid cell line is cholinergic and shown to behave like motor neurons forming synapses with skeletal muscle myotubes [17-20].

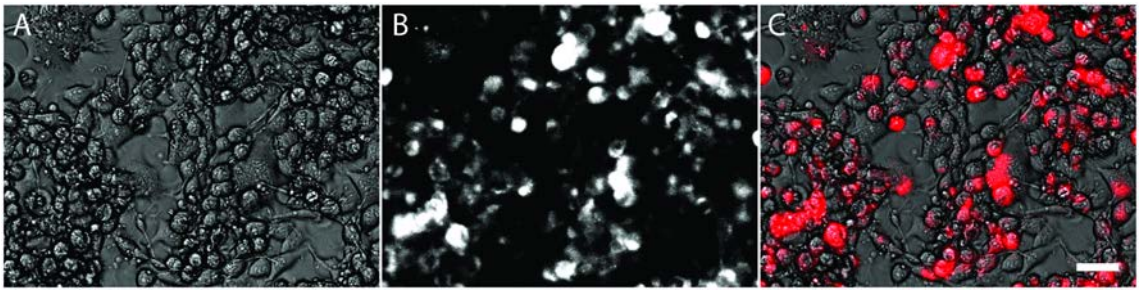

Figure 20: mCherry-ChR2 transfected NG108-15 cells.
NG108-15 cells were transfected with mCherry-ChR2 expression vector using lentivirus. The cell line was selected using 5 µg/mL puromycin. (A) Bright field image of the NG108-15 cell line, (B) mCherry expression under fluorescent microscope, and (C) merged bright field and mCherry images. Scale bar: 50 µm.

To begin with, NG108-15 cell line was treated with lentivirus carrying mCherry-ChR2 expressing vector for selection and for light stimulation of neurons. After generating lentivirus in HEK293T cells and infecting NG108-15 cells, puromycin was used to select for the mCherry-ChR2 expressing cells (Figure 20). Roughly 70% of the cells were transfected 4 passages after infection.

Muscle Actuation via Light Stimulated Neurons: To better recapitulate physiologic mechanism of muscle contraction, the skeletal muscle tissue was actuated by stimulating ChR2 expressing neurons by light. Neuron triggered muscle contraction is advantageous than the other methods tried in similar µPW device because the ACh released by the innervating neurons are

responsible for sending signals, instead of direct stimulation via electrical current or forced calcium flux.

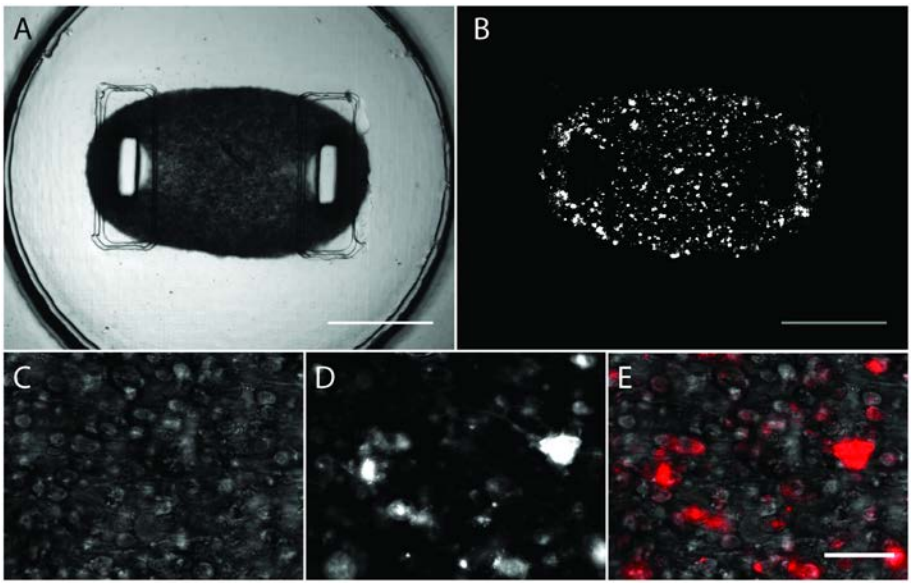

Figure 21: C2C12 and mCherry-ChR2 expressing NG108-15 coculture in μPW device. C2C12 and ChR2 transfected NG108-15 cells are cocultured in the micropillar microwell device at 1:1 cell number ratio. 3 mg/mL fibrin gel and 10% growth factor reduced Matrigel were used to support tissue formation. (A and C) Bright field image of the tissue, (B and D) mCherry fluorescent image of the tissue showing ChR2 transfected NG108-15 cells, and (E) combined images in C and D where mCherry expression is in red. Scale bars: 1 mm (A and B); 100 μm (C – E).

First, equal number of NG108-15 and C2C12 were mixed with 3 mg/mL fibrin and 10% growth-factor reduced Matrigel, and loaded μPW devices. NG108-15 was thoroughly mixed with C2C12 cells and formed tissue around the micro-pillars (Figure 21). The tissue was then cultured in differentiation medium 24 hours after seeding for additional two weeks. It is important to note that the spontaneous twitching of muscle tissue attenuated greatly after 2 weeks in differentiation (Supplementary Video 3), which was important to be able to discern between spontaneous versus stimulated muscle contraction. The neuron-muscle cocultured tissue was

light stimulated on differentiation day 15. As shown in Supplementary Video 4, minimum amount of spontaneous twitching was observed without light stimulation; however, upon stimulation using blue light, the muscle twitching was enhanced.

4.5 Conclusions

Long-term culture of skeletal muscle was challenging due to the detachment of the myotubes as they undergo fusion and spontaneous twitching. To aid a long-term culture of skeletal muscle tissue, fibrin and Matrigel matrix was mixed with skeletal myoblasts, and cultured in microsystems engineered devices comprising of micro-pillars that are capped with overhangs to anchor skeletal muscle tissues. The fabrication of such device was simplified using 3D printing technology, which allowed for easy modification of the shape and dimension of the pillars, which can be reverse engineered to meet stiffness requirement for force quantification.

Additionally, by leveraging recently discovered calcium channel ChR2, neurons were stimulated via light, which was then triggered muscle twitching. This is a significant achievement in tissue and neuroengineering in that the model mimics human physiology of skeletal muscle, functional, and easily quantifiable, which can be adopted for high-throughput screening system for much needed drug discovery and development efforts in neuromuscular degeneration. Further studies must be conducted such as using hESC or hiPSC derived MNs and skeletal muscles, in addition to exploring opportunities to add glial cells to generate human NMJ *in vitro.*

4.6 Experimental Section

Cell Lines and Cell Culture: NG108-15 and C2C12 cell lines were purchased form ATCC (Manassas, VA). NG108-15 cell line was maintained in DMEM (Life Technologies) supplemented with 10% FBS (Gibco), 1% penicillin-streptomycin (P/S, Gibco), and HAT supplement (Sigma). C2C12 cell line was maintained in DMEM supplemented with 10% FBS, 1% P/S, and 1 mM sodium pyruvate (Life Technologies). HEK293T cell line was a kind gift from Professor Justin Williams (University of Wisconsin, Madison) and maintained I DMEM supplemented with 10% FBS and 1% P/S.

Channel Rhodopsin 2 Expression in NG108-15: Plasmid containing mCherry channel rhodopsin 2 (ChR2) vector, pΔ8.9 plasmid containing *gag*, *pol*, and *rev* genes, and VSV-g envelop plasmid were kind gift from Professor Justin Williams (University of Wisconsin, Madison). *Escherichia coli* strains transduced with the plasmids were plated on Luria-Bertani (LB) containing agar petri-dish, selected with 50 µg/mL carbenicillin (Sigma), and one colony of each strain was expanded in 1 L LB medium flask on orbital shaker. Plasmids were purified using plasmid purification kit (Qiagen) and transfected into HEK293T cell line with 10 µg mCherry-ChR2, 7.5 µg pΔ8.9, and 5 µg VSV-g plasmids using BES buffered saline. 48 hours after transfection, lentiviral ChR2 containing spent medium was then collected, filtered, and applied directly to NG108-15 cell line, and selected with 5 µg/mL puromycin, sorted for the top 20% mCherry expressing population using flow cytometry.

Tissue Culture in µPW: The following mixture was prepared: C2C12 and NG108-15 mix at 5 million/mL density each, 87 µL of NG108-15 growth medium, 90 µL of fibrinogen (10 mg/mL stock), 30 µL of growth factor reduced Matrigel (BD Bioscience), and 18 µL of thrombin (50 U/mL stock). 20 µL of the mixture was used to load each micro-pillar well,

incubated for 5 minutes at 37 °C, fed with C2C12 growth medium supplemented with 1 mg/mL aminocaprionic acid (Sigma). After 24 hour incubation, the growth medium was replaced with differentiation medium formulated with Neurobasal media (Invitrogen) supplemented with 1x B27 (Invitrogen), 1x N2 (Invitrogen), 1x GS21 (GlobalStem), 1% GlutaMAX (Invitrogen), 1% P/S, and 1 mg/mL aminocaprionic acid. The differentiation medium was replaced daily for 14 – 20 days.

Master Mold Fabrication Using Photo Lithography: Photomasks for each layer was designed using Adobe Illustrator and printed on transparent transparency (Fineline Imaging). Standard soft lithography technique was used for fabricating the mold on silicon wafer. Briefly, (i) the first base layer was spun down with SU-8 50 (MicroChem) at 1000 rpm for 60 s, exposed with 300 mJ/cm^2 UV (L1 photomask), (ii) the second pillar layer was spun down with SU-8 100 at 500 rpm for 120 s, (iii) the third sacrificial layer was spun down with 85% SU-8 100 and 15% Shipley mixture at 1000 rpm for 30 s, exposed with 1000 mJ/cm^2 (L2 photomask) (iv) the fourth overhang layer was spun down with SU-8 at 1000 rpm for 45 s, which was exposed with 200 mJ/cm^2 (L3A photomask) for the overhang and 1500 mJ/cm^2 (L3B photomask) for the creating micro-wells, and (v) the fifth media hold layer was spun down with SU-8 100 at 1500 rpm for 45 s, exposed with 1500 mJ/cm^2 (L4 photomask). The silicon master was developed in propylene glycol monomethyl ester acetate (Sigma).

Master Mold Fabrication Using 3D Printer: The master mold was designed using SolidWorks 2013 and printed with Acura60 resin using Viper Si2 (UW Rapid Prototyping Consortium).

Polydimethylsiloxane (PDMS) Mold Fabrication: The PDMS polymer was mixed with cross linker at 20:1 ratio, degassed using vacuum pump, and poured onto the master molds. For

silicon SU-8 molds, the PDMS was cured for 4 hours at 80 °C whereas for 3D master mold was cured at room temperature for 48 hours, taken off the master molds, heated for additional 4 hours at 80 °C to ensure proper curing of the reagents.

Device Fabrication: The micro-pillar microwell devices were fabricated off of the PDMS molds. The PDMS molds were plasma treated and coated with silane (Sigma) overnight in vacuum chamber. PDMS was mixed with the curing reagent at 10:1 ratio, degassed and poured onto the silane coated PDMS mold, cured at 110 °C for 20 hours. The micro-pillar microwell devices were taken off of the PDMS mold, soxhlet extracted for at least 4 hours. The device was plasma treated, disinfected with 100% ethanol, and coated with 1% Pluronic F127 (Sigma) for at least 30 min at room temperature before seeding.

4.7 Supplementary Data

Supplementary Video 1: Spontaneous twitching of 9 days old C2C12 tissue cultured in device fabricated using photolithography technique.
The micro-pillars (200 x 1000 x 1000 μm in W x L x H) with overhangs held the skeletal muscle tissue anchored in place. The spontaneous twitching of the C2C12 tissue generated enough force to slightly move the pillars.

Supplementary Video 2: Spontaneous twitching of 12 days old C2C12 tissue cultured in 3D printed device.
The micro-pillars (100 x 800 x 1500 μm in W x L x H) with overhangs were 3D printed. The spontaneous twitching of 12 days old C2C12 tissue generates enough contractile force to bend the pillars. The displacement of the pillar is significant to be able to quantify force.

Supplementary Video 3: Spontaneous twitching of 14 days old C2C12 tissue cultured in 3D printed device.
The spontaneous twitching of 14 days old C2C12 tissue in 3D printed μPW device (100 x 800 x 1500 μm in W x L x H) decreases substantially compared to 12 days old tissue (Supplementary Video 2). The slowed down spontaneous twitching allows for discerning muscle contraction with external stimulation.

Supplementary Video 4: Light activation of ChR2 expressing NG108-15 cells stimulates C2C12 tissue contraction.
ChR2 expressing NG108-15 cell line was coculutred with C2C12 tissue and differentiated for 15 days in photolithography fabricated μPW device (pillar dimensions 200 x 1000 x 1000 μm in W x L x H). Blue light stimulation of ChR2 transfected in NG108-15 cells caused C2C12 contraction.

4.8 Acknowledgements

I thank Dr. Justin Williams at the University of Wisconsin-Madison for supplying plasmids for ChR2, VSV-g, and pΔ8.9, and HEK293T cell line. I also thank Robert Swader at the rapid prototype consortium in Wisconsin Institute for Discovery for consulting and printing 3D parts and an undergraduate student, Jiwon Lim, at the University of Wisconsin-Madison for conducting several tissue culture experiments.

Chapter 5 – Targeting Synaptic Vesicle 2 with the Non-Toxic Fragment of Botulinum Neurotoxin Type A for Neuroendocrine Malignancies

5.1 Abstract

Synaptic vesicle 2 (SV2) is highly expressed in neuroendocrine tumors (NETs) and has been recognized as a new biomarker for NETs. Despite the discovery of SV2 as a biomarker, no advance has been made that utilizes SV2 as a clinical target for treating NETs. In parallel, SV2 was identified as the protein receptor for botulinum neurotoxin type A (BoNT/A). We hypothesized that the nontoxic receptor-binding domain (HCR) of BoNT/A can be used as a ligand for targeting SV2 expressed in NET without imposing neurotoxicity. Our data suggest that HCR alone have potential for palliative therapy for slowly proliferating NETs with limited growth suppression function and it could also be used as a drug delivery vehicle for targeted therapy.

5.2 Introduction

Neuroendocrine (NE) malignancies are a highly heterogeneous group of neoplasms derived from hormone secreting neuroendocrine cells [84-86]. The uncontrolled hypersecretion of neurotransmitters and hormones causes debilitating symptoms, such as diarrhea, flushing, skin rashes, and heart failure, which characterizes these malignancies and can lead to morbidity [87]. According to the Surveillance, Epidemiology and End Result Registry, the incidence rate of NE tumors (NETs) was approximately 1 per 100,000 individuals in the United States in 1973, which steadily increased to 5 per 100,000 individuals comprising prevalence of 35 per 100,000 individuals in 2004. The patient outcome and mortality rate heavily depend on the

differentiation grade of the NETs. The median life expectancy decreases from over 10 years down to less than 1 year as the NETs progress from differentiated low-grade to undifferentiated high-grade stage, which account for about a half of the patients [88]. In gastrointestinal tract, NETs are the second most prevalent form of malignancies after colorectal cancer. Approximately 65% of all NETs originate from the gastrointestinal tract and 25% from the lung [88, 89].

Surgical removal is the most effective and curative treatment for NETs when possible; however, about half of the patients are diagnosed at later stages after lymph node and liver metastasis making surgery difficult for many cases [90, 91]. Treatments targeting somatostatin receptors (SSTRs) using somatostatin analogues (SSAs) have been the most successful palliative NET therapy [92]. Most notably, SSAs such as octreotide and lanreotide were shown to be effective in alleviating symptoms with limited anti-proliferative effect. Palliative therapies using SSAs have clinical benefits for low-grade slowly proliferating NETs since the patients survive for many years without malignant tissue volume related mortality. However, development of resistance to SSAs makes the therapy ineffective overtime [92] and only about half of the patients with the most prevalent gastrointestinal NETs respond to SSAs [84]. Moreover, due to the minimal anti-proliferative effect, SSAs are not used to treat high-grade aggressive NE cancers, which still rely on cytotoxic chemotherapy for treatment. Alternatively, SSA peptides conjugated with β-emitting radionuclides are being considered for treating high-grade metastatic and proliferative NE malignancies, but the clinical benefits are not consistent [93]. The application of interferon alpha (IFN-α) is approved by the European Medicines Agency for treating high-grade NE cancers but it accompanies severe side-effects affecting healthy tissues [92]. Tyrosine kinase inhibitors (TKIs) are under clinical evaluation [94] and several small

molecules that target insulin-like growth factor 1 receptor (IGF1R) or vascular endothelial growth factor receptor and platelet-derived growth factor receptor (VEGFR/PDGFR) are also being evaluated [92]. Recently, *sunitinib* and *everolimus* have shown clinical benefits for treating advanced pancreatic NE cancer extending the median progression-free survival by 5-6 months compared to placebo [95, 96]. Despite the advancements, recent studies suggest that *sunitinib* and *everolimus* promote metastasis with prolonged treatment limiting their use only for highly aggressive and advanced stage NE cancers [97, 98]. Other targeted therapies have been tested but the efficacies were limited [99, 100]. Taken altogether, most of the NET specific therapies available to date and under development target SSTRs, and untargeted delivery of therapeutic reagents is highly cytotoxic. Thus, identification of alternative clinical targets and development of drug delivery technologies are greatly in need.

In early 2000s, researchers found that synaptic vesicle 2 (SV2) proteins are abundantly expressed in NE tumor tissues, and they were recognized as a new biomarker of NETs [34-37]. There are three known isoforms of SV2, denoted SV2A, B and C, which are transmembrane transporters. Botulinum neurotoxin type A (BoNT/A) binds SV2A and C with high affinity, and also to gangliosides GT1b (as co-receptors) and then enters cholinergic neurons via synaptic activity [38, 70]. BoNT/A is a 150 kDa protein comprising three modular components: a 50 kDa heavy-chain receptor binding domain (HCR), a 50 kDa heavy-chain translocation domain (H_N), and a 50 kDa light-chain catalytic domain (LC). HCR recognizes the receptors, H_N repositions LC for endosomal escape, and LC cleaves its substrate, specifically SNAP25 for BoNT/A, imposing neurotoxicity [1]. Taking advantage of the modular design of the BoNTs, many efforts are being made to alter the target substrate of the LC, to replace the HCR with other ligands, or to use H_N to deliver biologics to the cytoplasm. Until now, most clinical applications of BoNT/A

have focused on regulating neurotransmitter release [4]. As one of the most notable applications of BoNT/A towards the treatment of NETs, Arsenault et al. replaced the HCR with various ligands such as ciliary neurotrophic factor (CNTF), tumor necrosis factor alpha (TNF-α), and epidermal growth factor (EGF), delivering LC to cells expressing the corresponding receptors. Replacing the ligands led to cleaving SNAP25 in NETs, a component of the soluble *N*-ethylmaleimide-sensitive fusion protein attachment protein receptor (SNARE) complex responsible for vesicle exocytosis, thereby sequestering hormone and neurotransmitter release [101]. However, the targeting ligands were not specific to NETs and were limited to blocking neurotransmitter release. More importantly, SV2 was not recognized as a target for NET specific therapies and drug delivery site.

In this study, we demonstrated that the recombinant HCR (rHCR) preferentially targets and enters NE cancer cell lines without the neurotoxicity of the full-length BoNT/A. Additionally, expression of NE differentiation markers chromogranin A (CgA) and achaete-scute complex 1 (ASCL1) were significantly reduced when treated with rHCR, especially in lung and pancreatic NE cancer cell lines [87, 102]. Our data suggest that SV2 proteins are promising targets for treating and delivering drugs to NETs, and rHCR may have palliative therapeutic potential and an application for a drug delivery vehicle.

5.3 Materials and Methods

Cell lines and cell culture: The following cell lines were purchased from ATCC (Manassas, VA): NG108-15, A439, H727, H226, and TT. All cell lines purchased from ATCC were maintained as instructed by the manufacturer, except TT cell line was maintained in RPMI-1640 supplemented with 10% fetal bovine serum (FBS; Gibco) and 1% penicillin-streptomycin

(P/S; Gibco). MZ-CRC-1, FTC-236, TPC-1, HTh7, and Panc-1 cell lines were received from Dr. Herbert Chen Lab. BON cell line was cultured and maintained in Dr. Chen Lab throughout the study. MZ-CRC-1, FTC-236, and BON cell lines were maintained in Dulbecco's modified Eagle's medium (DMEM) supplemented with 10% FBS and 1% P/S. TPC-1 and HTh7 cell lines were maintained in RPMI-1640 supplemented with 10% FBS and 1% P/S. Panc-1 cell line was maintained in DMEM supplemented with sodium pyruvate, 10% FBS and 1% P/S. Cell line identities were verified by short tandem repeat (STR) analysis either at the end of the experiments (H727, A549, H226, and TT) or after vial thaw (NG108-15, FTC-236, TPC-1, and HTh7). For BON cell line, a vial containing the authenticated cell line was received directly from Dr. Evers, which was then immediately expanded and stored in liquid nitrogen. All cell lines were maintained no more than 25 passages post vial thaw.

BoNT/A and rHCR: BoNT/A was received from Eric Johnson Lab (University of Wisconsin) and rHCR was received from Dr. Joseph T. Barbieri (Medical College of Wisconsin, Milwaukee, WI). rHCR was produced and purified as previously described [103].

Fluorescent microscopy: Cells were fixed with 4% paraformaldehyde and permeabilized with Triton-X 100. The samples were then stained with the primary rabbit anti-BoNT/A (Eric Johnson Lab) and mouse SV2 (DSHB) antibodies. For the secondary antibodies, anti-rabbit AlexaFluor 488 and anti-mouse AlexaFluor 568 (Life Technologies) were used. Hoechst (Life Technologies) was used to stain nucleus. All images were acquired using Nikon Eclipse Ti inverted fluorescent microscope with PlanFluor 20x objective (Nikon Instrument), and images were captured using Nikon DS-Qil Mc CCD camera and acquired using NIS-Element Version D 3.10 software. For image analysis, refer to Figure S4.

Image analysis: The captured images were threshold selected and used as regions of interest (ROI). The mean RFU within the ROI of BoNT/A or rHCR untreated samples was subtracted from the treated sample for quantification (Supplementary Figure 7). All images were processed and analyzed using ImageJ.

SNAP25 cleavage assay: All SNAP25 expressing cells were plated on 96-well plate at ~ 40,000 cells/well and incubated for 48 hours. After 48 hours, spent media was carefully aspirated and the cells were fed with 50 μl of fresh media containing desired concentration of BoNT/A. Cells were then incubated for additional 48 hours and lysed directly with LDS buffer for Western blot.

Western blot: The primary antibodies for the following were used to run western blot: anti-SV2A (Synaptic Systems); anti-SV2C (Synaptic systems); anti-SNAP25 (Synaptic Systems); anti-β-actin (Sigma-Aldrich); anti-BoNT/A was a kind gift from Eric Johnson Lab (University of Wisconsin-Madison); anti-CgA, anti-ASCL1, anti-GAPDH were kind gifts from Dr. Herbert Chen. The following secondary antibodies were used: anti-mouse IRDye 800 (Li-Cor); anti-guinea pig IRDye 800 (Li-Cor); anti-mouse HRP and anti-rabbit HRP (Invitrogen). For Western blot of SV2A, SV2C, and SNAP25, cell lysates were mixed with LDS buffer and loaded into 4-12% Bis-Tris NuPAGE gel (Life Technologies). The gel was transferred onto a 0.2 μm Mini Nitrocellulose Transfer Pack by Trans-Blot Transfer System (Bio-Rad). Li-Cor Odyssey two-channel infrared imager was used for detecting SV2A, SNAP25, and β-actin (Li-Cor), whereas SV2C was detected using Bio-Rad ChemiDoc^{TM} System. For SNAP25 cleavage assay, 12% Bis-Tris NuPAGE gel was used instead and optical densitometry tool in ImageJ (NIH) was used to determine percent cleavage of SNAP25.

Statistical analysis: GraphPad Prism 6 software (GraphPad) was used to compute one-way ANOVA followed by Tukey's multiple comparison test except for Figure 24, which was analyzed by Student's 2-tailed t test. $P \leq 0.05$ was considered significant

.

5.4 Results and Discussion

We first verified expression of BoNT/A protein receptors SV2A and C [38] in human NE cancer cell lines—bronchopulmonary carcinoid H727, medullary thyroid cancer (MTC) MZ-CRC-1 and TT, and pancreatic carcinoid BON–and compared to the non-NE cancer cell lines—lung adenocarcinoma A549, mesothelioma H226, follicular thyroid cancer FTC-236, anaplastic thyroid carcinoma HTh7, and papillary thyroid carcinoma TPC-1, and pancreatic adenocarcinoma Panc-1 (Table 3). A Western blot analysis revealed that all of the tested NE cancer cell lines express SV2A and C except for H727, which only expresses SV2A. Interestingly, a non-NE cancer cell line FTC-236 also expresses both SV2A and C, but at lower molecular weights (Figure 22). SNAP25, the substrate of BoNT/A that mediates vesicular exocytosis, is expressed in all tested NE cancer cell lines and in A549, which indicates partial adoption of neuronal characteristics (Figure 22) [104].

BoNT/A enters peripheral neurons upon association with the receptors via calcium-mediated SV2 recycling activities [4, 70]; therefore, we hypothesized that rHCR can be used as a ligand to target SV2 positive NE cancer cells. We treated MTC, pancreatic carcinoid and non-NET cell lines with 5 ng μL^{-1} of BoNT/A for 24 hours. The treatment concentrations were determined in a low SV2 expressing H727 cell line (Supplementary Figure 4). The cell lines were then fixed and immunocytochemically labeled with BoNT/A antibody and observed under fluorescent microscope. The BoNT/A NE cancer cell lines MZ-CRC-1, TT, and BON showed

strong fluorescent signals but not in the non-NE cancer cell lines H226, FTC-236, and TPC-1 (Supplementary Figure 5).

Table 3: List of human cancer cell lines tested.
The origins and types of both neuroendocrine (■) and non-neuroendocrine (□) cell lines are listed.

	Cell Line	Origin	Type	Reference
	NG108-15	Brain	Neuroblastoma and glioma	[105, 106]
■	H727	Lung	Bronchopulmonary typical carcinoid	[107, 108]
□	A549	Lung	Human adenocarcinoma	[109]
□	H226	Lung	Squamous cell carcinoma; mesothelioma	[110]
■	MZ-CRC-1	Thyroid	Human metastatic medullary thyroid carcinoma	[111, 112]
■	TT	Thyroid	Human medullary thyroid carcinoma	[111]
□	FTC-236	Thyroid	Human lymph node metastasis of a follicular thyroid cancer	[113]
□	HTh7	Thyroid	Human anaplastic thyroid carcinoma	[114, 115]
□	TPC-1	Thyroid	Papillary thyroid carcinoma	[115, 116]
■	BON	Pancreas	Epithelioid carcinoma, pancreatic carcinoid	[117]
□	Panc-1	Pancreas	Adenocarcinoma	[118]

Interestingly, BoNT/A does not appear to target FTC-236 cells despite SV2A and C expressions (Figure 22). SV2 are glycoproteins and the lower molecular weights of SV2

observed in FTC-236 suggests lack of proper glycosylation. Previous studies demonstrated a significant reduction of BoNT/A and E entry into neurons when N-glycosylation at N537Q of SV2A was missing [119]. Moreover, the absence of SNAP25 expression indicates lack of SNARE complex, which regulates the neurotransmitter release. Thus, the impaired binding affinity of BoNT/A to SV2 paired with missing SNARE complex responsible for calcium-mediated SV2 endocytosis could explain lack of accumulation of BoNT/A in FTC-236 cells despite the expression of SV2A and C.

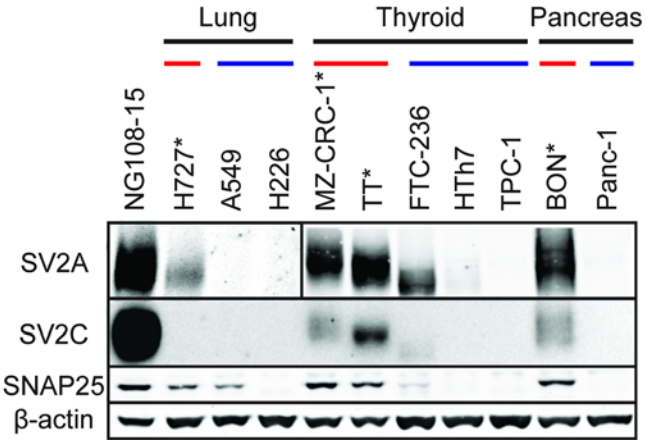

Figure 22: Expression pattern of SV2A and C and SNAP25 in various human cancer cell lines.
Western blot of a neuronal cell line, NG108-15, NE cancer cell lines (indicated with red line above the blot and asterisk), and non-NE cancer cell lines (blue line). All NE cancer cell lines express SV2A and C, and SNAP25, except H727 only expresses SV2A. Non-NE cancer cell lines A549 expresses SNAP25 and FTC-236 expresses SV2A and C but at lower molecular weights. Note that SV2A expression in NG108-15 and H727 cell lines was weak, and Western blot analysis was performed separately.

Although the full-length BoNT/A is clinically used for localized delivery at a very low dosage [4], it is not practical for treating NE cancers due to the small size of nodules and spreading to distant secondary sites, which requires systematic delivery of the therapeutic reagents. The systematic delivery of BoNT/A would cause severe paralysis and even death [1];

therefore, the toxicity imposing catalytic LC domain of BoNT/A must be removed before the systemic delivery. We hypothesized that rHCR will retain SV2 and GT1b receptor binding affinity enabling the use of rHCR as a ligand to target NETs.

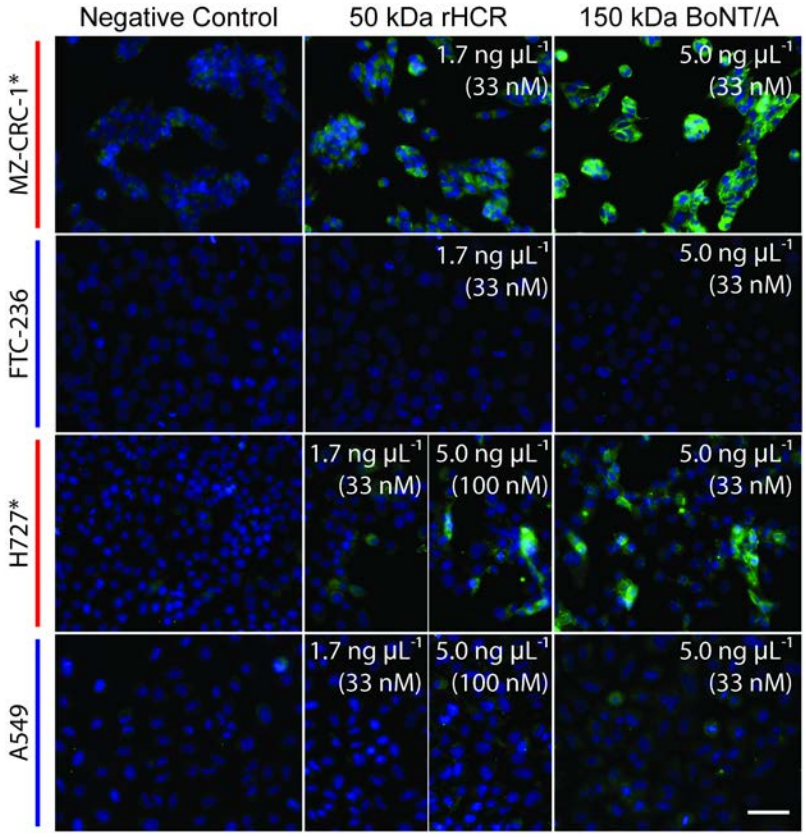

Figure 23: rHCR and BoNT/A target NE cancer cell lines.
NE cancer cell lines MZ-CRC-1 and H727 and non-NET cell lines FTC-236 and A549 were treated with rHCR and BoNT/A for 24 hours. Cells were then fixed and stained for nucli using Hoechst (blue), and labeled with anti-BoNT/A primary antibody. Fluorescent microscope images of rHCR (green, middle panels), and BoNT/A (green, right panels) are displayed. Both NE cancer cell lines showed strong fluorescent signal above the background. A549 cell line showed above the background fluorescent signal whereas FTC-236 did not. Scale bar: 20 µm.

NE cancer cell lines MZ-CRC-1 and H727 and non-NE cancer cell lines FTC-236 and A549 were either treated with BoNT/A or rHCR for 24 hours, followed by immuno-cytochemically labeling with anti-BoNT/A primary antibody. Two different concentrations of

rHCR were tested either matching the molar or mass concentrations of rHCR to BoNT/A at 33 nM or 5 ng μL^{-1} respectively to assess detection sensitivity. Upon 24-hour treatment, positive fluorescent signal was observed in both MZ-CRC-1 and H727 cells (Figure 23 and Supplementary Figure 4). The lower fluorescent intensity of the cells treated with rHCR was mainly due to less binding sites for the primary antibody on rHCR (Supplementary Figure 6). No fluorescent signal was detected in FTC-236 in accordance to our previous observation (Figure 23); however, noticeable amounts of fluorescent signal was observed in the non-NET lung adenocarcinoma A549 (Figure 23), which expressed SNAP25 but not SV2A and C (Figure 22).

It is important to note the association of rHCR and BoNT/A to A549 cells. In previous studies, greater amount of BoNT/A was coimmunoprecipitated with SV2 compared to gangliosides alone, and increased amount of BoNT/A was coimmunoprecipitated when gangliosides were added to SV2 rich mouse brain extract [38, 120]. In addition, reduced BoNT/A activity was observed in ganglioside-depleted neuroblastoma [50]. Collectively, BoNT/A can target gangliosides alone, although to a lesser extent without SV2. Although A549 is not a NE cancer cell line, the expression of SNAP25 revealed possible partial neuronal characteristics [104], and thus may express gangliosides, which are abundant in neuronal cells.

We then quantified the relative fluorescent intensity (RFU) of immunocytochemically labeled rHCR on treated cells (RFU) as described in Supplementary Figure 7. In the lung cell lines, RFUs of H727 and A549 were significantly greater than in H226 (p = 0.0003 and 0.0012 respectively) but failed to show statistical significance between H727 and A549 (Figure 24A). Although not statistically significant, perceptible difference was observed between the two tested pancreatic cancer cell lines BON and Panc-1 (Figure 24B; p = 0.07). Moreover, rHCR

preferentially targeted thyroid NE cancer cells as opposed to the non-NE cancer cell lines (Figure 24C; $p \leq 0.0001$).

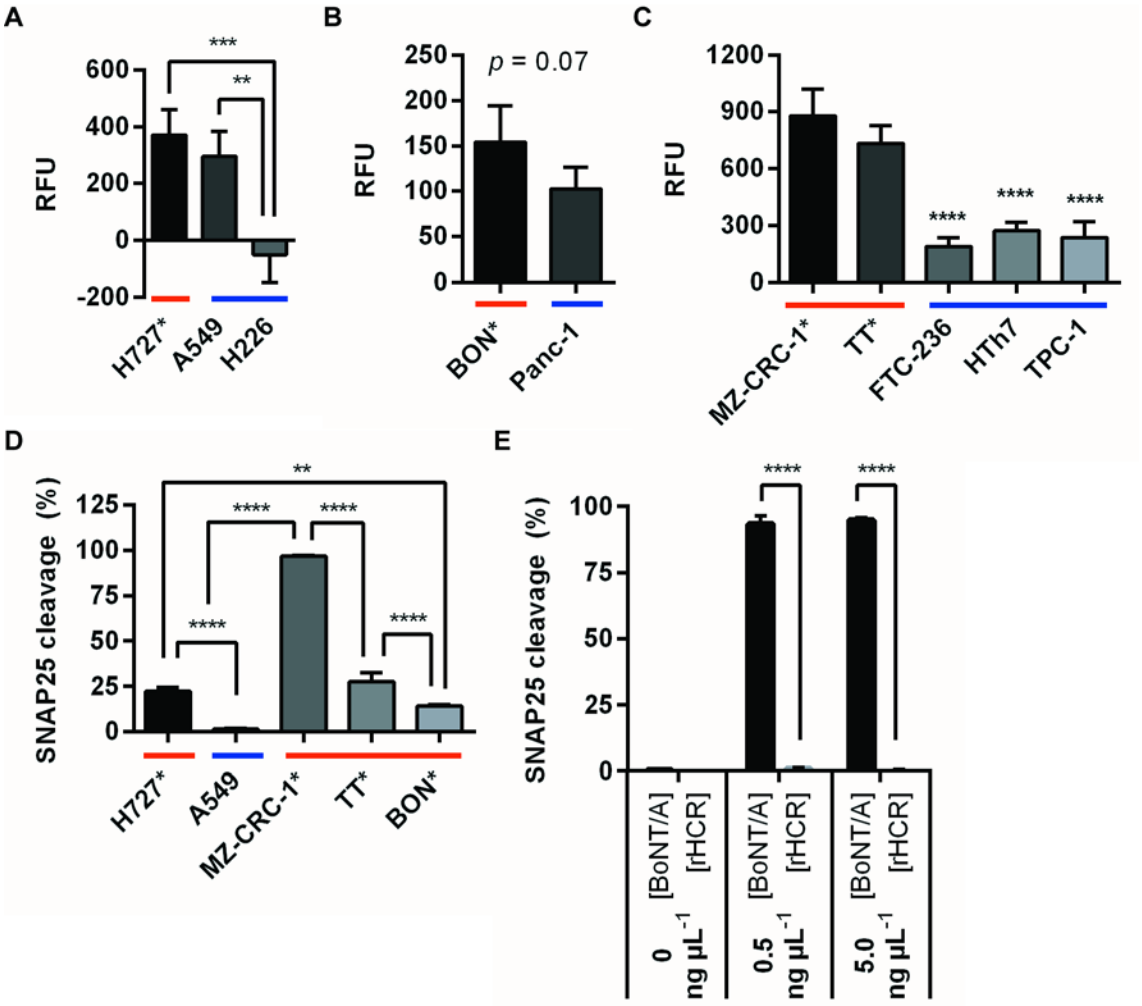

Figure 24: Quantitative analysis of rHCR targeting and entering NE cancer cell lines via image analysis and adopting SNAP25 cleavage assay.
(A) NE cancer cells (red and asterisk) and non-NE cancer cells (blue) originating from (A) lung, (B) pancreas, and (C) thyroid were treated with 5 ng μL^{-1} (100 nM) of rHCR, incubated for 24 hours, and immunocytochemically labeled with anti-BoNT/A antibody. The mean relative fluorescent intensity (RFU) of the cells were quantified and plotted. (D) All SNAP25 expressing cell lines were treated with 5 ng μL^{-1} (33 nM) of BoNT/A and analyzed for SNAP25 cleavage by Western blot. MTCs were most sensitive to BoNT/A followed by bronchopulmonary and pancreatic carcinoids. No SNAP25 cleavage was observed in the non-NE cell line A549 indicating NE specific internalization of rHCR. (E) No SNAP25 was cleaved in NG108-15 cells when treated with rHCR whereas nearly all SNAP25 was cleaved when treated with BoNT/A indicating rHCR is not neurotoxic. For all experiments, error bars represent standard deviation at $n = 4$; ** $p \leq 0.01$; *** $p \leq 0.001$; **** $p \leq 0.0001$.

Although rHCR specifically targeted thyroid NE cancer cells, no statistically significant difference was observed in lung and pancreas cancer cells between the NE and non-NE origin. To assess whether rHCR can be used as a drug delivering ligand, we studied at the internalization of BoNT/A into NE cancer cells by adopting SNAP25 cleavage assay [73]. The assay involves treating the cells with the full-length BoNT/A, which then cleaves SNAP25 upon endocytosis. By measuring the percent cleavage of SNAP25, we can infer the relative amount of BoNT/A that entered the cells, which is also proportional to the amount of rHCR in the cells.

Interestingly in the lung cancer cell lines, the SNAP25 was cleaved only in H727 cells (Figure 24D, Supplementary Figure 8A-B). This result indicates that both BoNT/A and rHCR may target A549 cells but are not endocytosed (Figure 23, Figure 24A, Supplementary Figure 8B). As previously noted, calcium is required for synaptic activities and SV2 recycling, which are necessary for the entry of BoNT/A into the cells [70]. Despite the possible partial neuronal characteristics of A549 cells, they lacked expression of SV2A and C, the transmembrane transporters that in part regulate neurotransmitter release [121, 122]. Therefore, A549 cells neither have proper vesicular activity nor machinery for BoNT/A to enter the cells. The SNAP25 cleavage in lung NE cancer cells showed that rHCR can be used as a NE cancer targeting drug delivery ligand since endocytosis is required for targeted therapies. In the metastatic MTC cell line MZ-CRC-1, nearly all SNAP25 was cleaved and was significantly more than that of the non-metastatic MTC cell line TT (Figure 24D, Supplementary Figure 8C-D). Metastatic MTCs are aggressive cancers with limited clinical success [123]. Nevertheless, our data suggested that rHCR can effectively target metastatic MTC, potentially opening new therapeutic development opportunities. SNAP25 expressed in pancreatic NE cancer cell line BON was also cleaved (Figure 24D, Supplementary Figure 8E). Collectively, BoNT/A can

target thyroid, lung, and pancreas NE cancer cell lines (p = 0.0015 between H727 and BON; not labeled in Figure 24D). Finally, SNAP25 in a neuronal cell line, NG108-15, was cleaved only when treated with the full-length BoNT/A (Figure 24E, Supplementary Figure 8F) indicating that rHCR will not cause botulism implicated toxicity.

The preferential NET targeting was encouraging and we further sought to test whether rHCR alone could have palliative treatment effects on NETs. SSA and SSTR association inhibits adenylyl cyclase activities, which activates potassium channel while deactivating calcium channels that leads to lower bioactive hormone and neurotransmitter production [124, 125]. Although the function of SV2 proteins are not yet fully elucidated, evidences suggest that they work with or affect the function of calcium channels [121]. We hypothesized that calcium signaling across the plasma membrane will be disrupted upon association with rHCR thereby suppressing the production of bioactive hormones.

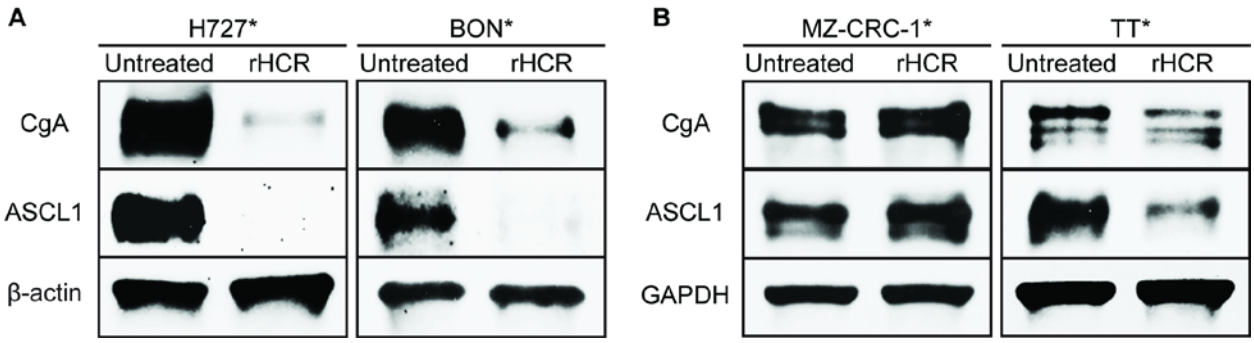

Figure 25: Suppression of CgA and ASCL1 in rHCR treated NE cancer cell lines.
(A) Lung and pancreatic NE cancer cell lines, H727 and BON respectively, were treated with a single dose of rHCR at 5 ng μL^{-1} (100 nM) and incubated for three days. Significantly reduced amount of NE differentiation markers, CgA and ASCL1, was observed. (B) Thyroid NE cancer cell lines were treated with 5 ng μL^{-1} (100 nM) of rHCR for four days, with retreatment on day two. Significant reduction of CgA and ASCL1 was observed in TT cell line, but not in MZ-CRC-1 cell line.

CgA and ASCL1 are both NET markers that are used for predicting clinical efficacies, and which were shown to correlate with the NE cancer treatment efficacies [87]. We treated lung and pancreatic NE cancer cell lines, H727 and BON respectively, with 100 nM of rHCR for three days and performed Western blot analysis. The expression of CgA and ASCL1 was significantly decreased after treating with rHCR (Figure 25A). Additionally the expression of CgA and ASCL1 was also significantly reduced in TT cells when treated with 100 nM of rHCR for four days with retreatment after two days although no change was observed in MZ-CRC-1 cells (Figure 25B). MTCs are also prone to be more resistant to SSAs treatment (our experimental observation) and metastatic MTCs are especially difficult to treat. Although our data showed that the metastatic MTC cell line was more susceptible to BoNT/A uptake, the signaling and mechanism relating to CgA and ASCL1 suppression seem to involve downstream signaling upon rHCR and SV2 binding.

In summary, we successfully demonstrated that SV2A and C are expressed in NE cancer cell lines except for H727, which only expresses SV2A. Moreover, rHCR has a potential for suppressing the production of bioactive hormones in NETs revealing palliative therapeutic potential and rHCR can be used as a targeting ligand for drug delivery to NETs. Follow up *in* vivo studies must be conducted to verify clinical benefits of rHCR and the specificity of rHCR to NETs to further support our data. We plan to conjugate fluorescent proteins to rHCR to enable preclinical animal studies, direct quantification, and the assessment of rHCR accumulation in NETs. Additionally, we are interested in understanding mechanisms of how rHCR suppresses NE differentiation markers CgA and ASCL1 and further testing the reduction of bioactive hormones and neurotransmitters. Although rHCR was not effective in suppressing CgA and

ASCL1 in metastatic MTCs, they take up more rHCR than the other tested NE cancer cells and, therefore, rHCR can be used as the drug delivery vehicle towards developing targeted therapy.

5.5 Supplementary Data

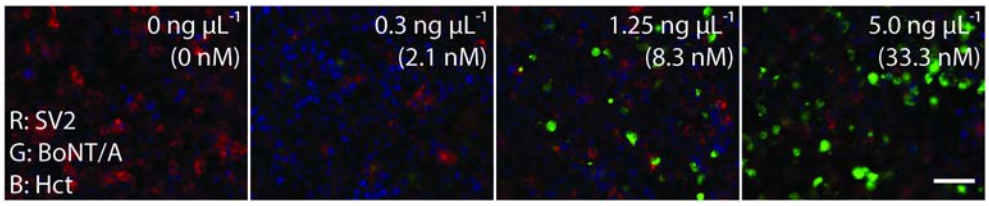

Supplementary Figure 4: BoNT/A targets lung NE cancer cell line H727 in a dose-dependent manner.
H727 cells were treated with varying concentrations of BoNT/A (green) up to 33.3 nM for 24 hours and immunocytochemically labeled. The fluorescent intensity increased with the increased amount of BoNT/A concentration. The anti-SV2 primary antibody recognizes all three isoforms of SV2 (red). The nucleus was labeled with Hoechst (blue). Scale bar: 20 µm.

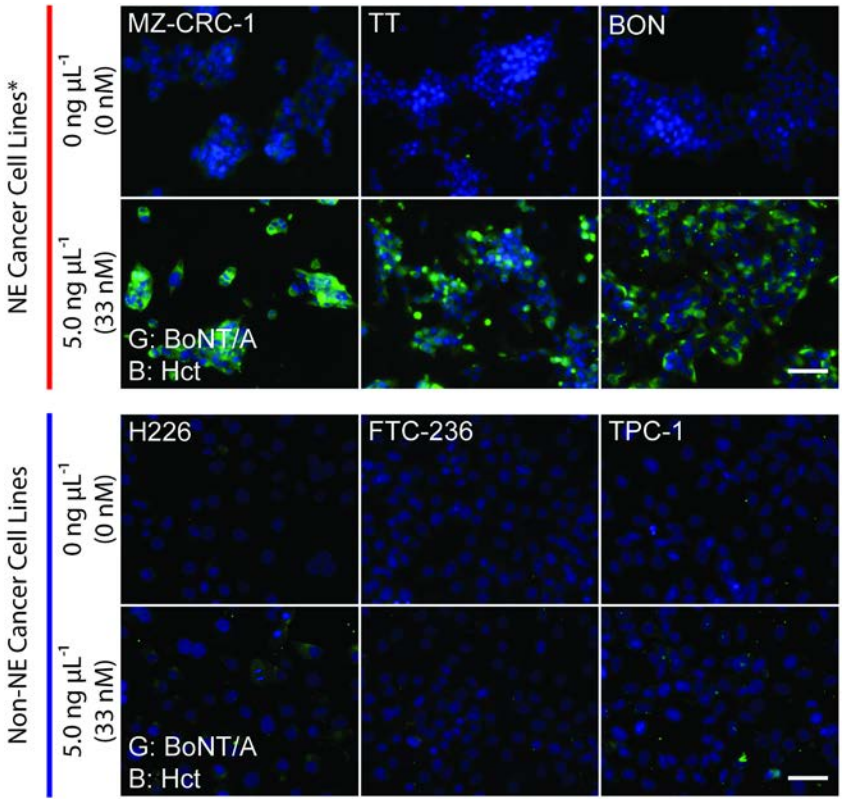

Supplementary Figure 5: The full-length BoNT/A targets NE cancer cells.
Three NE cancer and three non-NE cancer cell lines were treated with 5 ng μL^{-1} of BoNT/A and incubated for 24 hours. Cells were fixed and stained for nucli using Hoechst (blue) and immunocytochemically labeled with anti-BoNT/A antibody (green). Fluorescent microscope images indicate BoNT/A specifically targets NE cancer cell lines. Scale bar: 20 µm.

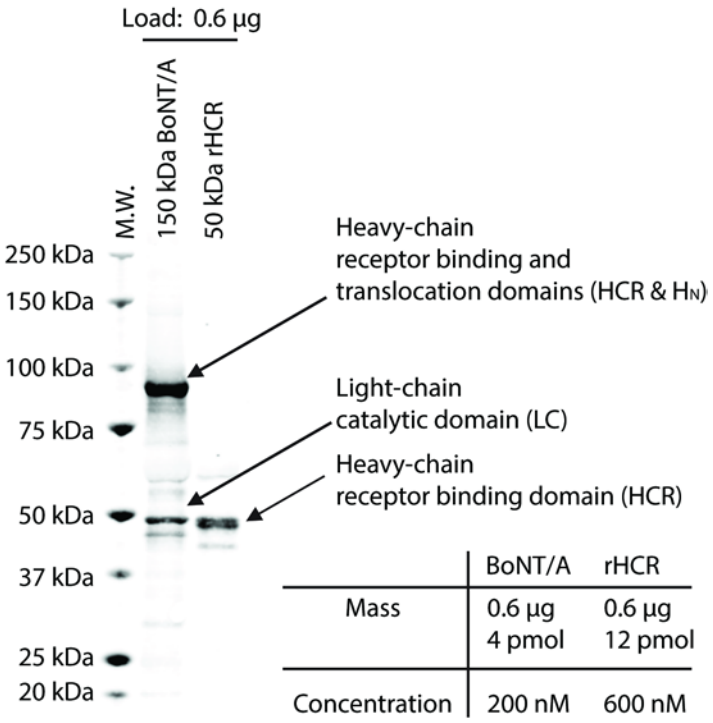

Supplementary Figure 6: Western blot of the full-length BoNT/A and rHCR.
An equal amount of purified BoNT/A and rHCR were loaded and labeled with the anti-BoNT/A primary antibody. The purified BoNT/A was reduced with 100 mM DTT to break down disulfide bonds between the heavy and light-chains shown at 100 kDa and 50 kDa molecular weight bands respectively. Western blot showed that more binding sites are available on the full-length BoNT/A than rHCR.

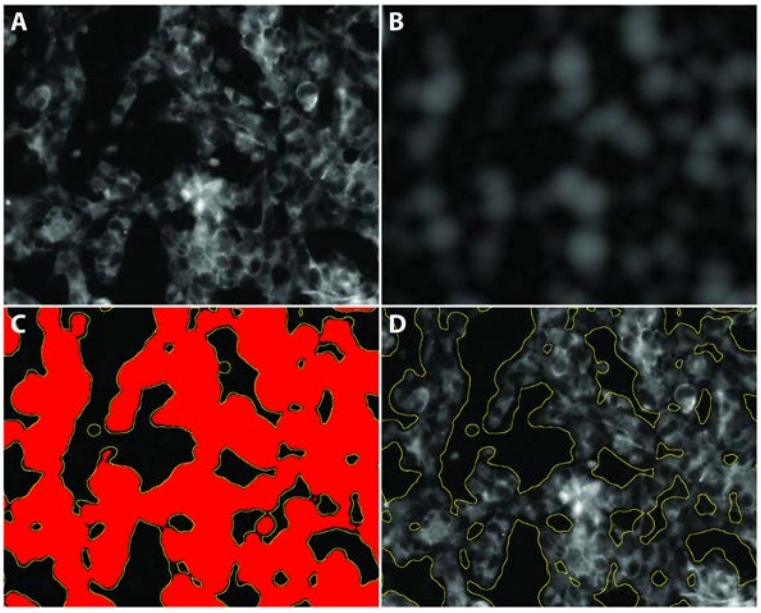

Supplementary Figure 7: Image analysis steps.
(A) Image was loaded onto ImageJ software for processing. (B) Background was created around the cells using image processing tool in ImageJ. (C) The background was threshold selected using threshold tool in ImageJ. (D) The threshold was used to select regions of interest and overlaid on the original image. The mean fluorescent intensity (RFU) or the fluorescent intensity distribution histogram was computed for quantification.

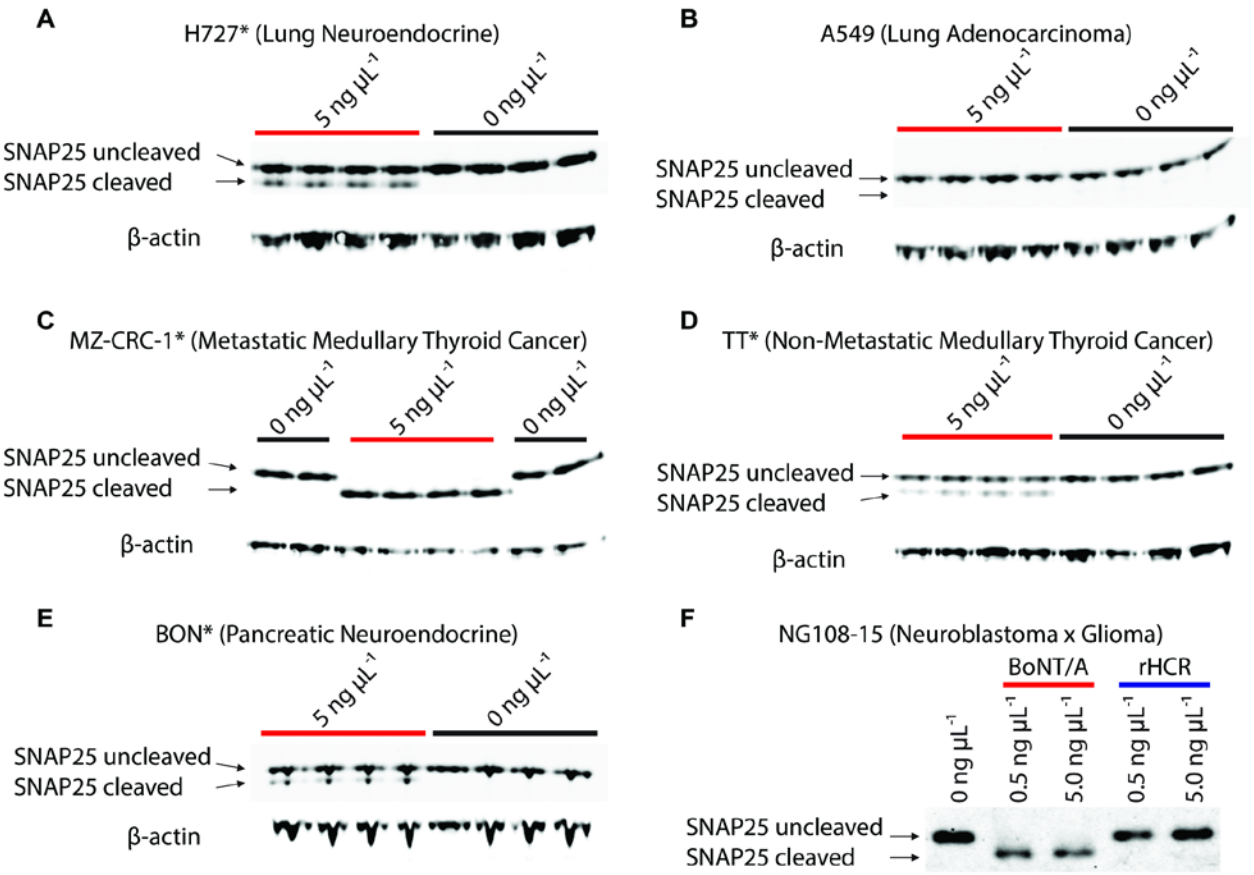

Supplementary Figure 8: BoNT/A cleaves SNAP25 only in NE cancer cell lines.
(A-B) Lung cancer cell lines, (C-D) thyroid cancer cell lines, and (E) pancreatic cancer cell line that expressed SNAP25 were treated with 5 ng μL^{-1} of BoNT/A and incubated for 48 hours. No SNAP25 cleavage was observed in (B) lung adenocarcinoma A549, which did not express SV2A and SV2C, which indicates that BoNT/A was not endocytosed into the cells. (F) A neuronal cell line, NG108-15, was treated with BoNT/A or rHCR at 0.5 and 5.0 ng μL^{-1}. Nearly all SNAP25 was cleaved when treated with the full-length BoNT/A; however, SNAP25 was not cleaved when treated with rHCR. For all SNAP25 assays, the cells were directly lysed using LDS buffer post 48-hour treatment and transferred blots were analyzed using Odyssey Imager (Li-Cor) to assess relative amount of SNAP25 cleaved.

5.6 Acknowledgements

We thank Dr. Eric Johnson, Sabine Pellett and William Tepp at the University of Wisconsin-Madison and Dr. Joseph Barbieri at the Medical College of Wisconsin, Milwaukee, WI for supplying BoNT/A and rHCR for this study. We also thank the University of Wisconsin

Translational Research Initiative in Pathology laboratory, in part supported by the UW Department of pathology and Laboratory Medicine and UWCCC grant P30 CA014520, for use of its facilities and services.

Funding: This research was supported by the U.S. Department of Homeland Security Science and Technology Assistance Agreement No. 2007-ST-061-000003, National Center for Food Protection and Defense (2010-ST-061-FD0001), NIH/NCI R01 CA121115, the American Cancer Society MEN2 Professorship, a Caring for Carcinoid Foundation-American Association for Cancer Research grant, and by the National Research Service Award (NRSA) T32 EB011434.

Disclaimer: The views and conclusions contained in this document are those of the authors and should not be interpreted as necessarily representing the official policies, either expressed or implied, of the U.S. Department of Homeland Security. The Department of Homeland Security does not endorse any products or commercial services mentioned in this publication.

Chapter 6 – Future Directions

6.1 Biosensor for Detecting Botulinum Neurotoxins

In this thesis, I started off with the challenges and progresses made in reliably quantifying the amount and catalytic activity of BoNT/A. In Chapter 2, I cocultured Schwann cells and showed significant improvement in the detection sensitivity as well as culturing the cells in a microscale cell culture system. Later in Chapter 3, I used Taguchi's design-of-experiment followed by step-by-step approach in optimizing media to achieve BoNT/A detection limit below 1 LD_{50} U. Although the cell-based assay that I developed is sensitive and can replace mouse bioassay, there is still much room for improvements.

As part of the project described in Chapter 4, I expressed ChR2 in NG108-15 cells, which can fire action potentials via light stimulation. It would be interesting to culture ChR2 transfected NG1080-15 cells, differentiate them in the media that I developed in Chapter 3, and periodically expose the cells with blue light to activate neurons after treating them with BoNT/A. As demonstrated by coculturing with Schwann cells, which increases synaptic activities of motor neurons, I suspect more BoNT/A will enter the cells with increased synaptic activity enhanced by light stimulation. Collectively, (i) coculturing NG108-15 and Schwann cells at microscale, (ii) using the optimize medium for the assay, and (iii) stimulating neurons with light in combination may even further improve the detection sensitivity.

The limitation of cell-based assay lies in the reliance on Western blot for analysis. Although we could not get the primary antibody that specifically recognizes BoNT/A cleaved SNAP25 [126], using this antibody will allow developing ELISA for the end-point measurement replacing Western blot. Additionally, our lab developed microfluidic-based phase separation

technique that can be used as the end-point measurement that has higher throughput than conventional ELISA [127]. Finally, the μPW device can be used to detect muscle paralysis upon BoNT/A treatment, which the method I described in Chapter 4. Although the method is not yet ready for an application, I can envision that that quantifying muscle paralysis *in vitro* in the near future.

6.2 *In Vitro* Organotypic Model Development – Neuromuscular Junction

The most reliable form of NMJ so far has been extracting primary motor neurons and skeletal myoblasts from mice and culturing them on petri-dishes. This method has severe limitations including (i) sacrificing animal for obtaining cells, (ii) culturing on a surface as an adherent culture limiting the quantification of muscle force, (iii) laborious steps in assessing the formation of functional synapses with electrophysiology, and (iv) detachment of the cells from the surface overtime.

Leveraging microsystems fabrication technique widely used in microelectromechanical systems, I was able to build micro-pillar micro-well device with overhangs that allows anchoring skeletal muscle tissues. However, similar engineered cell culture systems and tools were not widely adopted in the neuroscience research field due to the required access to cleanroom and equipment for the fabrication, in addition to challenges in reproducing the shape and size of the master mold. I solved these challenges by replacing the photolithography with 3D printing that obsoletes need for such facility where the master mold can be easily ordered through rapid prototyping companies and simply pouring PDMS to make devices. Additionally, the 3D printing created high aspect ratio features, where I was able to print 100 μm x 800 μm x 1500 μm (width x length x height) size pillars.

The device can be used to coculture skeletal muscle and MNs derived from hESCs and hiPSCs, to truly generate human *in vitro* model of NMJ. Additionally, expressing ChR2 into MNs will enable *in situ* quantification of the function, and configured for automated high-throughput screening platform towards the discovery of novel therapeutic targets and drugs for the patients suffering from various neuromuscular diseases and degeneration.

The first generation of the device is merely an improved replica of the device pioneered by Professor Christopher Chen's group [79]. The device does not compartmentalize MNs and skeletal myotubes, thus the dendrites of MNs may form synapses with myotubes possibly triggering false positive signals. Instead, I envision an improved design that can physically separate the two cell types recapitulating human anatomy while teasing out noises from dendrites. hESC and iPSC cell lines that are transfected with inducible ChR2 vector can be established to add light activation function, eliminating pharmacological and electrophysiological stimulation that complicates system and signals. Using inducible vector for ChR2 might serve to better direct stem cell fate towards desired lineage, and unfiltered ambient light may trigger ChR2 activation sending calcium signal across the cell membrane interfering with the differentiation. Moreover, by advancing the fabrication and design, we can introduce other players such as Schwann cells in PNS, and astrocytes and oligodendrocytes in CNS. Adding these components may be crucial in developing disease models.

Motor neuron diseases are not confined within the defects in MNs, but affected by other neighboring cells. Recent studies demonstrated toxicity of amyotrophic lateral sclerosis (ALS) astrocytes to MNs [128, 129], replenish of immature oligodendrocytes after degeneration impaired neuromuscular function [130], and neuroinflammation caused by activated astrocytes and microglia [131] with superoxide dismutase 1 (SOD1) mutation can lead to ALS. Adding to

the complexity, SOD1 mutation, one of several mutations identified in familial ALS, restricted to skeletal muscle showed muscle impairment without damaging MNs in one study [132] although others showed MN degeneration in similar studies [133, 134]. Furthermore, reduction of ALS-linked dismutase in Schwann cells accelerated, instead of delaying, disease progression especially when coupled with insulin-like growth factor 1 (IGF-1) [135]. Similarly, suppressing the expression of survival motor neuron 1 (SMN1) in tissues other than MNs induced type I spinal muscular atrophy (SMA1) [136]. These evidences support that studying neuromuscular diseases cannot be limited to a single cell type, but contributions from other players must be taken into account.

To achieve such advancement in generating disease models *in vitro*, strong collaboration among engineers, biologists, and developmental scientists must be established. With the emergence of gene editing technique such as CRISPR-Cas9, familial neuromuscular degeneration and dystrophies can be fixed or induced in iPSCs. Side-by-side comparisons of the tissue engineered diseased and corrected models will be critical.

6.3 Signaling in Neuromuscular Junction

In the past, significant challenges in developing a functional NMJ was in part due to the complexity of the intercellular signals involving, at minimum, motor neurons (MNs), skeletal muscle fibers, and Schwann cells. Recently, keratinocyte was found to cap terminal Schwann cells supporting structural integrity of the synapses with possibly other intercellular signaling to support maintenance and development of the synapses [40]. Additionally, explanted skeletal muscle fibers cultured *in vitro* (primary skeletal muscle cells) survived for a much shorter time period compared to the culture containing MNs [137, 138]. Retrospectively, skeletal muscle

fibers secrete various neurotrophic factors such as transforming growth factor-beta (TGFβ), basic fibroblast growth factor (bFGF), brain-derived neurotrophic factor (BDNF), and neurotrophin-3 (NT-3) promoting survival of MNs through retrograde signaling [139, 140]. These evidences suggest that MNs and skeletal muscle fibers need to work in concert for survival.

Moreover, MNs and skeletal muscles cooperatively seem to differentiate post-synaptic end of NMJ prior to motor neuron innervation, also known as AChR clustering or pre-patterning of muscle fiber. A neural factor agrin was discovered and shown to promote post-synaptic differentiation by activating muscle specific kinase (MuSK) responsible for the AChR clusting [141-143]. However, subsequent studies reveal confounded results competing neural agrin induced [144, 145] versus aneural activation of MuSK in post-synaptic differentiation and pre-pattering of myotubes at NMJ [146]. Despite much effort, evidence continued to point at different directions indicating that there might be unidentified players that mediate agrin-MuSK interactions. Delineating the mechanism may reveal developmental defect in MNs and skeletal muscle tissues to better understand degenerative diseases and discover targets for treatments. Therefore, access to human and physiologically relevant *in vitro* NMJ model will enable understanding complex signaling, thus foster basic and translational sciences.

Supporting previous literatures that intercellular signaling events among the different cell types forming NMJ are interdependent to each other, I discovered an interesting developmental phenomenon. So far, both developmental and neurodegenerative researches focused on the effects on MNs imposed by the surrounding tissues. Naturally, the contribution of MNs to development of surrounding tissues and regeneration was overlooked. I found intriguing evidence that MNs are involved in the skeletal muscle development and regeneration. When I introduced hESC derived MNs into the human myoblast culture *in vitro*, the development of

process of myoblast into myotubes was accelerated and was much more efficient. Significant activation of myogenin, a transcriptional factor involved in the development of myotubes, strikingly higher expression of myosin heavy chain (MYH), and the formation of myotubes were observed in the culture containing hESC derived MNs (Figure 26).

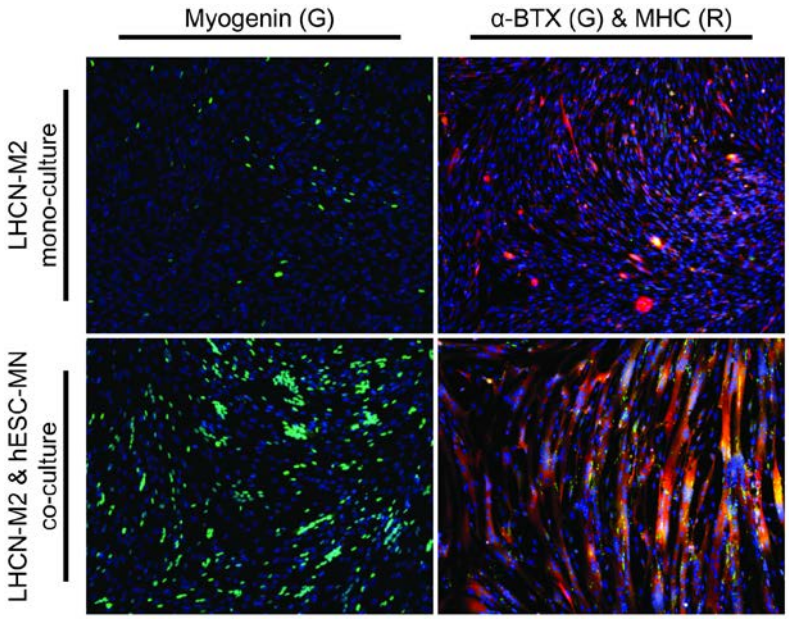

Figure 26: hESC derived motor neurons accelerate skeletal muscle development and maturation.
Increased activation of myogenin and expression of MYH was observed in human skeletal myoblast cells (LHCN-M2) cultured with hESC derived motor neurons (hESC-MN). Hoechst nuclear staining is shown in blue.

My preliminary data suggests MNs is actively involved in the skeletal muscle development and possibly in regeneration, which poses an interesting question to the mechanism of skeletal muscle dystrophies and degeneration—are muscle wasting diseases such as Duchenne muscular dystrophy a truly muscle disease or is it motor neuron disease? It is important to

dissect out the mechanism of these devastating diseases to identify targets for treatment and be able to discover therapeutics to help patients. Thus, it is essential to understand the intercellular interactions through systems of biology and technology development to model diseases.

To begin with, I'd be interested in understanding the role of retinaldehyde dehydrogenase 2 (RALDH-2), which is strongly expressed in limb innervating MNs [147]. RALDH-2 is the main source of RA, a potent cell differentiation factor, which is controlled by limb mesenchyme and MNs [148-150]. It will be interesting to see the transcriptional control of RALDH-2 in limb innervating MNs in relation to *Hox* expression—regulator of MN specification in spinal cord—and how they are inter-related towards muscle development and defects, in addition to neural development.

Additionally, insulin-like growth factor 1 (IGF-1) signaling in skeletal muscle development is another interesting area for research. The release of IGF-1 in neurons is controlled by synaptotagmin 10 mediated neuroendocrine exocytosis [151]. IGF-1 is upregulated via activation of sonic hedgehog (Shh), which was shown to promote differentiation of primary mouse satellite cells that replenish skeletal myotubes. Smoothened mediated MAPK/ERK and PI3K/Akt pathways are involved in the promotion of myotubes regeneration through downstream effector glycogen synthase kinase 3 beta (GSK3β) [152, 153]. GSK3β activation destabilizes β-catenin, sharing Wnt signaling pathway that is regulated by RA. In MNs, SMN1 spliced isoform axonal-SMN (a-SMN) increases production of IGF-1 [154]. Thus it seems possible that MNs with SMA1 phenotype have defective machinery to produce or secrete IGF-1 delaying muscle development as shown in SMA1 defective human fetus [136]. Taken together, I hypothesize that RA and IGF-1 controlled by MNs enhance skeletal muscle

development and regeneration by activating Wnt pathway independently or in concert, which plays a putative role in NMJ development [155].

The two proposed singling pathways are just the start, and more players and complex signaling can be delineated by close collaboration with systems biology experts to narrow down targets and pathways to investigate. Additionally, having a physiologically relevant *in vitro* model of NMJ will serve as a valuable tool to demonstrate mechanisms of the complex interactions among different cellular players, and define these pathways and molecular mechanisms.

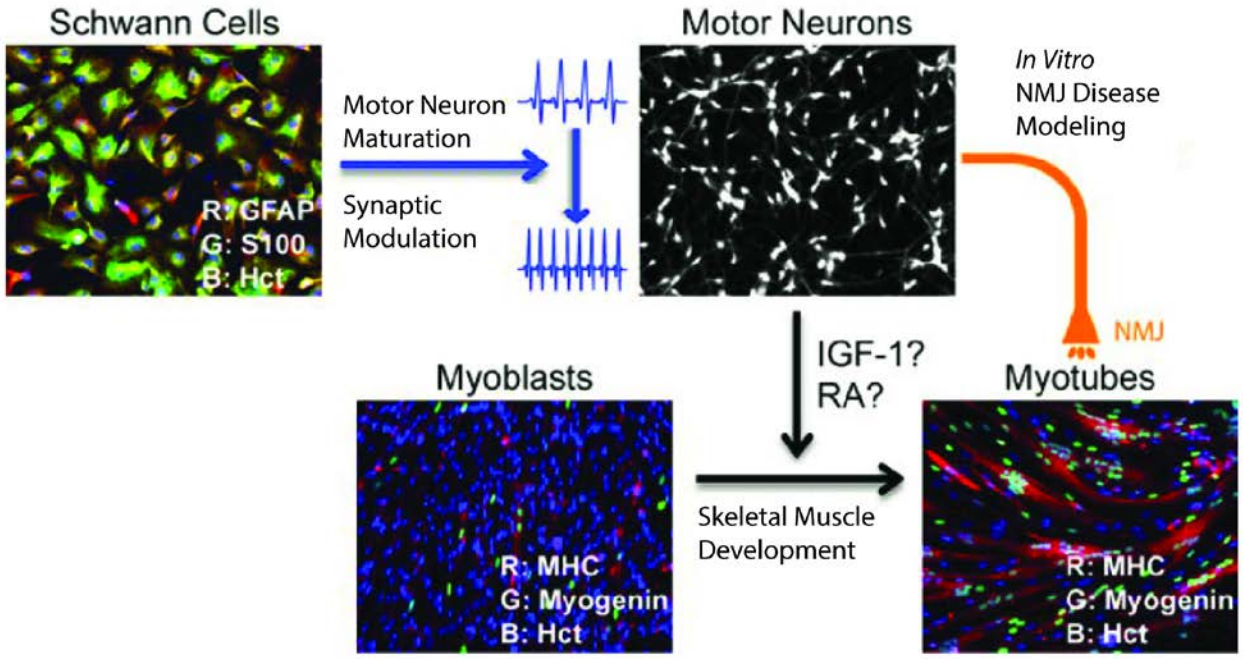

Figure 27: Schematic of future research directions.
Schwann cells modulates synaptic activities of MNs, which then signals, either concurrently or seuqentially, skeletal myoblasts for development and maturation. IGF-1 and RA signaling pathways may play an important role in the development of mature and functioning NMJ.

6.4 Novel Applications of Botulinum Neurotoxin for Neuroendocrine Malignancies

Botulinum neurotoxin type A has been the tying theme of my thesis. The early efforts was on the development a biosensor that can quantify the activity of BoNT/A for the protection against bioterrorism and the safety of patients using BoNT/A analogues for treatment. The sensor development led to interesting project that can potentially have great impact in biomedical research—generation NMJ model *in vitro* by adopting microsystems engineering tools. In addition to the "engineering" approaches in tissue engineering, I investigated potential utility of BoNT/A in neuroendocrine malignancies, which I made a very intriguing discovery.

The function of heavy-chain receptor binding domain of BoNT/A (HCR) has been limited to binding to its receptors SV2 and GT1b. Through my thesis research, I found that HCR alone has an interesting function that suppresses CgA and ASCL1 expressions in human neuroendocrine cancer cells. CgA and ASCL1 are known neuroendocrine differentiation marker, of which the reduction in their expression was correlated with the suppression of bioactive hormone production that has clinical benefits in palliating symptoms of neuroendocrine malignancies. Taking the newly discovered function of HCR, I'd be interested in conducting preclinical studies using animal models carrying neuroendocrine cancers to test clinical efficacies of HCR. Moreover, in collaboration with drug delivery experts, it would be interesting to conjugate HCR with drug carrying nanoparticles to target neuroendocrine cancers to treat highly aggressive malignancies in the future to provide therapies alternatives to SSAs.

In addition to the clinical utility of HCR, the suppression of CgA and ASCL1 in neuroendocrine cells upon HCR treatment may lead to discovering a novel signaling pathway. Such investigation will foster research in cellular plasticity in dedifferentiating neuroendocrine cells and identifying additional clinical targets for neuroendocrine malignancies.

6.5 Conclusions

My thesis evolved from developing biosensor for toxin detection to microsystems engineering, tissue engineering, and translational research. Through this work, I laid out a foundation that will enable (i) generation of functional *in vitro* model of NMJ, (ii) clinical applications of BoNT/A in treating neuroendocrine malignancies, (iii) discovery of intercellular signaling pathways triggering the development of NMJ, and (iv) a novel function and signaling of HCR in reducing bioactive hormone production. The studies I conducted are preliminary and the beginning of many exciting science and engineering projects to come.

Abbreviations

ACh: acetylcholine

AChR: acetylcholine receptor

Akt: protein kinase B

ALS: amyotrophic lateral sclerosis

ASCL1: achaete-scute complex 1

a-SMN: axonal-survival motor neuron

bFGF: basic fibroblast growth factor

CNS: central nervous system

BDNF: brain-derived neurotrophic factor

BoNT: botulinum neurotoxin

CgA: chromogranin A

ChR2: channel rhodopsin 2

CMT: Charcot-Marie-Tooth disease

CNS: central nervous system

ELISA: enzyme-linked immunosorbent assay

ERK: extracellular signal-regulated kinase

GABAergic neurons: gamma aminoisobutyric acid neurons

GFAP: glial fibrillary acidic protein

GSK3β: glycogen synthase kinase 3 beta

HCR: heavy-chain receptor binding domain of botulinum neurotoxin

H_N: heavy-chain translocational domain of botulinum neurotoxin

hESC: human embryonic stem cells

hiPSC: human induced pluripotent stem cells

IGF-1: insulin-like growth factor 1

LC: light-chain catalytic domain of botulinum neurotoxin

MAPK: mitogen-activated protein kinase

MN: motor neuron

μPW: micro-pillar micro-well

MTC: medullary thyroid cancer

MuSK: muscle specific kinase

MYH: myosin heavy chain

NE: neuroendocrine

NET: neuroendocrine tumor

NT-3: neurotrophin-3

NMJ: neuromuscular junction

OCT: octreotide

PI3K: phosphoinositide 3-kinase

PNS: peripheral nervous system

Pur: purmorphamine

RA: retinoic acid

rHCR: recombinant heavy-chain receptor binding domain of botulinum neurotoxin

Shh: sonic hedgehog

SNARE: Soluble *N*-ethylmaleimide-sensitive factor attachment protein receptor complex

SMA: spinal muscular atrophy

SMA1: spinal muscular atrophy type 1

SMN1: survival motor neuron 1

SOD1: superoxide dismutase 1

SSA: somatostatin analogue

SSTR: somatostatin receptor

SV2: synaptic vesicle 2 protein

TGFβ: transforming growth factor-beta

Bibliography

1. Montal, M., *Botulinum neurotoxin: a marvel of protein design.* Annu Rev Biochem, 2010. **79**: p. 591-617.

2. Barash, J.R. and S.S. Arnon, *A novel strain of Clostridium botulinum that produces type B and type H botulinum toxins.* J Infect Dis, 2014. **209**(2): p. 183-91.

3. Arnon, S.S., et al., *Botulinum toxin as a biological weapon: medical and public health management.* JAMA, 2001. **285**(8): p. 1059-70.

4. Masuyer, G., et al., *Engineered botulinum neurotoxins as new therapeutics.* Annu Rev Pharmacol Toxicol, 2014. **54**: p. 27-51.

5. Zhao, C.M., et al., *Denervation suppresses gastric tumorigenesis.* Science Translational Medicine, 2014. **6**(250): p. 250ra115-250ra115.

6. Bandala, C., et al., *Effect of botulinum toxin A on proliferation and apoptosis in the T47D breast cancer cell line.* Asian Pac J Cancer Prev, 2013. **14**(2): p. 891-4.

7. Chuang, Y.C. and M.B. Chancellor, *The application of botulinum toxin in the prostate.* J Urol, 2006. **176**(6 Pt 1): p. 2375-82.

8. Frisk, M.L., et al., *Self-Assembled Peptide Monolayers as a Toxin Sensing Mechanism within Arrayed Microchannels.* Analytical Chemistry, 2009. **81**(7): p. 2760-2767.

9. Strotman, L.N., et al., *Facile and rapid DNA extraction and purification from food matrices using IFAST (immiscible filtration assisted by surface tension).* Analyst, 2012. **137**(17): p. 4023-8.

10. Pellett, S., et al., *Comparison of the primary rat spinal cord cell (RSC) assay and the mouse bioassay for botulinum neurotoxin type A potency determination.* J Pharmacol Toxicol Methods, 2010. **61**(3): p. 304-10.

11. Whitemarsh, R.C., et al., *Novel application of human neurons derived from induced pluripotent stem cells for highly sensitive botulinum neurotoxin detection.* Toxicol Sci, 2012. **126**(2): p. 426-35.

12. Kao, I., D.B. Drachman, and D.L. Price, *Botulinum toxin: mechanism of presynaptic blockade.* Science, 1976. **193**(4259): p. 1256-8.

13. Hu, B.Y. and S.C. Zhang, *Differentiation of spinal motor neurons from pluripotent human stem cells.* Nat Protoc, 2009. **4**(9): p. 1295-304.

14. Boulting, G.L., et al., *A functionally characterized test set of human induced pluripotent stem cells.* Nat Biotechnol, 2011. **29**(3): p. 279-86.

15. Minna, J., et al., *Genes for neuronal properties expressed in neuroblastoma x L cell hybrids.* Proc Natl Acad Sci U S A, 1971. **68**(1): p. 234-9.

16. Minna, J., D. Glazer, and M. Nirenberg, *Genetic dissection of neural properties using somatic cell hybrids.* Nat New Biol, 1972. **235**(60): p. 225-31.

17. McGee, R., et al., *Regulation of acetylcholine release from neuroblastoma x glioma hybrid cells.* Proc Natl Acad Sci U S A, 1978. **75**(3): p. 1314-8.

18. Christian, C.N., et al., *Pharmacologic responses of cells of a neuroblastoma X glioma hybrid clone and modulation of synapses between hybrid cells and mouse myotubes.* Brain Res, 1978. **147**(2): p. 261-76.

19. Nelson, P., C. Christian, and M. Nirenberg, *Synapse formation between clonal neuroblastoma X glioma hybrid cells and striated muscle cells.* Proc Natl Acad Sci U S A, 1976. **73**(1): p. 123-7.

20. Nelson, P.G., et al., *Formation of synapses between cells of a neuroblastoma X glioma hybrid clone and mouse myotubes.* Brain Res, 1978. **147**(2): p. 245-59.

21. Kingham, P.J., et al., *Adipose-derived stem cells differentiate into a Schwann cell phenotype and promote neurite outgrowth in vitro.* Exp Neurol, 2007. **207**(2): p. 267-74.

22. Nicholls, J.G., *From neuron to brain*. 5th ed. 2012, Sunderland, Mass.: Sinauer Associates. xxiii, 621, 93 p.

23. Umbach, J.A., et al., *Functional neuromuscular junctions formed by embryonic stem cell-derived motor neurons.* PLoS One, 2012. **7**(5): p. e36049.

24. Das, M., et al., *Differentiation of skeletal muscle and integration of myotubes with silicon microstructures using serum-free medium and a synthetic silane substrate.* Nat Protoc, 2007. **2**(7): p. 1795-801.

25. Das, M., et al., *A defined long-term in vitro tissue engineered model of neuromuscular junctions.* Biomaterials, 2010. **31**(18): p. 4880-8.

26. Ullian, E.M., K.S. Christopherson, and B.A. Barres, *Role for glia in synaptogenesis.* Glia, 2004. **47**(3): p. 209-16.

27. Ullian, E.M., et al., *Schwann cells and astrocytes induce synapse formation by spinal motor neurons in culture.* Mol Cell Neurosci, 2004. **25**(2): p. 241-51.

28. Cao, G. and C.P. Ko, *Schwann cell-derived factors modulate synaptic activities at developing neuromuscular synapses.* J Neurosci, 2007. **27**(25): p. 6712-22.

29. Feng, Z. and C.P. Ko, *Schwann cells promote synaptogenesis at the neuromuscular junction via transforming growth factor-beta1*. J Neurosci, 2008. **28**(39): p. 9599-609.

30. Woodhoo, A. and L. Sommer, *Development of the Schwann cell lineage: from the neural crest to the myelinated nerve.* Glia, 2008. **56**(14): p. 1481-90.

31. Chen, Z.L., W.M. Yu, and S. Strickland, *Peripheral regeneration.* Annu Rev Neurosci, 2007. **30**: p. 209-33.

32. Chen, S. and J.T. Barbieri, *Engineering botulinum neurotoxin to extend therapeutic intervention.* Proc Natl Acad Sci U S A, 2009. **106**(23): p. 9180-4.

33. Colasante, C., et al., *Botulinum Neurotoxin Type A is Internalized and Translocated from Small Synaptic Vesicles at the Neuromuscular Junction.* Molecular Neurobiology, 2013. **48**(1): p. 120-127.

34. Portela-Gomes, G.M., A. Lukinius, and L. Grimelius, *Synaptic vesicle protein 2, A new neuroendocrine cell marker.* Am J Pathol, 2000. **157**(4): p. 1299-309.

35. Jakobsen, A.M., et al., *Expression of synaptic vesicle protein 2 (SV2) in neuroendocrine tumours of the gastrointestinal tract and pancreas.* J Pathol, 2002. **196**(1): p. 44-50.

36. Nilsson, O., et al., *Importance of vesicle proteins in the diagnosis and treatment of neuroendocrine tumors.* Ann N Y Acad Sci, 2004. **1014**: p. 280-3.

37. Bumming, P., et al., *Gastrointestinal stromal tumors regularly express synaptic vesicle proteins: evidence of a neuroendocrine phenotype.* Endocr Relat Cancer, 2007. **14**(3): p. 853-63.

38. Dong, M., et al., *SV2 is the protein receptor for botulinum neurotoxin A.* Science, 2006. **312**(5773): p. 592-6.

39. Chaddock, J.A. and K.R. Acharya, *Engineering toxins for 21st century therapies.* FEBS J, 2011. **278**(6): p. 899-904.

40. Thomson, S.R., et al., *Using induced pluripotent stem cells (iPSC) to model human neuromuscular connectivity: promise or reality?* J Anat, 2012. **220**(2): p. 122-30.

41. Eroglu, C. and B.A. Barres, *Regulation of synaptic connectivity by glia.* Nature, 2010. **468**(7321): p. 223-31.

42. Hakami, R.M., et al., *Gaining ground: assays for therapeutics against botulinum neurotoxin.* Trends Microbiol, 2010. **18**(4): p. 164-72.

43. Cai, S., B.R. Singh, and S. Sharma, *Botulism diagnostics: from clinical symptoms to in vitro assays.* Crit Rev Microbiol, 2007. **33**(2): p. 109-25.

44. Phillips, R.W. and D. Abbott, *High-throughput enzyme-linked immunoabsorbant assay (ELISA) electrochemiluminescent detection of botulinum toxins in foods for food safety and defence purposes.* Food Additives & Contaminants: Part A, 2008. **25**(9): p. 1084-1088.

45. Bagramyan, K., et al., *Attomolar detection of botulinum toxin type A in complex biological matrices.* PLoS One, 2008. **3**(4): p. e2041.

46. Pancrazio, J.J., et al., *Development and application of cell-based biosensors.* Ann Biomed Eng, 1999. **27**(6): p. 697-711.

47. Pellett, S., et al., *Sensitive and quantitative detection of botulinum neurotoxin in neurons derived from mouse embryonic stem cells.* Biochem Biophys Res Commun, 2011. **404**(1): p. 388-92.

48. Whitemarsh, R.C.M., et al., *Novel and highly sensitive cell model for botulinum neurotoxin detection using human neurons from induced pluripotent stem cells.* Toxicon, 2013. **68**: p. 78-79.

49. Purkiss, J.R., et al., *Clostridium botulinum neurotoxins act with a wide range of potencies on SH-SY5Y human neuroblastoma cells.* Neurotoxicology, 2001. **22**(4): p. 447-53.

50. Yowler, B.C., R.D. Kensinger, and C.L. Schengrund, *Botulinum neurotoxin A activity is dependent upon the presence of specific gangliosides in neuroblastoma cells expressing synaptotagmin I.* J Biol Chem, 2002. **277**(36): p. 32815-9.

51. Fernandez-Salas, E., et al., *Botulinum neurotoxin serotype a specific cell-based potency assay to replace the mouse bioassay.* PLoS One, 2012. **7**(11): p. e49516.

52. Whitemarsh, R.C., et al., *Model for studying Clostridium botulinum neurotoxin using differentiated motor neuron-like NG108-15 cells.* Biochem Biophys Res Commun, 2012. **427**(2): p. 426-30.

53. Dong, M., et al., *Using fluorescent sensors to detect botulinum neurotoxin activity in vitro and in living cells.* Proc Natl Acad Sci U S A, 2004. **101**(41): p. 14701-6.

54. Reddy, L.V., et al., *Glial cells maintain synaptic structure and function and promote development of the neuromuscular junction in vivo.* Neuron, 2003. **40**(3): p. 563-80.

55. Domenech, M., et al., *Cellular observations enabled by microculture: paracrine signaling and population demographics.* Integr Biol (Camb), 2009. **1**(3): p. 267-74.

56. Paguirigan, A.L. and D.J. Beebe, *From the cellular perspective: exploring differences in the cellular baseline in macroscale and microfluidic cultures.* Integr Biol (Camb), 2009. **1**(2): p. 182-95.

57. Young, E.W. and D.J. Beebe, *Fundamentals of microfluidic cell culture in controlled microenvironments.* Chem Soc Rev, 2010. **39**(3): p. 1036-48.

58. Young, E.W., et al., *Microscale functional cytomics for studying hematologic cancers.* Blood, 2012. **119**(10): p. e76-85.

59. Walker, G.M. and D.J. Beebe, *A passive pumping method for microfluidic devices.* Lab Chip, 2002. **2**(3): p. 131-4.

60. Duffy, D.C., et al., *Rapid Prototyping of Microfluidic Systems in Poly(dimethylsiloxane).* Anal Chem, 1998. **70**(23): p. 4974-84.

61. Xia, Y. and G.M. Whitesides, *Soft Lithography.* Annu rev Mater Sci, 1998. **28**: p. 153-84.

62. Regehr, K.J., et al., *Biological implications of polydimethylsiloxane-based microfluidic cell culture.* Lab Chip, 2009. **9**(15): p. 2132-9.

63. National Institute of Health, *Report on the ICCVAM-NICEATM/ECVAM Scientific Workshop on Alternative Methods to Refine, Reduce or Replace the Mouse LD50 Assay for Botulinum Toxin Testing.* . National Institute of Health, 2008

64. Nirenberg, M., et al., *Modulation of synapse formation by cyclic adenosine monophosphate.* Science, 1983. **222**(4625): p. 794-9.

65. Tojima, T., et al., *Acquisition of neuronal proteins during differentiation of NG108-15 cells.* Neurosci Res, 2000. **37**(2): p. 153-61.

66. Hai, M., et al., *Comparative analysis of Schwann cell lines as model systems for myelin gene transcription studies.* J Neurosci Res, 2002. **69**(4): p. 497-508.

67. Saharinen, J. and J. Keski-Oja, *Specific sequence motif of 8-Cys repeats of TGF-beta binding proteins, LTBPs, creates a hydrophobic interaction surface for binding of small latent TGF-beta.* Mol Biol Cell, 2000. **11**(8): p. 2691-704.

68. Young, E.W., et al., *Rapid prototyping of arrayed microfluidic systems in polystyrene for cell-based assays.* Anal Chem, 2011. **83**(4): p. 1408-17.

69. Lam, A.J., et al., *Improving FRET dynamic range with bright green and red fluorescent proteins.* Nat Methods, 2012. **9**(10): p. 1005-12.

70. Keller, J.E., F. Cai, and E.A. Neale, *Uptake of botulinum neurotoxin into cultured neurons.* Biochemistry, 2004. **43**(2): p. 526-32.

71. Singh, A.K., L.H. Stanker, and S.K. Sharma, *Botulinum neurotoxin: where are we with detection technologies?* Crit Rev Microbiol, 2013. **39**(1): p. 43-56.

72. Kiris, E., et al., *Embryonic stem cell-derived motoneurons provide a highly sensitive cell culture model for botulinum neurotoxin studies, with implications for high-throughput drug discovery.* Stem Cell Res, 2011. **6**(3): p. 195-205.

73. Hong, W.S., et al., *A Microscale Neuron and Schwann Cell Coculture Model for Increasing Detection Sensitivity of Botulinum Neurotoxin Type A.* Toxicol Sci, 2013.

74. Cressey, D., *Neuroscientists claim growing pains.* Nature, 2009. **459**(7243): p. 19-19.

75. Chen, Y., et al., *NS21: re-defined and modified supplement B27 for neuronal cultures.* J Neurosci Methods, 2008. **171**(2): p. 239-47.

76. Vandenburgh, H., et al., *Drug-screening platform based on the contractility of tissue-engineered muscle.* Muscle Nerve, 2008. **37**(4): p. 438-47.

77. Sakar, M.S., et al., *Formation and optogenetic control of engineered 3D skeletal muscle bioactuators.* Lab Chip, 2012. **12**(23): p. 4976-85.

78. Boudou, T., et al., *A microfabricated platform to measure and manipulate the mechanics of engineered cardiac microtissues.* Tissue Eng Part A, 2012. **18**(9-10): p. 910-9.

79. Legant, W.R., et al., *Microfabricated tissue gauges to measure and manipulate forces from 3D microtissues.* Proc Natl Acad Sci U S A, 2009. **106**(25): p. 10097-102.

80. Foulds, I.G. and M. Parameswaran, *A planar self-sacrificial multilayer SU-8-based MEMS process utilizing a UV-blocking layer for the creation of freely moving parts.* Journal of Micromechanics and Microengineering, 2006. **16**(10): p. 2109-2115.

81. Bian, W., et al., *Mesoscopic hydrogel molding to control the 3D geometry of bioartificial muscle tissues.* Nat Protoc, 2009. **4**(10): p. 1522-34.

82. Bian, W. and N. Bursac, *Engineered skeletal muscle tissue networks with controllable architecture.* Biomaterials, 2009. **30**(7): p. 1401-12.

83. Hinds, S., et al., *The role of extracellular matrix composition in structure and function of bioengineered skeletal muscle.* Biomaterials, 2011. **32**(14): p. 3575-3583.

84. Barakat, M.T., K. Meeran, and S.R. Bloom, *Neuroendocrine tumours.* Endocr Relat Cancer, 2004. **11**(1): p. 1-18.

85. Pinchot, S.N., et al., *Carcinoid tumors.* Oncologist, 2008. **13**(12): p. 1255-69.

86. Chen, H., et al., *The North American Neuroendocrine Tumor Society Consensus Guideline for the Diagnosis and Management of Neuroendocrine Tumors: Pheochromocytoma, Paraganglioma, and Medullary Thyroid Cancer.* Pancreas, 2010. **39**(6): p. 775-783.

87. Massironi, S., et al., *Chromogranin A in Diagnosing and Monitoring Patients with Gastro-Entero-Pancreatic Neuroendocrine Neoplasms. A Large Series from a Single Institution.* Neuroendocrinology, 2014.

88. Yao, J.C., et al., *One hundred years after "Carcinoid": Epidemiology of and prognostic factors for neuroendocrine tumors in 35,825 cases in the United States.* Journal of Clinical Oncology, 2008. **26**(18): p. 3063-3072.

89. Taal, B.G. and O. Visser, *Epidemiology of neuroendocrine tumours.* Neuroendocrinology, 2004. **80 Suppl 1**: p. 3-7.

90. Metz, D.C. and R.T. Jensen, *Gastrointestinal neuroendocrine tumors: pancreatic endocrine tumors.* Gastroenterology, 2008. **135**(5): p. 1469-92.

91. Demirkan, B.H. and B. Eriksson, *Systemic treatment of neuroendocrine tumors with hepatic metastases.* Turk J Gastroenterol, 2012. **23**(5): p. 427-37.

92. Barbieri, F., et al., *Neuroendocrine tumors: insights into innovative therapeutic options and rational development of targeted therapies.* Drug Discov Today, 2013.

93. Gulenchyn, K.Y., et al., *Radionuclide therapy in neuroendocrine tumours: a systematic review.* Clin Oncol (R Coll Radiol), 2012. **24**(4): p. 294-308.

94. Ye, L., L. Santarpia, and R.F. Gagel, *The evolving field of tyrosine kinase inhibitors in the treatment of endocrine tumors.* Endocr Rev, 2010. **31**(4): p. 578-99.

95. Raymond, E., et al., *Sunitinib malate for the treatment of pancreatic neuroendocrine tumors.* N Engl J Med, 2011. **364**(6): p. 501-13.

96. Yao, J.C., et al., *Everolimus for advanced pancreatic neuroendocrine tumors.* N Engl J Med, 2011. **364**(6): p. 514-23.

97. Ebos, J.M.L., et al., *Accelerated Metastasis after Short-Term Treatment with a Potent Inhibitor of Tumor Angiogenesis.* Cancer Cell, 2009. **15**(3): p. 232-239.

98. Pool, S.E., et al., *mTOR inhibitor RAD001 promotes metastasis in a rat model of pancreatic neuroendocrine cancer.* Cancer Res, 2013. **73**(1): p. 12-8.

99. Mohammed, T.A., et al., *A pilot phase II study of valproic acid for treatment of low-grade neuroendocrine carcinoma.* Oncologist, 2011. **16**(6): p. 835-43.

100. Lubner, S.J., et al., *A preclinical and clinical study of lithium in low-grade neuroendocrine tumors.* Oncologist, 2011. **16**(4): p. 452-7.

101. Arsenault, J., et al., *Stapling of the botulinum type A protease to growth factors and neuropeptides allows selective targeting of neuroendocrine cells.* J Neurochem, 2013. **126**(2): p. 223-33.

102. Castro, D.S., et al., *A novel function of the proneural factor Ascl1 in progenitor proliferation identified by genome-wide characterization of its targets.* Genes Dev, 2011. **25**(9): p. 930-45.

103. Baldwin, M.R., et al., *Characterization of the antibody response to the receptor binding domain of botulinum neurotoxin serotypes A and E.* Infect Immun, 2005. **73**(10): p. 6998-7005.

104. Bailey, J.A. and D.K. Lahiri, *Neuronal differentiation is accompanied by increased levels of SNAP-25 protein in fetal rat primary cortical neurons - Implications in neuronal*

plasticity and Alzheimer's disease. Integrated Molecular Medicine for Neuronal and Neoplastic Disorders, 2006. **1086**: p. 54-65.

105. Hamprecht, B., *Structural, electrophysiological, biochemical, and pharmacological properties of neuroblastoma-glioma cell hybrids in cell culture.* Int Rev Cytol, 1977. **49**: p. 99-170.

106. Hamprecht, B., et al., *Culture and characteristics of hormone-responsive neuroblastoma X glioma hybrid cells.* Methods Enzymol, 1985. **109**: p. 316-41.

107. Takahashi, T., et al., *p53: a frequent target for genetic abnormalities in lung cancer.* Science, 1989. **246**(4929): p. 491-4.

108. Brandt, D.W., S.J. Pandol, and L.J. Deftos, *Calcium-stimulated parathyroid hormone-like protein secretion: potentiation through a protein kinase-C pathway.* Endocrinology, 1991. **128**(6): p. 2999-3004.

109. Giard, D.J., et al., *In vitro cultivation of human tumors: establishment of cell lines derived from a series of solid tumors.* J Natl Cancer Inst, 1973. **51**(5): p. 1417-23.

110. Phelps, R.M., et al., *NCI-Navy Medical Oncology Branch cell line data base.* J Cell Biochem Suppl, 1996. **24**: p. 32-91.

111. Cooley, L.D., et al., *Cytogenetic characterization of three human and three rat medullary thyroid carcinoma cell lines.* Cancer Genet Cytogenet, 1995. **80**(2): p. 138-49.

112. Zhu, W., et al., *Medullary thyroid carcinoma cell lines contain a self-renewing CD133+ population that is dependent on ret proto-oncogene activity.* J Clin Endocrinol Metab, 2010. **95**(1): p. 439-44.

113. Demeure, M.J., et al., *Invasion by cultured human follicular thyroid cancer correlates with increased beta 1 integrins and production of proteases.* World J Surg, 1992. **16**(4): p. 770-6.

114. Carlsson, J., et al., *Formation and growth of multicellular spheroids of human origin.* Int J Cancer, 1983. **31**(5): p. 523-33.

115. Schweppe, R.E., et al., *Deoxyribonucleic acid profiling analysis of 40 human thyroid cancer cell lines reveals cross-contamination resulting in cell line redundancy and misidentification.* J Clin Endocrinol Metab, 2008. **93**(11): p. 4331-41.

116. Saiselet, M., et al., *Thyroid cancer cell lines: an overview.* Front Endocrinol (Lausanne), 2012. **3**: p. 133.

117. Evers, B.M., et al., *Establishment and characterization of a human carcinoid in nude mice and effect of various agents on tumor growth.* Gastroenterology, 1991. **101**(2): p. 303-11.

118. Lieber, M., et al., *Establishment of a continuous tumor-cell line (panc-1) from a human carcinoma of the exocrine pancreas.* Int J Cancer, 1975. **15**(5): p. 741-7.

119. Dong, M., et al., *Glycosylated SV2A and SV2B mediate the entry of botulinum neurotoxin E into neurons.* Mol Biol Cell, 2008. **19**(12): p. 5226-37.

120. Simpson, L.L. and M.M. Rapport, *Ganglioside inactivation of botulinum toxin.* J Neurochem, 1971. **18**(7): p. 1341-3.

121. Chang, W.P. and T.C. Sudhof, *SV2 renders primed synaptic vesicles competent for Ca2+ -induced exocytosis.* J Neurosci, 2009. **29**(4): p. 883-97.

122. Nowack, A., et al., *SV2 regulates neurotransmitter release via multiple mechanisms.* Am J Physiol Cell Physiol, 2010. **299**(5): p. C960-7.

123. Martins, R.G., et al., *Medullary thyroid cancer: options for systemic therapy of metastatic disease?* J Clin Oncol, 2006. **24**(11): p. 1653-5.

124. Bertherat, J., et al., *Somatostatin Receptors on Thyrotropin-Secreting Pituitary-Adenomas - Comparison with the Inhibitory Effects of Octreotide Upon Invivo and Invitro Hormonal Secretions.* Journal of Clinical Endocrinology & Metabolism, 1992. **75**(2): p. 540-546.

125. Csaba, Z. and P. Dournaud, *Cellular biology of somatostatin receptors.* Neuropeptides, 2001. **35**(1): p. 1-23.

126. Ekong, T.A., I.M. Feavers, and D. Sesardic, *Recombinant SNAP-25 is an effective substrate for Clostridium botulinum type A toxin endopeptidase activity in vitro.* Microbiology, 1997. **143 (Pt 10)**: p. 3337-47.

127. Berry, S.M., E.T. Alarid, and D.J. Beebe, *One-step purification of nucleic acid for gene expression analysis via Immiscible Filtration Assisted by Surface Tension (IFAST).* Lab Chip, 2011. **11**(10): p. 1747-53.

128. Nagai, M., et al., *Astrocytes expressing ALS-linked mutated SOD1 release factors selectively toxic to motor neurons.* Nat Neurosci, 2007. **10**(5): p. 615-22.

129. Haidet-Phillips, A.M., et al., *Astrocytes from familial and sporadic ALS patients are toxic to motor neurons.* Nat Biotechnol, 2011. **29**(9): p. 824-8.

130. Kang, S.H., et al., *Degeneration and impaired regeneration of gray matter oligodendrocytes in amyotrophic lateral sclerosis.* Nat Neurosci, 2013. **16**(5): p. 571-9.

131. Philips, T. and W. Robberecht, *Neuroinflammation in amyotrophic lateral sclerosis: role of glial activation in motor neuron disease.* Lancet Neurol, 2011. **10**(3): p. 253-63.

132. Dobrowolny, G., et al., *Skeletal muscle is a primary target of SOD1G93A-mediated toxicity.* Cell Metab, 2008. **8**(5): p. 425-36.

133. Wong, M. and L.J. Martin, *Skeletal muscle-restricted expression of human SOD1 causes motor neuron degeneration in transgenic mice.* Hum Mol Genet, 2010. **19**(11): p. 2284-302.

134. Dupuis, L., et al., *Muscle mitochondrial uncoupling dismantles neuromuscular junction and triggers distal degeneration of motor neurons.* PLoS One, 2009. **4**(4): p. e5390.

135. Lobsiger, C.S., et al., *Schwann cells expressing dismutase active mutant SOD1 unexpectedly slow disease progression in ALS mice.* Proc Natl Acad Sci U S A, 2009. **106**(11): p. 4465-70.

136. Martinez-Hernandez, R., et al., *The developmental pattern of myotubes in spinal muscular atrophy indicates prenatal delay of muscle maturation.* J Neuropathol Exp Neurol, 2009. **68**(5): p. 474-81.

137. Kobayashi, T., V. Askanas, and W.K. Engel, *Human muscle cultured in monolayer and cocultured with fetal rat spinal cord: importance of dorsal root ganglia for achieving successful functional innervation.* J Neurosci, 1987. **7**(10): p. 3131-41.

138. Askanas, V., et al., *De novo neuromuscular junction formation on human muscle fibres cultured in monolayer and innervated by foetal rat spinal cord: ultrastructural and ultrastructural--cytochemical studies.* J Neurocytol, 1987. **16**(4): p. 523-37.

139. Connor, E.A. and M.A. Smith, *Retrograde Signaling in the Formation and Maintenance of the Neuromuscular-Junction.* Journal of Neurobiology, 1994. **25**(6): p. 722-739.

140. Wu, H., W.C. Xiong, and L. Mei, *To build a synapse: signaling pathways in neuromuscular junction assembly.* Development, 2010. **137**(7): p. 1017-33.

141. Vogel, Z., Sytkowsk.Aj, and Nirenber.Mw, *Acetylcholine Receptors of Muscle Grown in-Vitro.* Proceedings of the National Academy of Sciences of the United States of America, 1972. **69**(11): p. 3180-&.

142. Fischbac.Gd and S.A. Cohen, *Distribution of Acetylcholine Sensitivity over Uninnervated and Innervated Muscle Fibers Grown in Cell-Culture.* Developmental Biology, 1973. **31**(1): p. 147-162.

143. Jessell, T.M., R.E. Siegel, and G.D. Fischbach, *Induction of Acetylcholine Receptors on Cultured Skeletal-Muscle by a Factor Extracted from Brain and Spinal-Cord.* Proceedings of the National Academy of Sciences of the United States of America, 1979. **76**(10): p. 5397-5401.

144. Lin, S., et al., *The role of nerve-versus muscle-derived factors in mammalian neuromuscular junction formation.* Journal of Neuroscience, 2008. **28**(13): p. 3333-3340.

145. Tourovskaia, A., N. Li, and A. Folch, *Localized acetylcholine receptor clustering dynamics in response to microfluidic focal stimulation with agrin.* Biophys J, 2008. **95**(6): p. 3009-16.

146. Kim, N. and S.J. Burden, *MuSK controls where motor axons grow and form synapses (vol 11, pg 19, 2008).* Nature Neuroscience, 2008. **11**(2): p. 238-238.

147. Lacombe, J., et al., *Genetic and functional modularity of Hox activities in the specification of limb-innervating motor neurons.* PLoS Genet, 2013. **9**(1): p. e1003184.

148. Berggren, K., et al., *Differential distribution of retinoic acid synthesis in the chicken embryo as determined by immunolocalization of the retinoic acid synthetic enzyme, RALDH-2.* Dev Biol, 1999. **210**(2): p. 288-304.

149. Berggren, K., et al., *Expression and regulation of the retinoic acid synthetic enzyme RALDH-2 in the embryonic chicken wing.* Dev Dyn, 2001. **222**(1): p. 1-16.

150. Ji, S.J., et al., *Mesodermal and neuronal retinoids regulate the induction and maintenance of limb innervating spinal motor neurons.* Dev Biol, 2006. **297**(1): p. 249-61.

151. Cao, P., A. Maximov, and T.C. Sudhof, *Activity-dependent IGF-1 exocytosis is controlled by the Ca(2+)-sensor synaptotagmin-10.* Cell, 2011. **145**(2): p. 300-11.

152. Madhala-Levy, D., et al., *Cooperation between Shh and IGF-I in promoting myogenic proliferation and differentiation via the MAPK/ERK and PI3K/Akt pathways requires smo activity.* Journal of Cellular Physiology, 2012. **227**(4): p. 1455-1464.

153. Schiaffino, S. and C. Mammucari, *Regulation of skeletal muscle growth by the IGF1-Akt/PKB pathway: insights from genetic models.* Skelet Muscle, 2011. **1**(1): p. 4.

154. Locatelli, D., et al., *Human axonal survival of motor neuron (a-SMN) protein stimulates axon growth, cell motility, C-C motif ligand 2 (CCL2), and insulin-like growth factor-1 (IGF1) production.* J Biol Chem, 2012. **287**(31): p. 25782-94.

155. Korkut, C. and V. Budnik, *WNTs tune up the neuromuscular junction.* Nature Reviews Neuroscience, 2009. **10**(9): p. 627-634.